



HAL
open science

Modelling and control of actuated lower limb exoskeletons : a mathematical application using central pattern generators and nonlinear feedback control techniques

Michael Oluwatosin Ajayi

► **To cite this version:**

Michael Oluwatosin Ajayi. Modelling and control of actuated lower limb exoskeletons : a mathematical application using central pattern generators and nonlinear feedback control techniques. General Mathematics [math.GM]. Université Paris-Est, 2016. English. NNT : 2016PESC1021 . tel-01531927

HAL Id: tel-01531927

<https://theses.hal.science/tel-01531927v1>

Submitted on 2 Jun 2017

HAL is a multi-disciplinary open access archive for the deposit and dissemination of scientific research documents, whether they are published or not. The documents may come from teaching and research institutions in France or abroad, or from public or private research centers.

L'archive ouverte pluridisciplinaire **HAL**, est destinée au dépôt et à la diffusion de documents scientifiques de niveau recherche, publiés ou non, émanant des établissements d'enseignement et de recherche français ou étrangers, des laboratoires publics ou privés.

**MODELLING AND CONTROL OF ACTUATED LOWER LIMB
EXOSKELETONS:
A Mathematical Application using Central Pattern Generators and
Nonlinear Feedback Control Techniques**

by

Michael Oluwatosin Ajayi

Submitted in partial fulfilment of the requirements for the degree

DOCTORAT SIGNAL, IMAGE, AUTOMATIQUE

in the

UNIVERSITÉ PARIS-EST ET MSTIC

Co-Tutelle

TSHWANE UNIVERSTIY OF TECHNOLOGY

Directeur de these : Prof. Karim Djouani

Directeur de these : Prof. Yskandar Hamam

Rapporteur : Prof. Benallegue Abdelaziz

Rapporteur : Prof. Ferrerira Antonie

Examineur : Prof. Van Wyk B. Jacobus

Examineur : Prof. Amirat Yacine

Examineur : Prof. Rocaries Francois

Examineur : Prof. Kurien Anish

Date of Defence : 15 November 2016

Declaration

“I hereby declare that the thesis submitted for the degree D Tech: Control Engineering, at the Tshwane University of Technology, is my own original work and has not previously been submitted to any other institution of higher education. I further declare that all sources cited or quoted are indicated and acknowledged by means of a comprehensive list of references” .



M.O. Ajayi

Dedication

This thesis is dedicated to God, my family and loved ones.

Acknowledgements

I would like to thank my supervisor Prof. Karim Djouani, and my co-supervisor, Prof. Yskandar Hamam, for their guidance and support throughout the course of this study. Many thanks also go to my friends and colleagues who made my time at Tshwane University of Technology, Pretoria campus worthwhile.

I acknowledge all the management staff of the French South African Institute of Technology (F'SATI), department of electrical engineering, and the faculty of engineering and the built environment; I treasure your tireless assistance towards making things work whenever I run into difficulties that require your attention.

I also appreciate the Tshwane University of Technology, National Research Foundation (NRF) and Research and Innovation Support and Advancement (RISA) for the funds made available to me for the proper completion of this study.

Finally, thanks to my mother, Mrs. Victoria Ojo, my pastor, Pastor Ebenezer George and his wife, Pastor Stella George and also my fiancée, Miss Omotola Ibukunoluwa Johnson for their encouragement, prayers and love.

Abstract

Wearable robotic system in recent years has become a well sought after mechanism in the field of bio-mechatronics engineering due to the various possibilities it possesses. These possibilities encompass the assistive and rehabilitative protocols rendered to disabled and elderly people, in order to enable them to regain control of their limbs and of course increase the abilities of able-bodied persons. It therefore clearly drives the motive of bringing back paraplegics back on their feet as well as executing difficult task beyond human ability.

Achieving the intended function of wearable robots requires the model dynamics of the physical system in relation to the tasks required to be performed by subjects. This demands a proper control measure which takes into account the safety of the wearer. For this purpose, bio-inspired control techniques and bounded nonlinear feedback controllers are considered. The latter control design ensures that the stipulated power required is not exceeded as well as the saturation of the actuator, while the former motivates the design of controllers based on the concept of Central Pattern Generators (CPG). CPGs are characterised as biological neural networks which can be represented by a set of coupled nonlinear oscillator situated in the spinal cord of mammals, having the capability of generating coordinated multidimensional rhythmic signals for the purpose of locomotion, under the control of simple input signals. These rhythmic signals are termed to be periodic or quasi-periodic in nature, hence performing this task in robotics

and animal motor control has been a perpetual research problem. The movement of the lower limb of humans, thus presents a platform to investigate and address this difficulty. In this thesis, the analysis, simulation, and control of joints which relate to the human lower limbs via CPGs and feedback control techniques with an aim of practically implementing the control strategies using a lower limb exoskeleton is presented. To accomplish this goal, it is expedient to have comprehensive knowledge of the anatomy, physiology and the normal gait biomechanics of the human lower limbs. Understanding the theories, principles and mathematical background of nonlinear oscillators are also required. Control strategies using the inverse and the forward dynamics approach based on different types of coupled nonlinear oscillators and nonlinear feedback control techniques were considered for single/multiple degrees of freedom (DoF). Simulations and results were presented using MATLAB/SIMULINK to verify the controller-human system ability to constantly and dynamically track and re-adapt its control parameters to maintain its desired motion dynamics, with reduced control torque values.

This work basically deals with two distinct methods of control systems; one which integrates bio-inspired methods with classical and nonlinear control techniques to govern the joints associated with human-in-the loop, and another which utilises bounded nonlinear feedback control techniques for the same purpose.

During this work, some of the components required to construct the physical prototype has been acquired and assembled, although not fully functional, preceding the testing on patients with lower limb disorders.

TABLE OF CONTENTS

DECLARATION	ii
DEDICATION	iii
ACKNOWLEDGEMENTS	iv
ABSTRACT	v
GLOSARRY	xx
1.. Problem Settings	1
1.1. Introduction	1
1.2. Background	3
1.3. Problem Statement	5
1.3.1. Sub-Problem 1	7
1.3.2. Sub-Problem 2	7
1.3.3. Sub-Problem 3	9
1.3.4. Sub-Problem 4	10
1.3.5. Sub-Problem 5	11
1.3.6. Sub-Problem 6	13
1.3.7. Sub-Problem 7	15

1.4. Hypotheses of the Study	16
1.5. Contribution of the Study	17
1.6. Outline of Thesis	19
CHAPTER 2.. Literature Review	21
2.1. Introduction	21
2.2. Human Lower Limb Modelling	21
2.2.1. Human Lower Limb Anatomical structure	22
2.3. Human Gait Modelling	24
2.4. Central Pattern Generators (CPGs)	28
2.4.1. Modelling CPGs	29
2.4.2. Neural Oscillators as CPGs	30
2.4.3. Coupled Oscillators	32
2.5. Exoskeletons	33
2.5.1. Multi-joints Exoskeletons	35
2.5.2. Single-joint Exoskeletons	39
2.6. Conclusion	45
CHAPTER 3.. Analysis of Knee-Ankle Orthosis Modelling: An In-	
verse Dynamics Approach using Adaptive Coupled Oscillators	47
3.1. Introduction	47
3.2. Knee-Ankle Orthosis System	48
3.3. CPG Design	49
3.3.1. Adaptive Frequency Oscillator (AFO)	50

3.3.2.	Coupled AFO	51
3.4.	Mathematical Model	52
3.4.1.	Dynamic Model	52
3.4.2.	Coupled AFO (Joints Coupling)	53
3.4.3.	Signal Estimator	54
3.4.4.	Torque Estimator	55
3.4.5.	Human Torque	55
3.5.	Numerical Simulation & Results	56
3.5.1.	Reference Trajectories and Physiological Parameters	56
3.5.2.	Results	57
3.6.	Conclusions and Future Works	61

CHAPTER 4.. Shank-Foot Trajectory Control: A Forward Dynamics

	Approach using Computed-Torque Control	62
4.1.	Introduction	62
4.2.	Shank-Foot Model	65
4.3.	Dynamic Equation of Motion	65
4.4.	Path Generation: Desired & Internally Generated Trajectory	67
4.5.	Computed-Torque Control	68
4.5.1.	Computed-Torque PID Control	69
4.5.2.	Computed-Torque simple PD Control	69
4.6.	Numerical Simulations	71
4.7.	Discussion	73
4.8.	Conclusion and Further Works	74

CHAPTER 5.. Rhythmic Trajectory Design and Control	76
5.1. Introduction	76
5.2. CPG Model Design	78
5.2.1. Coupled van der Pol Oscillators	78
5.2.2. Periodic Sequence	80
5.3. Human-Exoskeleton Dynamics	83
5.3.1. Lagrangian equation of motion	83
5.3.2. Phase Transition	89
5.4. Exoskeleton control	90
5.4.1. Matrix transformation analysis	91
5.4.2. Feedback linearisation	94
5.4.3. Desired trajectory mapping	96
5.5. Numerical simulation	96
5.5.1. Simulation results	97
5.5.2. Analysis of results	98
5.6. Conclusion and Future works	100
CHAPTER 6.. Bounded Control of an Actuated Lower Limb Orthosis .	103
6.1. Introduction	103
6.2. Observer-based Bounded Control of an Actuated Lower Limb orthosis . .	104
6.2.1. Mathematical Description of the Knee-Ankle Orthosis	105
6.2.2. High Gain Observer Structure and Estimation	107
6.2.3. Control Law	111

6.2.4.	Saturation Function	112
6.2.5.	Closed Loop System	112
6.2.6.	Stability Analysis	113
6.2.7.	Orthosis Control	116
6.2.8.	Simulations Results	117
6.2.9.	Conclusion and Future Work	121
6.3.	Bounded Control of a Full Exoskeleton Device with 4 Degree of Freedom	122
6.3.1.	Introduction	122
6.3.2.	Trajectory Design	123
6.3.3.	Human-Exoskeleton Dynamics	124
6.3.4.	Exoskeleton control	124
6.3.5.	Numerical simulation	126
6.3.6.	Conclusion and Further Works	130
6.4.	Conclusion	130
CHAPTER 7.. Conclusion, Future Works & Recommendation		131
7.1.	Introduction	131
7.1.1.	Conclusion	131
7.1.2.	Further Works	136
7.1.3.	Recommendation	137
7.2.	Conclusion	137

APPENDIX A.. Nonlinear Oscillators	160
A.1. Introduction	160
A.2. Van der Pol Oscillator	161
A.3. Matsuoka Oscillator	163
A.4. Hopf Oscillator	165
A.4.1. Single Frequency Signal	168
A.4.2. Multi-Frequency Signal	169
A.5. Coupled Oscillators System	169
A.5.1. Learning Multi-Frequency Signal	170
A.6. Inverted Pendulum Control	173
A.6.1. Inverted Pendulum Dynamics	174
A.6.2. Adaptive Frequency Oscillator	174
A.7. Conclusion	176
APPENDIX B.. Stability Theory	178
B.1. Vectors and Matrix Norms	178
B.1.1. Vector Norms	178
B.1.2. P-norms	178
B.1.3. Matrix Norms	179
B.1.4. Existence and Uniqueness of Solutions	180
B.2. Lyapunov Stability Theory	181
B.2.1. Asymptotic Stability	181
B.2.2. Globally Stable	182

B.2.3. Exponential Stability	182
B.2.4. Locally Positive Definite Functions	183
B.2.5. Positive Definite Functions	183
B.2.6. Decrescent Functions	184
B.2.7. The Indirect Lyapunov	185
B.2.8. Lasalle's Invariance Principle	185
APPENDIX C.. Transformed Inertia Matrix - Relative Angles	186
C.1. Inertia matrix	186

LIST OF TABLES

3.1.	Physiological Parameters.	57
4.1.	Physiological Parameters.	71
5.1.	Values of Oscillators Parameters	78
5.2.	Physiological Parameters	97

LIST OF FIGURES

1.1.	Conceptual scheme of the motion control of a musculoskeletal system.	3
2.1.	Anatomical structure of the human lower limb.	24
2.2.	Gait cycle - Components.	25
2.3.	Neural Network.	32
2.4.	Classification of the Coupling of Oscillators.	34
2.5.	Bleex suit (Left) & Ekso suit (Right)	37
2.6.	ReWalk suit (Left), Mindwalker suit (Middle) & elegs suit (Right).	39
2.7.	Hip exoskeleton (Left), Knee exoskeleton (Middle) - EICOSI orthosis & MIT AAFO (Right).	43
3.1.	Shank-Foot Model.	50
3.2.	Block diagram of the human knee and ankle + orthosis.	52
3.3.	Structure of CPG coupling.	54
3.4.	Top-Left: Position trajectory of knee and ankle with adaptive oscillator synchronisation. Top-Right: Assistive and Human torque. Bottom: Bottom: Tracking error result of knee and ankle with adaptive oscillator synchronisation.	58

3.5.	Top-Left: Human (muscular) torque and assistive torque simulation of knee and ankle $\kappa = 0.5$. Top-Right: Human (muscular) torque and assistive torque simulation of knee and ankle $\kappa = 0$. Bottom-Left: Human and assistive torque simulation of knee and ankle $\kappa = 1$ with disturbance. Bottom-Right: Position trajectory of knee and ankle with adaptive oscillator synchronisation in the presence of disturbance.	59
4.1.	Exoskeleton "test-bed".	64
4.2.	Shank-Foot Desired Points.	67
4.3.	Top-Left: Angular position trajectory tracking based on Computed-Torque PID controller. Top-Right: Angular velocity trajectory tracking based on Computed-Torque PID controller. Bottom: Applied torque.	72
4.4.	Left: Angular position trajectory tracking based on Computed-Torque simple PD controller. Right: Applied Torque	73
5.1.	Nature of Coupling between the Oscillators	79
5.2.	Stick diagram of joint angles profile evolution. Left: Fast succession. Right: Phases captured in frames	80
5.3.	Hip and Knee trajectories generated via van der Pol oscillators and phase plots.	81
5.4.	Phase transition of the CPG walking gait - <i>SSP left leg, DSP & SSP right leg</i>	82
5.5.	Five-Link planar biped model. This is modelled to depict a single support phase.	85

5.6.	Block diagram of a closed loop control system (Computed-Torque Control).	95
5.7.	Hip and Knee angular position and velocity trajectory tracking for both legs.	98
5.8.	Control Torque τ_{q0} & τ_{q1}	99
5.9.	Control Torque τ_{q2} & τ_{q3}	99
5.10.	Control Torque τ_{q4}	100
6.1.	Block diagram of the Observer-Based Controller.	117
6.2.	Top-Left: Knee-Ankle position trajectory tracking. Top-Right: Knee-Ankle velocity trajectory tracking. Bottom-Left: Knee-Ankle torque input and estimated torque. Bottom-Right: Knee-Ankle saturation torque input. For $\tau_h = 0$	118
6.3.	Top-Left: Knee-Ankle position trajectory tracking. Top-Right: Knee-Ankle velocity trajectory tracking. Bottom-Left: Knee-Ankle torque input. Bottom-Right: Knee-Ankle human torque input (resistive torque). For $\tau_h \neq 0, \kappa = 0.1$	119
6.4.	Top-Left: Knee-Ankle position trajectory tracking. Top-Right: Knee-Ankle velocity trajectory tracking. Bottom-Left: Knee-Ankle torque input. Bottom-Right: Knee-Ankle human torque input (resistive torque). For $\tau_h \neq 0, \kappa = 0.2$	120
6.5.	Top-Left: Knee-Ankle position trajectory tracking. Top-Right: Knee-Ankle velocity trajectory tracking. Bottom-Left: Knee-Ankle torque input. Bottom-Right: Knee-Ankle human torque input (assistive torque). For $\tau_h \neq 0, \kappa = 0.1$	121

6.6.	Left: Physical joint angles. Right: Joint angle profile evolution for a single step (skick diagram).	124
6.7.	Top: Relative angular position tracking. Bottom: Driving torque output. q_0 & q_1	128
6.8.	Top: Relative angular position tracking. Bottom: Driving torque output. q_2, q_3 & q_4	128
6.9.	Error in degrees.	129
A.1.	Graph of x and \dot{x} as function of time and the trajectory in the phase plane (limit cycle).	162
A.2.	Structural view of the Matsuoka oscillator.	164
A.3.	Left: Graph of x and v as a function of time. Right: The trajectory in the phase plane (limit cycle).	164
A.4.	Graph of x and v as a function of time and the trajectory in the phase plane (limit cycle).	166
A.5.	Left: AFO frequency convergence to $F(t)$ with varied ω . Right: AFO frequency convergence to $F(t)$ with varied ϵ	168
A.6.	Structure of a pool of AFO used in the reproduction of a given multi-frequency signal.	171
A.7.	Top-Left: Coupled AFO frequency convergence to $P_{teach}(t)$. Bottom-Left: Amplitude α . Top-Right: Error Signal $F(t)$. Bottom-Right: Signal evolution of P_{teach} and $Q_{learned}$	172
A.8.	Inverted pendulum.	174
A.9.	Angular position tracking of the inverted pendulum.	176

GLOSSARY

AAFO	Active Ankle Foot Orthoses
AFO(s)	Adaptive Frequency Oscillator(s)
CAD	Computer Aided Design
CNS	Central Nervous System
CPG(s)	Central Pattern Generator(s)
DoF	Degree of Freedom
DSP	Double Support Phase
EEG	Electroencephlogram
EMG	Electromyogram
HMC	Human Motion Control
HMI	Human Machine Interface
IMU	Inertial Measurement Unit
MSF	Muscular Stiffness Force
PAFO	Powered Ankle Foot Orthosis
PD	Proportional Derivative
PID	Proportional Integral Derivative
PSAO	Particularly-Shaped Adaptive Oscillators
ROM	Range of Motion
SCI	Spinal Cord Injury(Injured)
SSP	Single Support Phase
STS	Sit-to-Stand
ZMP	Zero Point Moment

CHAPTER 1. Problem Settings

In this chapter, essential information necessary to justify the proposition in this research work as they concern wearable robot with human-in-the-loop is discussed. The need for the use of efficient mathematical models of systems, robust control methods, CPG-based models and controllers required for proper evaluation of biomechanical design consideration are elaborated.

1.1 Introduction

Disabilities in the lower limb of humans may be accident-related or pathology-related. In any of these cases the resultant effect could be linked to a nerve or muscular injury which may lead to improper motor functions and eventually paralyses. In a bid to provide solution to people with these disabilities, the need for rehabilitative and assistive devices to support mobility of such individual is paramount. Although, several supports have been provided by use of exoskeleton and orthotic devices, a largely readily available supportive device for assistive measure for persons with lower limb disability has been the wheelchair ([Acosta-Marquez and Bradley \(2005\)](#)). Nevertheless, paraplegic's desires to be back on their feet can only be achieved via exoskeleton.

Exoskeletons are known to be articulated mechanical systems which require actuators and sensors to perform its supportive duties. Since the number of actuators an animal

can power depends on the size of the animal, a considerable scaling of the actuator size to meet the force and stroke needs of the exoskeletal/orthotic devices must be a task to accomplish ([Herr \(2009\)](#)). This certainly will bring about enormous computational issues, based on the number of Degrees of freedoms (DoF) possess by the musculoskeletal systems of humans.

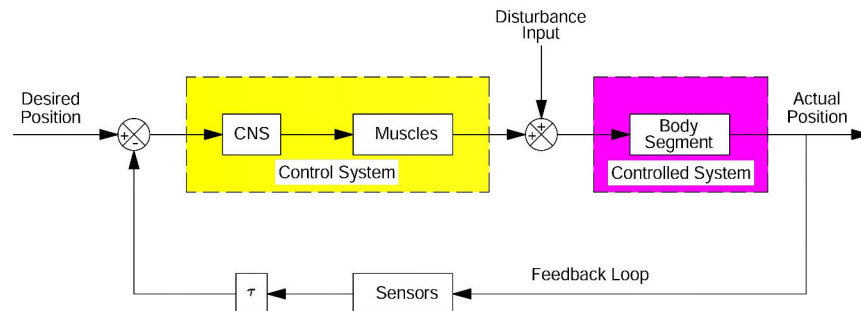
Machine aided bipedal walking presents a very difficult task because of its lack of support (for example; crutches). Hence, the control system is a critical factor if a successful design is to be accomplished. As stated in ([Kato \(1983\)](#)), factors which must be considered by the control system include; the synchronic nature of limbs control i.e. must occur at the same period or phase, the need for control of the positioning and acceleration of the limbs, control strategies employed should be able to incorporate adaptation to the environment and finally, the optimum control of energy requirements must be taken into consideration. These factors form the basis of a well-designed control law when adhered to appropriately; nevertheless, several control methods have not been able to fully incorporate these factors in a satisfactory manner.

Planning walking patterns for biped systems is centered around achieving stable walking in various environments, be it rough surfaces, up and down slopes or regions containing obstacles ([Huang, Yokoi, Kajita, Kaneko, Arai, Koyachi and Tanie \(2001\)](#)). Several methods have been proposed for gait synthesis in an attempt to solve a particular need which could be to ensure static stability ([Zheng and Shen \(1990\)](#)), or rather to ensure dynamic stability. A large number of researchers did concentrate more on dynamic walking stability and this has led to planning walking synthesis based on zero point moment (ZMP) ([Vukobratovic and Juricic \(1969\)](#)), omnidirectional biped walking ([Behnke \(2006\)](#)), CPG-generated walking patterns ([Zielińska \(1996\)](#)) and limit cycle walking ([Hobbelen \(2008\)](#)) among others. In addition to ensuring dynamic stability of the gait synthesis, there is a need for such gait to allow the use of small torque and velocity of

the actuators at each joint.

1.2 Background

Generally, in Human Motion Control (HMC) (either in performing a predefined task or a gait pattern), a proper knowledge of the mechanical and control behaviour of the musculoskeletal system is expedient. This necessitates the study of the neuromusculoskeletal system with focus on the role of joints, bones, muscles, sensors and the central and peripheral nervous system. The neuromusculoskeletal system can be modelled as a feedback or feedforward control system; however the former is addressed in this work due to the fact that it best suits the concept of motion control in humans. A feedback control system conceptual scheme could be seen to involve the linkage system (body segments), actuators (muscles), sensors (proprioceptive and tactile sensors, visual and vestibular system) and the controller (Central Nervous System, (CNS)) (see Fig. 1.1).



(van der Kooij, Koopman and van der Helm (2008))

Figure 1.1: Conceptual scheme of the motion control of a musculoskeletal system.

The desired position (signal from the brain) is compared with the actual position of the limb, and the CNS sends a neural signal to the muscles. The muscles then exert forces on the skeletal system which will start moving if it is not constrained by the environment. As seen in the Fig. 1.1, two inputs are considered. The desired position input which

is transferred to the actual position in order to track the behaviour of the system, and the disturbance input which is introduced with an intention to deviate the system from its intended position. These disturbance forces may be friction acting on the human body. τ represents the time-delays caused by transport and processing in the nervous system. This concept allows the modelling of the exoskeleton in conjunction with the movement pattern of humans. The desired position is defined as the desired trajectory while the actual position represents the limbs movement irrespective of the disturbance encountered.

Muscles are very integral parts in developing a human motion control system because they serve as the actuators needed to propel the said movement or actions carried out by humans. It is therefore a necessity that the biological idea behind the principle of muscle operation is applied when using actuators in exoskeleton, hence the term "bio-inspired" model. Certainly, the muscle structure is known to be very complex and highly nonlinear, but its dynamics may be modelled considering several assumptions and simplifications as needed. Based on the neuromusculoskeletal system, there are at least 20 or more DoF involved in human walking motion ([Chan \(2000\)](#)). These numerous DoF may become problematic when included in the mathematical model of the human gait pattern, which may eventually cause a drawback in fulfilling the engineering control tasks. It becomes paramount to reduce the number of DoF associated with the human movement; while restricting the muscle actuation to the behaviour of each joint required to participate in the actualisation of a certain control task.

The modelling and processing of information for the control of the human locomotion typically involves the application of finite state machines, linear control, neuronal networks, adaptive control and fuzzy control ([Pons, Moreno, Brunetti and Rocon \(2007\)](#)) and of course nonlinear control. Nevertheless, they could fall within the broad class of the feedback and feedforward control system. In a bid to closely incorporate the factors

needed to be considered by a control system as stated above, and also bearing in mind that the exoskeleton is been worn by humans, the neural network and the bounded non-linear feedback control system model was adopted. This neural network control system is typically oscillator-based and it is made to act as CPGs which automatically mimic the function of the CNS in human, which may also be used as a desired trajectory. In some cases it may be utilised as an estimator of observed data.

This work basically focus on applying adequate controls to joint actuators of a lower limb exoskeleton so as to execute defined trajectories of the human limbs for the purpose of rehabilitation and also to provide assistance via a feedback of an estimated torque by the exoskeletal device or human contribution.

1.3 Problem Statement

Over the years, several methods have been used to model the human lower limb exoskeleton for the purpose of providing a proper solution for the rehabilitation and assistance of individuals with lower limb disabilities. Some of these methods have failed to fulfill its purpose due to enormous assumptions within the mathematical modelling of the exoskeleton, the human gait model and the control method adopted, which may not typically agree with the functions of the neuromusculoskeletal system. A good number of these assumptions negate the ability to design a reliable rehabilitative and assistive protocol for humans with lower limb disorders. Although a level of success have been achieved by some research groups ([Ferris, Sawicki and Domingo \(2005\)](#); [Hassani, Mohammed and Amirat \(2013\)](#)), a need to further investigate the complexity associated with human movement and walking for the purpose of proposing a practicable rehabilitative and assistive technique for lower limb extremity is required, without undermining the safety of the wearer.

Control and model designs which have CPGs as their bedrock have proven to be very effective in the control of lower limb exoskeleton, nevertheless, these designs rarely include the mathematical dynamics of the exoskeleton but rather make use of virtual software or rather the CPG dynamics itself (de Pina Filho, Dutra and Raptopoulos, 2005; Veskos and Demiris, 2006; de Pina Filho, Santos and Dutra, 2006; Mondal, Nandy, Verma, Shukla, Saxena, Chakraborty and Nandi, 2011) to stimulate the exoskeleton actuators with an objective of accomplishing the task required. Some others which are not CPG-based model may utilise certain kinematic modelling packages to achieve the purpose of their design such as in (Yali and Xingsong, 2008; Zhao and Xu, 2008; Ferrati, Bortolotto and Pagello, 2013). Designing an effective CPG-based controller relies majorly on understanding the functionalities of the targeted physical system under control (Habib, Liu, Watanabe and Izumi (2007)).

Since CPGs may be modelled by sets of different type of oscillators and used as inputs to control certain physical systems; this type of control designs often excludes the kinematics and dynamics of the system under consideration. Hence, do not give proper insight on how these tasks are achieved and also seldom provide a good perception on which approach could be best used for the task in question.

This thesis, therefore aim at designing practically effective models that will assist patients having lower limb disorders with a motive to helping them regain their motor functions. CPG-based models specifically for rehabilitative and assistive purposes were addressed. These CPG-based models are either used for the generation of the physical system trajectories or together with classical control techniques. The validation of these models will be investigated in conjunction with the nonlinear dynamic equation of motion of the envisaged exoskeleton. In addition to this, a bounded control torque and a feedback linearisation technique will be developed for rehabilitative and assistive purposes also. Lyapunov-based stability proof that guarantees asymptotic stability of

the lower limb exoskeleton will be performed. Hence, this will automatically serve as a blue print towards practical implementations of exoskeletons' design motive.

1.3.1 Sub-Problem 1

Nonlinear oscillators have received increased interest in the field of engineering, biology and physical science. It has been considered a very significant tool for modelling in these fields and hence it is becoming widely used in the modelling and control of wearable robots. This interest is based on their synchronisation capabilities with other oscillators or with external driving signals ([Righetti, Buchli and Ijspeert \(2009\)](#)). These oscillators which are represented by nonlinear dynamical equations have as an attribute a phenomenon known as "limit cycle behaviour". This allows them to be used as CPGs. Nevertheless, designing a CPG model requires the definition of certain "points" closely interconnected with each other. This includes; the general architecture of the CPG, the type and topology of coupling, the waveforms, the effect of the input signals and the effect of the feedback signal ([Ijspeert \(2008\)](#)). It should then be noted that since there are no specific methodology for designing CPGs for the control of a particular task, it is therefore important to specify how CPGs interconnect with the physical system required to be controlled (i.e the human lower limb exoskeleton). The mathematical theory and background of three major oscillators used in the field of robotics will be analysed with specifics on the "points" given above. These oscillators are the Hopf oscillator (adaptive), Matsuoka oscillator and Van der Pol oscillator.

1.3.2 Sub-Problem 2

Oscillators are said to be coupled if they allow themselves to interact in some way. It may then be stated that coupled oscillators refer to a number of oscillators connected by means of a spring or a stretchy cord with certain coordination between them. Springs are

likened to be the coupling terms between them and as such provide a medium by which the oscillators interact with each other. In general, coupling may be classified into two broad categories, namely; direct coupling and global coupling. The nature of coupling and the number of oscillator required to be coupled is a reflection of the system required to be modelled. The idea behind this development is based on the fact that most systems are connected together in a certain manner so as to achieve the purpose they are made for. Coupled nonlinear oscillators may be used in control systems of locomotion as CPGs to generate desired trajectories or in a way track the given trajectory of wearable robots. Wearable robots are basically anthropometric in nature and therefore modelled in accordance to the anatomical behaviour of the human lower limb. The human lower limbs are considered to be made up of links termed "rigid segments" (thigh and shank) and mechanically connected via joints (hip, knee and ankle). These joints enable movements and thus determine the DoF these limbs possess. However, lower numbers of DoF are being assumed for the purpose of simplification (Pons *et al.* (2008)) so as to reduce its complexity.

Research based on coupled oscillators have always been done using virtual simulation software without mathematically using the dynamic equation of motion of the system to be controlled such as in (Buchli and Ijspeert (2004)) among others. Although they tend to reduce the computational issues associated with the multiple DoF of relevant physical systems, it does not give a clear insight on how the system interacts with the CPG to physically yield the motion dynamics.

With regard to the above, the coupled adaptive Hopf oscillator will be used in the control of the knee-ankle orthosis to demonstrate its coupling effect. In addition, the shank-foot trajectory control using Matsuoka oscillators and computed torque control will also be used to exploit this effect.

1.3.3 Sub-Problem 3

The objective of rehabilitation is to perform specific movements that exercise and hence improve motor unit plasticity of the patient thereby influencing motor recovery and minimising functional deficits (Díaz, Gil and Sánchez (2011)). Rehabilitation therefore could be implemented manually or robotically (i.e. by the use of a robotic tool). Rehabilitation robotics is a branch of robotics which provides a platform for the design of robots in the form of orthosis/exoskeleton for the purpose of providing physiotherapy to persons with physical disability. Conventional manual rehabilitation is associated with excessive time, energy and resources (physiotherapist) hence disadvantageous compared to robotic-based rehabilitation (Kordasz, Kuczkowski and Sauer (2011)). Research on the efficiency of robotic therapy has shown that rehabilitation technologies provide new alternatives for repetitive training sessions that can increase efforts to improve the therapy performance. This is also intended to reduce the burden on physiotherapists and assess quantitatively the level of motor recovery by measuring force and movement patterns ((Díaz, Gil and Sánchez, 2011; Dollar and Herr, 2008)).

Robotic therapy may be performed on *traditional robotic platforms or robot-assisted platforms* (Ronsse, Vitiello, Lenzi, Van Den Kieboom, Carrozza and Ijspeert (2010)). The former is basically used to drive the patient's limb along a pre-specified trajectory using stiff position control as in Colombo, Wirz, Dietz *et al.* (2001), thereby making the patient passive during the whole training sessions. Although this proved to be a drawback, (Kordasz, Kuczkowski and Sauer (2011)) addressed the possibility for traditional robotic platforms to work in passive and active mode, depending on the recovery stage of the patients.

The "assistance-as-needed" approach known as the robot-assisted platform helps provide assistance for movement to subjects when they are incapable of completing the movement task (Wolbrecht, Chan, Reinkensmeyer and Bobrow (2008)). This allows

patients to be active during the entire physiotherapy session and assisted only when required, thereby improving the patients muscle activity (Israel, Campbell, Kahn and Hornby (2006)). In (Ronsse, Vitiello, Lenzi, Van Den Kieboom, Carrozza and Ijspeert (2010)), a novel assistance method was proposed for rhythmic movement of the forearm about the elbow using a single adaptive oscillator. The features associated with this method commensurate with that of Electromyogram (EMG)-based assistive device (Sankai (2006)), since its level of assistance is same at steady-state for the subject and virtually no pre-specified trajectory is needed.

To investigate the rehabilitative and assistive protocol using CPGs to perform rhythmic movements of the lower limb about the knee and ankle, the coupled adaptive Hopf oscillator will be used, based on an inverse dynamic approach. A comparison of the torque using Matsuoka oscillators and traditional robotic platforms for rehabilitation will also be examined, employing a forward dynamics approach (using Lagrange's principle for its dynamic equation of motion) while exploiting its natural dynamics¹.

1.3.4 Sub-Problem 4

The use of traditional robotic platform for the control of lower limb exoskeletons/orthoses has been in existence over a century. Existing works on this topic are either related to single DoF or multiple DoF (Ajayi, Djouani and Hamam (2014)). In either of the cases, the purpose of the exoskeleton control is to help the wearer to restore a level its motor function either partially or completely. A lot of these existing works concentrate more on using classical PD or PID control methods (Walsh, Pasch and Herr, 2006a; Tsukahara, Kawanishi, Hasegawa and Sankai, 2010; Kong and Tomizuka, 2009). These controllers

¹Ability for movement to occur around the joints naturally hence, does not require complicated method of control

are known to be weak against model uncertainties² and disturbance³ (Mefoued, Mohammed and Amirat (2011)). These effects could result in increased power required by the exoskeleton and consequently a high torque, which may be dangerous to the wearer. Furthermore, the use of control methods which are intuitive such as hybrid fuzzy (Zhang, Yang, Chen, Zhang and Dong (2008)) and neuro-fuzzy approaches (Kiguchi, Tanaka and Fukuda (2004)) may not ensure the stability of the physical system since there is no prove to guarantee such.

The need for a bounded control⁴ is therefore expedient. This is to somewhat guarantee the safety of the wearer. Although, in (Rifai, Hassani, Mohammed and Amirat (2011)), the EICOSI⁵ (Exoskeleton Intelligently COmmunicating and Sensitive to Intention) orthosis, was controlled via a bounded control torque based on nested saturations with gravity compensation, it was only applied at the knee joint level.

Based on the above, the generalisation of this control law and its application to the hip and knee joint of both legs while walking will be proposed. This is purposed to prevent problems related to nonlinearities as mentioned above. Stability proof will be presented.

1.3.5 Sub-Problem 5

One of the interesting features of wearable robots is the fact that it enables healthy wearers to perform stressful activities easily over a lengthy period of time. This sole attribute has made its use in the domain of rehabilitation and assistance quite appreciated, with an extension to the medical, military and agricultural field. Wearable robots are electro-mechanical devices driven by on-board actuators in order to induce the movement of the embodied limbs. However, by inducing this movement, there remains a

²Uncertainties such as inertial and frictional effects, elastic coefficients of the leg may vary among users.

³Disturbance which may occur as a result of the user wrong movement.

⁴Bounded control literally refers to the control of a system within certain bounded variables.

⁵An orthotic device used for the rehabilitation of subjects with knee joint disabilities.

possibility that there may be a contribution of these limbs through the activities of the muscles, hence delivering a part of the torque during rehabilitation or rather determining the user intention to develop a specific movement.

In the near future, it is envisaged that the number of elderly people in world population will increase considerably, therefore this will further increase the burden of treating the health risks associated with aging by physiotherapists ([Dellon and Matsuoka \(2007\)](#)). Robotic therapy solutions which give rise to the use of intelligent machines capable of offering solutions that promote motor recovery and better understanding of motor control, ([Dollar and Herr, 2008](#); [Hesse, Schmidt, Werner and Bardeleben, 2003](#)) remains the only efficient way to alleviate physiotherapists from this time and energy consuming exercise. Robotic solutions could either be assistive, rehabilitative or both depending on the purpose of the design.

In rehabilitative robotics, the solutions developed are aimed at optimising existing therapeutic approaches in order to improve or cure motor lost functions after a disabling encounter, while, assistive robotics provides solutions that will assist and interact with individuals with reduced motor functionalities so as to help them increase their self-reliance and sustaining a fulfilling lifestyle within their personal environment ([Guglielmelli, Johnson and Shibata \(2009\)](#)). However, there exists a technical similarity between them, in that the primary subject of interest is centered on the motor performance of the patient.

In utilising robotic systems for assistance and rehabilitation the wearer could be passive or active throughout the whole session of training. When passive, the wearer voluntary movement tends to be limited since the lower-limb rehabilitation device is only designed to assist the user to follow pre-defined movement patterns with the aid of certain control methods. Although this method have been proven to be an effective therapeutic measure ([Westlake and Patten](#); [Colombo, Jorg and Dietz, 2000](#); [Mefoued, Mohammed and Amirat, 2011](#); [Pohl, Werner, Holzgraefe, KroczeK, Wingendorf, Hoölig, Koch and](#)

Hesse, 2007), the need for patients to be actively involved in robotic therapy brings about more success in the results obtained (Hogan, Krebs, Rohrer, Palazzolo, Dipietro, Fasoli, Stein, Hughes, Frontera, Lynch *et al.* (2006)). One rehabilitative method which further validate this proof is the "assist-as-needed" paradigm (Cai, Fong, Otoshi, Liang, Burdick, Roy and Edgerton, 2006; Edgerton and Roy, 2009; Banala, Kim, Agrawal and Scholz, 2009; Vallery, van Asseldonk, Buss and van der Kooij, 2009).

Most often the contribution of the wearers may be determined using on-board sensors like EMG, Electroencephalogram (EEG), Inertial Measurement Unit (IMU), camera, etc and adequate algorithms to detect and classify the intention. Electromyography (EMG) control strategy is one that promote the user specific support for controllers by converting EMG signals to desired human torques which is then partly applied by the exoskeleton device ((Kiguchi, Iwami, Yasuda, Watanabe and Fukuda, 2003; Sawicki and Ferris, 2009). However, this method is somewhat sensitive to noise and sensor location (Lintzen (2011)).

With regard to the above, a high gain observer will be used to determine the extent of a wearer contribution for a specific exoskeleton control via a bounded nonlinear feedback controller applied to the knee and ankle joint level. Lyapunov stability theory will be used to find the condition for which the error between the states of the human-exoskeleton and the state of the high gain observer converge to zero.

1.3.6 Sub-Problem 6

The most complex movements of the human body is walking. This movement involves both legs and is often characterised as human gaits. Gaits may be referred to as periodic activities driven by muscles to activate the joints involved, which are stimulated by electrical signals transferred by neurons from the brain (Uyar, Baser, Baci and Özçivici (2009)). Planning walking patterns can sometimes be very rigorous with lots of opti-

misation required due to numerous constraints involved. One of the earliest method employed, involve the utilisation of model based mathematical studies where real measurements of the hip and knee joint angles of different healthy person are recorded under various conditions during bipedal walking to make certain conclusions relative to the characteristics of normal walking. Unfortunately, in synthesising a gait cycle for a particular biped physical system, researchers are faced with the task to develop joint profiles based on tangible gait characteristics which include; the walking speed, step length and step elevation (Mu and Wu (2003b)). This may seem unachievable using recorded human walking data in prescribing lower limb motion.

Currently, most humanoid robots uses the more advanced ZMP⁶ paradigm (Vukobratovic, Borovac, Surla and Stokic (1990)). However, there are certain drawbacks which may well question its absolute validity. These drawbacks include; firstly, the fact that the ZMP trajectory is first designed before the joint profile, not all desired ZMP can be achieved due to the limited range of motion of the hip. Secondly, utilising the ZMP method for the single support phase (SSP) may well be impossible unless the supporting foot is modelled as a separate link. As a way of resolving the issues posed by the ZMP, (Huang, Yokoi, Kajita, Kaneko, Arai, Koyachi and Tanie (2001)) developed a repeatable walking pattern plan for biped robots, but not without complicated constraint functions. Another researcher which could well be guilty of this is (Mu and Wu (2003b)), although, there was a significant reduction of the constraint function used in the joint trajectory planning.

Since biped robots are known to be easily tipped over, the concept of stability has to be taken seriously. Stability in bipedal walking may be divided into two class; the "generic one"⁷ and the "overly restrictive one" Hobbelen (2008). Achieving an optimal

⁶The ZMP is defined as the point on the ground about which the sum of the moments of all the active forces equal zero.

⁷The union of all viable states from which a biped walker is able to avoid a fall.

performance using the notion of the former may be quite expensive numerically and experimentally owing to the complex dynamics involved in walking. The latter, which could be referred to as sustained local stability⁸ requires local stabilisation and high stiffness control. This growing need for improved performance for biped walking robots has led to the development of the "limit cycle walking"⁹ paradigm. CPG-based model design of human gaits can somewhat be classified as limit cycle walking based on its limit cycle behaviour.

CPG-based walking pattern generation techniques developed by some researchers include those documented in (Liu, Habib, Watanabe and Izumi, 2008; Bay and Hemami, 1987; de Pina Filho, Dutra and Raptopoulos, 2005; Heralić, Wolff and Wahde, 2007; Mondal, Nandy, Verma, Shukla, Saxena, Chakraborty and Nandi, 2011; Inada and Ishii, 2004). With regard to this, the idea considered in (Bay and Hemami, 1987; Zielińska, 1996), will be used for the rhythmic trajectory design and control of a five-link biped exoskeleton ideated to be used for rehabilitative purposes. This will be achieved via a computed torque control to ensure a proper trajectory following of the rhythmic trajectory. The dynamic equation of the five-link biped exoskeleton will be derived based on the single support phase (SSP).

1.3.7 Sub-Problem 7

Although CPG-based techniques provides a unique and efficient way of acheving human gait, selecting initial conditions to identify double support phase (DSP) and the duration of the SSP may well be difficult to identify. To remedy this situation, the use of numerical methods such as time polynomial functions may be used to approximate the joint angles and therefore determine the sequence for the completion of one step having identified

⁸Gait is synthesised as a desired trajectory through state space which is continuously enforced by utilising suitable trajectory control strategy.

⁹This refers to nominally periodic sequence of steps that is stable as a whole but not locally stable at every instant in time.

when both feet are on the ground. This method eliminates the rigorous computational activities used to determine joint angles over a period of time. Using this ideology, an approximate joint trajectory for one (1) step could be achieved via coupled Van der Pol oscillators. This will then be applied as the desired joint trajectory of a five-link biped exoskeleton and continuously tracked with the aid of a bounded nonlinear feedback control. The repeatability of this gait may be validated by switching both legs at the end of the swing phase. The dynamic equation of motion of the SSP will be derived by means of Lagrange's principle and made to track this movement for the purpose of rehabilitation.

1.4 Hypotheses of the Study

This thesis primarily contributes to the area of rehabilitative and assistive robotics. Specifically, it introduces bio-inspired model by means of CPG modelling techniques used in the field of biomechatronics engineering. The primary objective of this thesis is to test the hypothesis that:

- (1.) the efficiency of robotic therapy in relation to rehabilitation technologies provide new alternatives for repetitive training sessions that may increase efforts to improve the therapy performance.
- (2.) robotic therapy reduces the burden on physiotherapists and assesses quantitatively the level of motor functions recovery.
- (3.) bio-inspired model offers properties such as system-environment interactions, self-stabilisation, energy efficiency by providing simplified control method.
- (4.) robot-assisted platform enables patients with lower-limb disorders to be passive or active during training sessions.

- (5.) observer-based feedback control methods may be used to verify the extent of human contribution during rehabilitation exercise.
- (6.) time polynomial functions could be a solution to effectively selecting proper initial conditions to generate repeatable gait.

It should be noted that, in a bid to prove the validity of this hypotheses, this thesis does so theoretically via computer simulations with an envisaged practical implementation.

1.5 Contribution of the Study

The eight (8) major contributions of this study are that:

- (a.) nonlinear oscillators could be used to design specific CPG-based models depending on the functions they are meant to perform. It does establish the fact that the type of oscillator used may differ based on the conceptual control approach.
- (b.) the coupling of nonlinear oscillator is done with a prior knowledge of the movement pattern envisaged. This coupling helps initiate the CPG interaction with the exoskeleton model and is achieved via the joints of the actuated lower limb exoskeleton.
- (c.) the integration of the CPG and the dynamic equations of exoskeleton could be largely affected by the value of the control parameters of CPG. This could be verified when the CPG output is applied to the exoskeleton at the joint level.
- (d.) designing rehabilitative and assistive protocols using CPGs are effective and gives satisfactory results even in the presence of environmental uncertainty.
- (e.) the safety of exoskeleton wearers could be enhanced by using bounded nonlinear feedback control based on nested saturation.

- (f.) rehabilitative walking could be achieved via CPG-based trajectory design.
- (g.) the implementation of conceptual rehabilitative walking procedures for humans using CPG-designed gait model could also be achieved by approximating the derived joint angles using numerical methods. This may be possibly more efficiency and computationally less complex.
- (h.) the extent of the wearer contribution can be determined by an observer-based feedback control.

These contributions are detailed in the articles highlighted below and within successive chapters:

- M. O. Ajayi, K. Djouani, and Y. Hamam, "Theory of adaptive oscillators: Mathematical principles and background," in AFRICON, 2013, 2013, pp. 1-6 (*Published*).
- M. O. Ajayi, K. Djouani, and Y. Hamam, "Analysis of Knee-Ankle Orthosis Modelling: An Inverse Dynamics Approach Using Adaptive Coupled Oscillator," in Simulation, Modeling, and Programming for Autonomous Robots. vol. 8810, D. Brugali, J. Broenink, T. Kroeger, and B. MacDonald, Eds., ed: Springer International Publishing, 2014, pp. 122-133 (*Published*).
- M. O. Ajayi, K. Djouani, and Y. Hamam, "Shank-foot trajectory control: A forward dynamics approach using computed-torque control." In 2014 IEEE-RAS International Conference on Humanoid Robots, pp. 652-657. IEEE, 2014. (*Published*).
- M. O. Ajayi, K. Djouani, and Y. Hamam, Inverted pendulum Control using Adaptive Oscillators (*Presented - TUT Research Day 2013*).

- M. O. Ajayi, K. Djouani, and Y. Hamam, Observer-based Bounded Control of an Actuated Lower Limb Exoskeleton, International Journal of Control and Automation Systems (IJCAS). (*Under review*).
- M. O. Ajayi, K. Djouani, and Y. Hamam, Rhythmic Trajectory Design and Control for Rehabilitative Walking in Patients with Lower Limb Disorder. International Journal of Humanoid Robotics. 2016 Apr 4:1650006. (*Published*).
- M. O. Ajayi, K. Djouani, and Y. Hamam, "Bounded control of a full-exoskeleton device with four (4) Degree of Freedom," In 2015 IEEE International Conference on Robotics and Biomimetics (ROBIO), pp. 2425-2430. IEEE, 2015. (*Published*).

1.6 Outline of Thesis

This thesis is structured into seven (7) chapters and its content mostly comprises of already published and unpublished articles and journals. It is organised in a ladder-like manner from the basic concept and formulation of CPGs through to the coupling structure and the eventual implementation on the human lower limb exoskeleton for rehabilitation and assistive purposes. Analysis of control strategies such as observer-based feedback control with nested saturation is also included. Proofs and propositions that guarantee the stability of the exoskeleton are highlighted.

In **Chapter 2**, the human lower limb modelling concept, CPG modelling techniques and applications in general, assistive and rehabilitative devices in relation to human lower limb movement, human gait modelling strategy and control strategies are detailed.

In **Chapter 3**, the application of CPG models in conjunction with classical control methods for rehabilitative and assistive measures are presented. The analysis is based on the knee and ankle joints of the patient in a seated position. Simulation and results

are analysed at the end of the chapter. A disturbance effect which exemplifies a state of inactivity of the human was also introduced.

In **Chapter 4**, nonlinear feedback control methods envisaged for the use of human lower limb rehabilitation are presented. CPGs were used to generate the trajectory of the exoskeleton internally. This analysis is based on the knee and ankle joints of the patient in a seated position also. Simulation results are demonstrated at the end of the chapter while also considering certain environmental disturbance effect.

In **Chapter 5**, the efficacy of rehabilitative walking in patients with lower limb disorder is investigated using the dynamics of a five-link biped exoskeleton. The trajectory design is based on coupled van der pol oscillators. Simulation results were obtained and analysed accordingly. This was also carried out in the presence of disturbance.

In **Chapter 6**, observer-based bounded feedback control of a lower limb exoskeleton at knee and ankle joint level is detailed. Analysis of the resultant simulated plots for rehabilitation with/without human contribution is presented. Stability proofs are derived. Environmental uncertainties are also considered. Furthermore, the modelling of the dynamic equation of motion of the SSP of a full exoskeleton device using Lagrangian principles and the approximation of joint angles using time polynomial functions is derived. The objective of this is to demonstrate the rehabilitative walking ideology using CPG-based human gait model as the joint angle trajectories. Results are presented to validate this design in the presence of disturbance.

Chapter 7 finally summarises the thesis, propose further works and provides meaningful recommendation.

CHAPTER 2. Literature Review

2.1 Introduction

In this chapter, modelling concepts associated to human lower limbs, human gait modelling strategies, CPGs modelling techniques, applications, and control methods are reviewed. Furthermore, assistive and rehabilitative strategies in relation to human lower limb movement are detailed accordingly.

2.2 Human Lower Limb Modelling

Models refer to the representation of reality, emphasising its most significant features. This makes it easy to comprehend the complex reality and further makes it controllable and analysable. Models could be based on mathematical models or empirical models which forms a replica of physical models. Empirical modelling refers to any type of computer modelling based on experimental data or observations collected in the real world, such as motion recordings of humans. In this context, the empirical model could then be achieved by inputting these data into modelling software such as Visual Nastran kinematic modelling package ([Acosta-Marquez and Bradley \(2005\)](#)) or ADAMS kinematic modelling package ([Zhao and Xu \(2008\)](#)). Mathematical models are simplified representations of real world entity and can be in equations or computer code. They depend solely on the kinematics and dynamics characteristics of the mechanism which

is described mathematically and used in the physical analogy of the system. This principle is considered in this thesis. Since models are formulated based on mathematical principles with a prior knowledge of the targeted physical system, the anatomical study of the human lower limb is expedient.

2.2.1 Human Lower Limb Anatomical structure

The human lower limb also known as the human lower extremity consists of the foot, leg, thigh and the gluteal region (see Fig. 2.1). This gives an idea of the joints typically considered in the lower extremity, and these include; the hip, knee and ankle joints. The main functions of the lower limb is to "support the body weight"¹ and assist in "human locomotion"². Carrying out these functions effectively requires the rigid segments of the limb referred to as the bones which are the hip bones (pelvis), thigh bone (femur) and the leg bone (tibia and fibula). Joints are the location at which bones connect. They are designed to allow movement and provide mechanical support, and are classified structurally and functionally. Structural classification is determined by the connection of bones between each other, while functional classification is determined by the degree of movement between the articulating bones. The hip joint may be characterised as a ball and socket type of joint with movements such as flexion, extension, abduction, adduction and circumduction. In a similar manner, knee and ankle joint relates to the hinge joint type with respective movements such as flexion/extension and plantarflexion/dorsiflexion. These movements are made possible through the articulation of the joints via the muscles. Muscles may then be defined as a band or bundle of fibrous tissue in a human body that has the ability to contract, producing movement in or maintaining the position of parts of the body. Based on this understanding, researchers have over the years

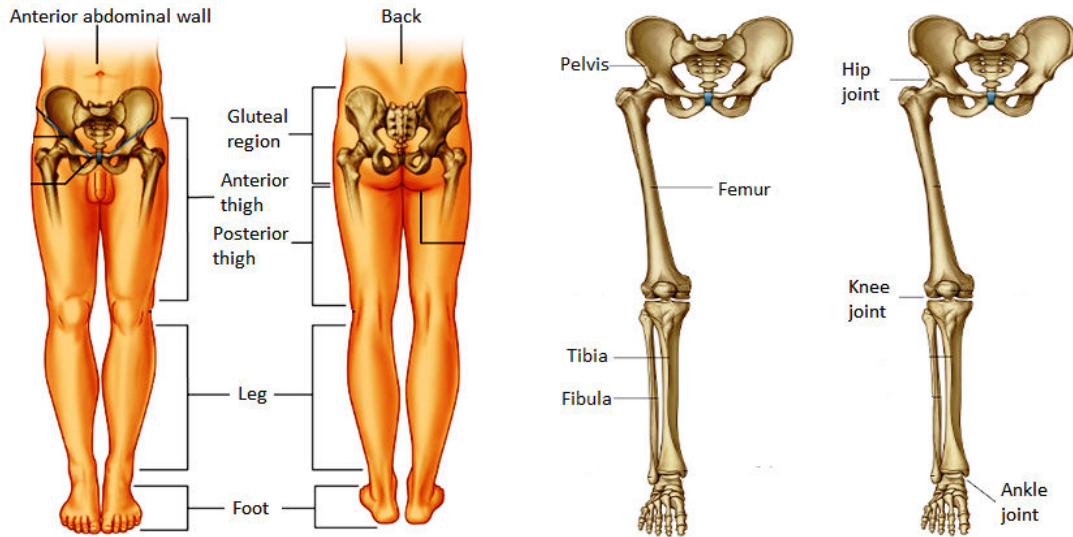
¹The ligaments at the hip and knee joints facilitate locking of these joints therefore reducing the amount of muscular energy required to maintain a standing position.

²To move the body through space. This involves integration of movements at all joints of the lower limb to place the foot on the ground and move the body over it.

mathematically developed musculoskeletal models of the human lower extremity. The dynamic behaviour of musculoskeletal system are mostly modelled by Newton's equation of motion or Lagrange's principles. The latter is preferred in this work because it eliminates the consideration of constraint forces, and rather focus on use of "generalised coordinates" like angle.

The main objective of modelling musculoskeletal system is to study how specific actuators contribute to movement coordination in healthy individuals and also to suggest rehabilitation strategies for lost motor functions in disabled patients, such as in the design of functional neuromuscular stimulation systems for persons with paralysed muscles (Khang and Zajac (1989)). This makes movement or motor coordination a focus research area. Works which clearly documented this motive can be found in (Hoy, Zajac and Gordon (1990)) and (Chittajallu and Kohrt (1996)). Hoy developed a musculoskeletal model of the human lower extremity for studies related to computer simulation of musculotendon function and muscle coordination during movement, while Chittajallu developed a planar knee model, FORM2D, which employs a novel force minimisation approach. This was proposed to serve as a tool for the study of ligament repair, providing information on ligament strain and knee mechanics during passive flexion. Motor coordination is the combination of body movements created with the kinematic (such as spatial direction) and kinetic (force) parameters that result in intended actions. These intended actions maybe walking, running, throwing or picking up an object, etc. Whatever the actions, it does involve the flexing or extension of one or more joints. Models needed to mathematically study and mimic these actions are therefore paramount. Periodic or quasi-periodic signals may be easily used to represent the motion of a particular joint but the most complicated movement in human is walking. Modelling a person's manner of walking (also known as human gait) provides a platform for which to correct individuals with gait disabilities. Human gait research have a wide range of applications

in medicine, ergonomics, sport science and technology (Wojtyra (2000)).



(Drake, Vogl and Mitchell (2014))

Figure 2.1: Anatomical structure of the human lower limb.

2.3 Human Gait Modelling

Human gait cycle may be regarded as a complete step or walking cycle. This cycle extends from heel strike to heel strike of one leg and includes the stance and swing phases of both legs. It can be divided into the 'single support phase'³ and the 'double support phase'⁴. Basically, it can be said that movements in gait cycle, spans from the time when the foot is on the ground (the stance phase which takes up 62% of the complete gait cycle) through when the foot is off the ground (the swing phase which takes up the remaining 38% of one complete gait cycle) (see Fig. 2.2).

History has it that research into the mechanics of body movement may be dated to about 3 centuries ago (Paul (2005)). Most of these researchers back then based their work on

³This is characterised by one limb moving forward while the other is in contact with the floor.

⁴This represent the instant when both limbs are in contact with the floor.

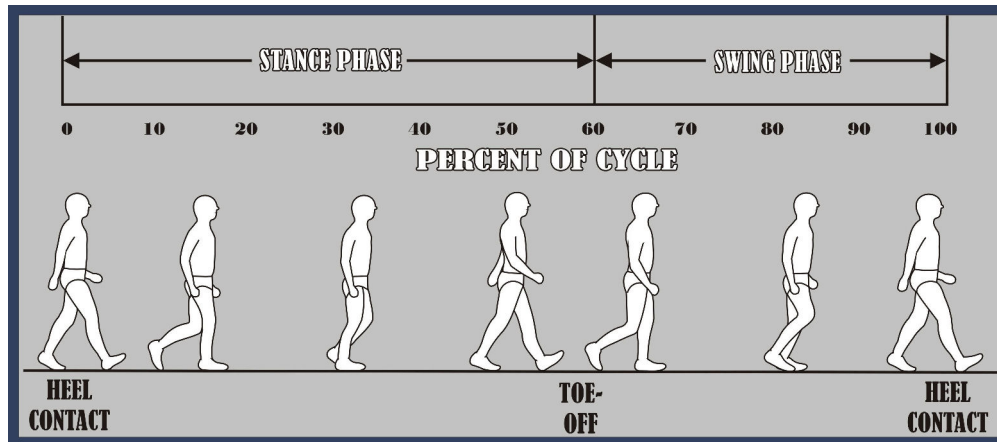


Figure 2.2: Gait cycle - Components.

the knowledge of anatomy and observations on the way in which human body carry out their daily activities. Their research was limited due to lack of equipment to measure the pattern of movement or forces developed during the process of human movement. It was not until 1836 that a telescope with calibrated graticule was used to measure the movement of specific anatomical points on human during walking ([Weber and Weber \(1836\)](#)). The development of a pneumatic system of measurement for the interpretation of temporal factors of gait ([Marey \(1873\)](#)) improved the analysis of the locomotion of human by using a stick diagram for this illustration. Series of pictures of the frontal and sagittal plane movements of test subjects achieved via the aid of cameras set up together was published in ([Muybridge \(1882\)](#)). This also set up the tone for researchers such as ([Braune and Fischer \(1895\)](#)) to investigate and provide information on the best method of load carriage by German soldiers with the aid of four (4) single plate cameras to view test subjects in a dark room. This research was sponsored by the German government. Further advancement in this research field received a boost when ([Eberhart, Inman, Saunders, Levens, Bresler and McCowan \(1947\)](#)) attempted a three dimensional movement analysis with a 35mm cine cameras operated simultaneously and also incorporated glass walkways having a mirror underneath to allow a further camera measure the areas of foot to ground contact. This article, produced at the Berkley campus of the Uni-

versity of California was centred on studies of normal locomotion with an intention of improving locomotion, prostheses and treatment of amputees. This was then followed by a publication (Inman, Eberhart *et al.* (1953)) from the same university which was included as a classic paper in orthopaedics (Charalambous (2014)) that describes the six major determinants of normal or pathological gaits. Later on, an improved body movement analysis tool in the form of EMG was then used in the analysis of human gaits as recorded in (Close and Todd (1959)) and (Basmajian (1962)).

The advent of devices capable of performing computation analysis provided a platform for which human locomotion could be prescribed using human kinematic data Zarrugh and Radcliffe (1979) studies on human walking pattern was based on this principle. It involves the description of a computer program used in the generation of absolute human walking data from predetermined relative motions. This was also investigated in (Vukobratovic, Borovac, Surla and Stokic (1990)). Synthesising joint profiles based on this principle are not well outlined due to the lack of freedom involved in selecting 'gait characteristics'⁵.

Designing functional recovery wearable systems with an objective to correct gait disabilities in subjects requires an effective normal human gait model since they are worn by humans. It is desired that biped exoskeleton used for this purpose imitate human locomotion. Bipedal robots may be used as a test bed to evaluate the accuracy of the assumed model. Several techniques have been used to develop joint profiles, but the question which arises is that, do they provide clearly defined methods for replicating human locomotion. Several techniques are available in the literature. Although they may have certain shortcomings, they have in one way or another contributed towards closely designing human-like walking patterns.

Tzafestas, Raibert and Tzafestas (1996) and Furusho and Masubuchi (1986) largely

⁵This relates to walking speed, step length and step elevation.

base their work on assumptions that does not provide a systematical way for synthesising joint profiles. [Hurmuzlu \(1993\)](#) developed a general approach based on discrete mapping techniques which overcomes difficulties encountered by others on the treatment of discontinuities and nonlinearities associated with bipedal gait. This model effectively addresses the specification of constraints function in the design of biped robot. However, the selection of specific initial conditions to identify the beginning and end of each step was not addressed. This problem was rectified by using numerical methods such as Fourier series expansion, ([Cabodevila and Abba \(1997\)](#)), time polynomial functions ([Red \(2000\)](#)), or periodic spline interpolation ([Shih \(1997\)](#)). A drawback polynomials might have may be the inducing of features which are not desired into joint profiles.

A key characteristic which a gait should have is stability. ZMP approach allows this feature to be guaranteed. Nevertheless, designing the desired ZMP trajectory before designing the hip motion presents a certain difficulty associated with limited hip motion and high hip acceleration. This difficulty was duly remedied in ([Huang, Yokoi, Kajita, Kaneko, Arai, Koyachi and Tanie, 2001](#); [Mu and Wu, 2003b](#)) but, may be guilty of complex constraint equation. Other walking pattern generation techniques include CPGs ([Liu, Habib, Watanabe and Izumi, 2008](#); [Bay and Hemami, 1987](#); [de Pina Filho, Dutra and Raptopoulos, 2005](#); [Heralić, Wolff and Wahde, 2007](#); [Mondal, Nandy, Verma, Shukla, Saxena, Chakraborty and Nandi, 2011](#); [Inada and Ishii, 2004](#)) and limit cycle walking [Hobbelen \(2008\)](#). These techniques could be used to generate stable periodic sequence of biped steps. However, identifying the joint angles at which the system is at a single support phase or double support phase may prove problematic. This will also have an effect on choosing appropriate initial conditions. In this work, the authors will also tend to address the possibility of extracting joint angle data from CPG-generated human-like walking pattern and then using polynomial functions, evaluate these data to represent a single support phase.

2.4 Central Pattern Generators (CPGs)

Central pattern generators (CPGs) are coordinated neural networks which are present in the spinal cords of living organisms. They act as signals responsible for motor neuron firing (activation of muscles for example) *in vivo*. This brings about the realisation of specific motor pattern observed *in vitro* in relation to the activation signal induced. CPGs are used to generate rhythmic patterned motion in absence of any rhythmic or central inputs (Hooper, 2000; Wu and Ma, 2010; Nor and Ma, 2014); and this has given rise to many researchers embarking on this philosophy for the control of robots mainly regarded as bio-inspired robotic control.

The ideology behind CPGs lies in the biological principles of the Central Nervous System (CNS) associated with the various limb/segmental behaviours of living animals (legged or creeping) such as terrestrial and aquatic locomotion, which entails walking, hopping and swimming to mention the least. The conceptual knowledge concerning the ability of the spinal cord being able to generate these locomotion in living animals had since being conceived in the early 20th century (de Pina Filho, Santos and Dutra (2006)). The CNS consists of two parts, namely; the brain and the spinal cord. Although, It is known that the brain is linked to all parts of the living animal passing information via the motor cortex responsible for its behavioural pattern, the spinal cord functions primarily in the transmission of neural signals between the brain and the rest of the body. The spinal cord contains neural circuits that is capable of independently generating complex rhythmic behaviours (motor output) without locomotive-related (proprioceptive) information (sensory inputs) (Brown, 1911, 1914; Field-Fote, 2000). This establish the fact that rhythmic pattern generation does not rely wholly on the CNS but that spinal cords possess autonomous network (circuit) of neurons which form the basis of Central Pattern Generators (CPGs).

2.4.1 Modelling CPGs

Based on biological concept, CPGs are regarded to be complex distributed network of inter-neurons present in spinal cords which are integrated into multiple reflex circuits systems (McCrea (1996)). The movement pattern generated is as a result of the certain activities between CPGs which makes up the entire reflex circuits and several feedback and feed forward modulatory signals, and therefore provides coordinated activation of various muscles for the control of joint movements in living organisms with respect to its environment Ivashko, Prilutsky, Markin, Chapin and Rybak (2003). The formulation of these spinal circuits which constitute the CPG model for the generation of rhythmic behavioural patterns with reference to locomotory control system is hence paramount Bay and Hemami (1987). In Ijspeert (2008) various CPGs models were examined and categorised as below;

- *Biological models*: used to investigate the generation of rhythmic activities in small neural circuits as in (Hellgren, Grillner and Lansner, 1992; Traven, Brodin, Lansner, Ekeberg, Wallén and Grillner, 1993; Wadden, Hellgren, Lansner and Grillner, 1997).
- *Connectionist models*: focus is on how network properties (half-centre network for example) is used to generate rhythmic activities as illustrated in (Williams, 1992; Buchanan, 1992; Wallén, Ekeberg, Lansner, Brodin, Traven and Grillner, 1992).
- *Oscillator models*: stresses the effect of inter-oscillator couplings and intrinsic frequency differences on the synchronisation and phase-lag of oscillatory centers. This was demonstrated in (Bay and Hemami, 1987; Cohen, Holmes and Rand, 1982; Matsuoka, 1987; Schöner, Jiang and Kelso, 1990; Kopell, Ermentrout and Williams, 1991; Collins and Richmond, 1994; Ijspeert, Crespi, Ryczko and Cabelguen, 2007).

- *Neuromechanical models*: This involves the use of the biomechanical model of the body and its environs in conjunction with the CPG for verification of the possible effect of sensory feedback on the body movement pattern. An example of these models was developed in (Nor and Ma, 2014; Ekeberg, 1993; Ijspeert, Hallam and Willshaw, 1999; Ijspeert, Crespi and Cabelguen, 2005; Inoue, Ma and Jin, 2004).

Neuromechanical models combines both the CPG design and the body mechanics design of the target physical system to be controlled, hence the CPG network required to simulate the locomotion of the system is first constructed. In addition to the above, modelling CPGs has to follow a certain procedure in order to meet the desired purpose of its design (Ijspeert (2008)). These procedures entail five (5) interconnected steps:

- The general architecture of the CPG, which involves the choice of the number and type of oscillators and also the type of control (position or torque control) to be adopted.
- The type and the topology of couplings. This does influence the phase relation between oscillators.
- The waveforms. It is directly proportional to shape of the limit cycle produced by the selected oscillator, but can be altered using filters.
- The effect of input signals (control parameters) on the frequency, amplitude and phase.
- The effect of feedback signals on the CPG as regard the environs of the body.

2.4.2 Neural Oscillators as CPGs

Oscillator model mathematically employs coupled nonlinear oscillators to mimic the dynamic behavioural pattern of mammals. It entails the use of one or more oscillators to

represent each neuron (representing a joint or segment) which is then coupled in a particular pattern to obtain a specific gait transition. Fig. 2.3 shows an exemplary structure of a neural network. It presents a general structure of coupling between neurons having specific connection weight, and how the output of each neuron can form the input to the other neuron depending on its coupling topology. These neurons can be actually represented by various types of oscillators depending on the approach considered by various researchers. Some of the oscillators that has been exploited for this purpose are; rayleigh oscillators (de Pina Filho, Santos and Dutra, 2006; Mondal, Nandy, Verma, Shukla, Saxena, Chakraborty and Nandi, 2011), Van der Pol oscillators (Bay and Hemami, 1987; Roy and Demiris, 2005), and also Stein and FitzHugh-Nagumo oscillators was utilised by Collins and Richmond in (Collins and Richmond (1994)). Furthermore, other vastly used oscillators by several researchers (although modified to suit the behavioural pattern to be established) include the Matsuoka oscillators proposed by Matsuoka in (Matsuoka, 1987, 1985) such as in (Kassim, Zainal and Arshad, 2008; Hein, Hild and Berger, 2008), the Hopf oscillators (adaptive) (Righetti and Ijspeert, 2006; Ronsse, Vitiello, Lenzi, Van Den Kieboom, Carrozza and Ijspeert, 2010; Righetti, Buchli and Ijspeert, 2005) and the phase oscillators (Nor and Ma, 2014; Cohen, Holmes and Rand, 1982; Buchli and Ijspeert, 2004; Conradt and Varshavskaya, 2003; Ijspeert and Crespi, 2007). The main interest in central pattern generations does not lie solely in the behavioural pattern of the oscillatory neural networks but rather on how the mechanisms which leads to stable rhythmic pattern occurs (Bay and Hemami (1987)), therefore it is necessary to analyse this mechanism.

Oscillators are used to characterise mechanisms that exhibits repeated periodical actions such as: some neurons, electric circuits, waves, cells, etc (de Pina Filho, Santos and Dutra (2006)). This behaviour is made possible because of the existence of closed trajectories having zero energy at each end of a periodic cycle. This allows the system to return to its

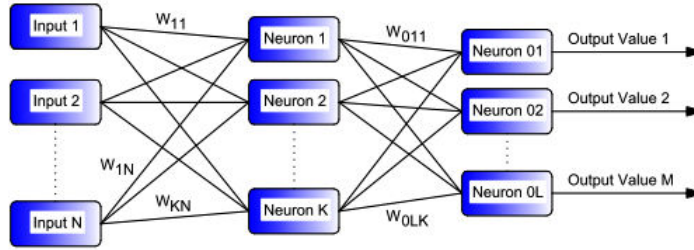


Figure 2.3: Neural Network.

stable periodic pattern after the state variable is perturbed (Ijspeert (2008)). This closed trajectories can be referred to as; *limit cycles*. Limit cycles could be stable, unstable or semi-stable. In this case we consider a stable limit cycle which can be defined as a closed trajectory in phase space having the property that at least one other trajectory spirals into it as time approaches infinity. This behaviour is inherent in oscillators and can be described by a differential equation.

2.4.3 Coupled Oscillators

The coupling of oscillators is established by certain coupling terms in the differential equations of the oscillators; hence, these coupling terms provide a medium by which the oscillators interact with each other. The manner at which oscillators are coupled depends on the type of oscillators used, but forms an integral part of the CPG model in such a way that the coupling method used has a direct influence on the purposed rhythmic behaviour. The coupling terms (weight) also help determine when synchronisation occurs in a coupled system.

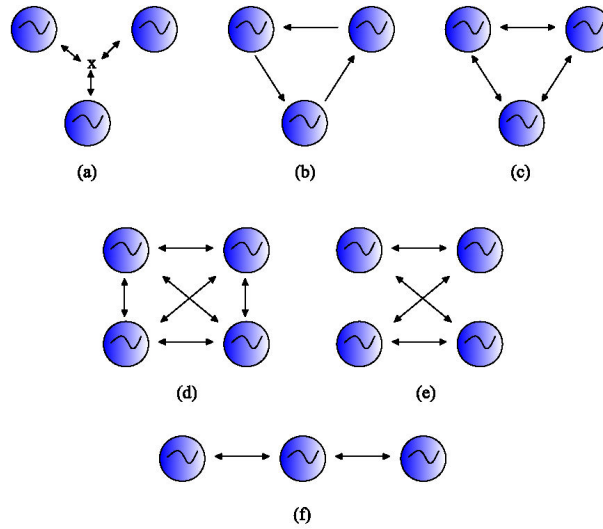
In general, coupling can be classified into two broad categories: *Direct coupling* and *Global coupling*. *Direct coupling* can be further divided into Mutual (i.e full coupling, local coupling and random coupling), Chain and Ring coupling (See Fig. 2.4 for a pictorial view of these types of coupling). Note that direct coupling could be either bidirectional or unidirectional. This was considered in (Nor and Ma (2014)) (unidirectional) and (Crespi

and Ijspeert (2008)) (bidirectional) both using phase oscillators for the modelling and control of a snake like robot. A mathematical analysis of direct coupling using Rayleigh oscillators was given in (de Pina Filho, Santos and Dutra (2006)) which was used in the modelling of bipedal robots. Bay and Hemami (1987) also used a set of coupled Van der Pol oscillators to generate control signals (CPG) for a simple biped locomotory system. Cohen, Holmes and Rand developed a theoretical model for generating locomotion in lamprey using coupled phase oscillators (Cohen *et al.* (1982)); an insight into inhibitory (- sign) and excitatory (+ sign) coupling was given. Mathematical models of neural rhythm generators were presented in (Matsuoka (1987)) using Matsuoka oscillators; it takes into account different coupled networks and different control mechanisms in rhythm pattern control.

Global coupling uses a single variable common to, and controlled by each oscillator in the CPG model to achieve its coupling goal (effect). The Kuramoto model basically employs global coupling for nonlinear oscillators (Daniels (2005)), and this idea was used in the coupling of adaptive Hopf oscillators (Righetti and Ijspeert (2006)) and also extended to the coupling of the augmented phase of the adaptive Hopf oscillators (Ronsse, Koopman, Vitiello, Lenzi, De Rossi, van den Kieboom, van Asseldonk, Carrozza, van der Kooij and Ijspeert (2011)). The main interest in this coupled network is how the phase, frequency and amplitude vary across the network.

2.5 Exoskeletons

Exoskeletons may be referred to as wearable robots fitted with mechatronics systems, designed to guarantee an harmonious working relationship with the human body (Rifai, Hassani, Mohammed and Amirat (2011)). Their main function include assisting able-bodied individuals perform rigorous task humanly impossible, and also to provide assistive and rehabilitative measures to physically challenged and elderly people, so as



The pictorial view of the major types of oscillators coupling are given according the alphabetical label as follows. (a) Global coupling (b) Local coupling (unidirectional) (c) Local coupling (bidirectional) (d) Full coupling (e) Random coupling. (a), (b) & (c) are regarded as mutual coupling while (d) & (e) are ring coupling and (f) Chain coupling.

Figure 2.4: Classification of the Coupling of Oscillators.

to support their mobility and as such help them regain control of their limbs ([Kazerooni, Racine, Huang and Steger \(2005\)](#)). The term "active orthosis" is mostly used to define the latter function.

The concept behind human exoskeletal devices may be perceived to have its root in studies carried out by researchers in the United States (US) and former Yugoslavia ([Dollar and Herr \(2008\)](#)), with focus on able-bodied person's joint augmentation by the US group of researcher while the latter focused on assistive innovations for disabled persons. Whichever function they were meant to perform, the number of lower limb joints involved in the design of the mechanical structure (exoskeleton) may be the only distinct feature common to both. Classifying exoskeleton based on this ideology may fall within the multi-joints or single-joint category.

2.5.1 Multi-joints Exoskeletons

Multi-joints exoskeletons relate to "full body exoskeleton"⁶ or exoskeleton which have more than one actuated joint. Here, some of the works based on multi-joints are documented.

The earliest joint augmentation device was first recorded in (Yagn (1890)). This device was intended to allow free flexure and motion of the legs and body but was never built to demonstrate its potency. In 1963, a conceptual paper titled "a powered aid for locomotion" written by Zaroodny of the US army described three (3) degree of freedom (DOF) device consisting pneumatic cylinder pivoted at hip and terminating at the toes via a specially made shoes (Zaroodny (1963)). It is known to be the first augmentation exoskeletal device ever built. Gilbert in (Gilbert (1966)) published a technical report detailing the first phase of a three-phase project to develop a powered exoskeleton which will aid the wearer to walk bend and turn with minimal constraints while dispatching its intended function of loading, unloading and moving cargo within designated areas of interest. The implementation of this powered exoskeleton tagged "Hardiman I Prototype" was carried out in 1971 (Makinson (1971)). It consists of thirty (30) actuated joints with twelve (12) of its joints partially tested at the time of publication. This project was supported by General Electric Research (Schenectady, NY). In 1986 (Moore (1986)) and 1989 (Rosheim (1990)), papers credited to Moore and Rosheim respectively were written for the augmentation of soldiers capability, although the latter further designed a twenty-six (26) DoF device with a 500 pound load capacity excluding the hands; he later on proposed an application to rehabilitation of handicapped persons.

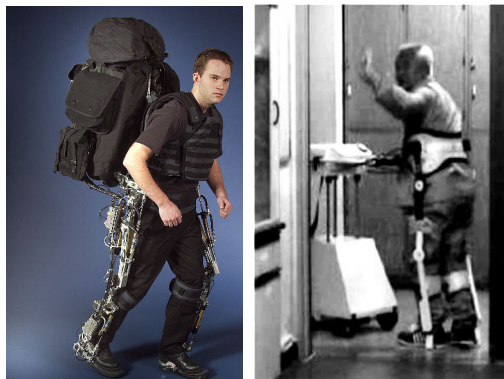
Zoss, Kazerooni, and Chu, were the first to demonstrate the first energetically au-

⁶They are considered to be biped exoskeleton which include hip, knee, ankle and upper body joints actuation with an attachment extended to enclose the chest.

onomous augmentation lower extremity exoskeletal device in (Zoss, Kazerooni and Chu (2005)) named Berkeley Exoskeleton (BLEEX). BLEEX has seven (7) DoF on each leg which is powered by linear hydraulic actuators, with three (3) DoF at the hip and ankle and one (1) DoF at the knee. It supports a load 75kg with a speed of 1.3m/s. Berkeley, and Sarcos Research Corporation (SARCOS) in Salt Lake City were both funded by the US Defence Advanced Research Projects Agency (DARPA), tagging the 50 million US dollar project as *Exoskeletons for Human Performance Augmentation* (see Fig. 2.5 (left)). SARCOS under the project Wearable Energetically Autonomous Robots (WEAR) was tasked to develop an autonomous wearable system fitted with base units to include the legs, torso and arm with the ability to contain energy storage, power systems and actuators; usage could include rescue and emergency operations. In 2006 a lightweight, under-actuated exoskeleton for load-carrying augmentation was developed. The exoskeleton had 3 DoF at the hip, one (1) DoF at the knee, two (2) DoF at the ankle and one (1) DOF at the foot. The mechanical system was tested with a load of 75lb payload and was able to transfer 90% of the weight (exoskeleton mass + payload) via the exoskeleton leg mass (Walsh, Paluska, Pasch, Grand, Valiente and Herr (2006b)). It was also a DARPA initiative funded program. The Japanese exoskeleton, called HAL-5 is an improvement on the earlier version of exoskeleton in Japan with an 100% capacity. This device was built to assist elderly people and people with lower limb disorder walk, climb stairs, and lift loads. However, it also help augment the capability of healthy humans (Guizzo and Goldstein (2005)).

The "active suit" became the first complete orthotic device designed for rehabilitative measure for patients with lower limb disorders (Hristic, Vukobratovic and Timotijevic (1981)). Some of these patients were able to exploit the use of this device to master walking once again. A similar device to the active suit designed to assist paraplegics regain lower limb motor functions was attained in University of Wisconsin (Seireg and

[Grundmann \(1981\)](#)). Powered by rotary hydraulic actuators, the device had three (3) DoF about the Hip and ankle and one (1) DOF about the knee. Other devices among many includes "EXPOS" ([Kong and Jeon \(2006\)](#)). EXPOS (exoskeleton for patients and the old) was initiated to carter for certain shortcomings as regard weight and volume of orthotic device for assistive walking in elderly people and patients. This tendon-driven device was established in Sogang University. The motors, drivers and batteries were separated from the caster walker in order to minimise the weight of the exoskeleton. It utilises certain sensing techniques for the synchronisation of the human and the robot. The Vanderbilt orthosis approach was intended to provide gait assistance to spinal cord injured (SCI) patients ([Quintero, Farris, Goldfarb *et al.* \(2011\)](#)). They are equipped with actuators at the both hips and knee joints. Its assistive torques is initiated via these joints in conjunction with a control structure. Recently, in ([Aoustin \(2015\)](#)) a seven-link planar biped equipped with a wearable walking assist device was proposed. However, assistance was only achieved at the hips level. This places assistive robotics as an active research field based a constant need to avoid continuous musculoskeletal disorders ([Ferris, Sawicki and Daley \(2007\)](#)).



([Zoss, Kazerooni and Chu \(2005\)](#)) & ([Kong and Jeon \(2006\)](#))

Figure 2.5: Bleex suit (Left) & Ekso suit (Right)

One of the most advanced exoskeletons is the "Ekso Suit" ([Ferrati, Bortoletto and Pag-](#)

ello (2013)). The Ekso Suit is an exoskeleton walking suit supported by a pair of crutches to establish stability (Strickland (2012)). It has four (4) motors distributed among both hips and knees of the device and supports 20kg weight via the skeletal legs (see Fig. 2.5 (right)). Advanced exoskeletal device have more improved technologies which necessitate better performance based on the intelligent concept envisaged. Some exoskeletons which may fall into this category are the "ReWalk" (Esquenazi, Talaty, Packel and Saulino (2012)), "eLEGS" (Wang, Wang, van Asseldonk and van der Kooij (2013)) and the "MINDWALKER" (Strausser and Kazerooni (2011)) (see Fig. 2.6) to mention a few. The ReWalk powered exoskeleton was designed to enable people with paraplegia due to SCI to carry out routine ambulatory functions. The hip and knee joints are powered to follow a predefined trajectory. This is achieved via a wrist-pad controller and a torso tilt sensor, which allow the user to perform functions like sitting, standing and walking. All subjects who partook in the trial of the ReWalk had strong positive comments regarding its use. The eLEGS adopted the use of a human machine interface (HMI)⁷ to enable the user interact with the exoskeleton by using natural gestures to perform standing, sitting and walking functions. The HMI utilises a unique sensor suite and a finite state automation to realise this task. The targeted subjects were also those with SCI. Similarly, the MINDWALKER powered exoskeleton which has five (5) DoFs and a weight of about 28kg excluding batteries, was designed to assist paraplegics regain locomotion capabilities. In (Ikehara, Nagamura, Ushida, Tanaka, Saegusa, Kojima and Yuge (2011)), a walking assistance device to assist elderly people who could walk independently but may be anxious about their muscle strength impairment was developed.

Exploring the learning mechanism and estimation capabilities of adaptive frequency oscillators (AFO), some researchers have been able to develop oscillator-based assistance for walking. In (Ronsse, Koopman, Vitiello, Lenzi, De Rossi, van den Kieboom, van

⁷HMI is a method by which the user commands the exoskeleton to the desired state.



(Esquenazi, Talaty, Packel and Saulino (2012)), (Strausser and Kazerooni (2011)) & (Wang, Wang, van Asseldonk and van der Kooij (2013))

Figure 2.6: ReWalk suit (Left), Mindwalker suit (Middle) & elegs suit (Right).

Asseldonk, Carrozza, van der Kooij and Ijspeert (2011)), an adaptive oscillator capable of predicting the future angular position of the user's joints, with reference to the pattern learned during preceding cycles was utilised. Its assistance mechanism was realised by attracting the joints to the predicted future position using a force field in a compliant lower-limb exoskeleton. The validation of this design was done only on the hip joint actuation. This estimation principle was also exploited in (Seo, Hyung, Choi, Lee and Shim (2015)), however, the new AFO developed could estimate gait cycle from joint angles without the need for foot contact sensors. For assistance, the gait assistance controller utilises the inputs from two hip joint angle sensors and estimates the gait cycle so as to generate assistive torques around hip joints. This new AFO is called particularly-shaped adaptive oscillator (PSAO).

2.5.2 Single-joint Exoskeletons

Single-joint exoskeletons are designed specifically for patients with a particular joint disorder. With regard to the lower limb, the joint of interest are the hip, knee and

ankle. Some research works on exoskeleton relevant to single-joints are presented here (see Fig. 2.7 for a pictorial view).

In walking, hip joints are said to be associated to the swing dynamic handling. However, it also plays a great role in providing support to the body weight during static and dynamic postures. Hip exoskeletons provide assistive measures to a patient with dysfunctional hip joint. Works related to this are documented accordingly.

In ([Aguirre-Ollinger \(2013\)](#)) an assistive method for hip movement assistance using AFO was proposed. This control algorithm involves two (2) modes; the learning mode and the assistive mode. In the learning mode, the average envelope of the muscle's EMG output is learned while the user moves in conjunction with the exoskeleton. This procedure entails the extraction of the phase and frequency of the leg's angle, and encoding the muscle EMG envelope using local weighted regression. In the assistive mode, the learned EMG envelope is reproduced as a function of the phase by the AFO. This signal serves as the generated assistive torque. Initial trials was performed using two (2) male participants to execute a uniform leg swing task for thirty (30) seconds, with and without assistance. In the result, there seems to be a timely coordination between the actuator output torque and the EMG activities.

A lower limb hip-orthosis powered by a pneumatic actuator was proposed in ([Do Nascimento, Vimieiro, Nagem and Pinotti \(2008\)](#)). In contrast to the use of EMG, Do Nascimento devised an alternative system that allows voluntary control of the orthosis by the patient. This alternative system entails employing the anthropometric parameters and movement constraints of the patient in the entire orthosis design. This information is used in the control system in order to monitor the hip joint angle so as to activate the pneumatic actuator. At minimum extension value, the actuator valve contracts and releases when the hip joint angle reaches a pre-set flexion value. A victim of poliovirus was used to test the functionality of the hip orthosis. Results obtained showed a satisfactory

performance of the controller.

Using the pneumatically powered hip exoskeleton proposed in (Ferris and Lewis (2009)), eight (8) healthy subjects were used to test the hypothesis that net muscle moment reduce about the joints when robotic assistance is provided (Lewis and Ferris (2011)). The exoskeleton is equipped with two (2) pneumatic cylinders together with other accessories to provide external torques, additional stability and quantify the assistance rendered by the exoskeleton. The control signal used is footswitch-based, and its function is to regulate the air pressure supplied to the pneumatic cylinder at a pre-set range of values within the gait cycle period. Subjects were made to walk with the exoskeleton unpowered and powered at a speed of 1.25 m/s for ten (10) minutes and thirty (30) minutes respectively. Results obtained indicated that the human-exoskeleton hip torques were almost equal under both instances, in spite of the kinematic differences.

In order to design an assisting mechanism that can completely assist the hip joint about its entire DoF, Yu proposed a six (6) DoF parallel mechanical system in (Yu, Liang and Ge (2011)). Its working principle is based on utilising direct parallel kinematical Jacobian to denote the velocity relation between the active joints and end-effector. This system is advantageous in the sense that it provides higher precision and stiffness. However, it is a more complex mechanism compared to serial mechanism. Experimental results showed that the system is applicable to human walking assisting control.

Knee joints are regarded to be the most complicated and important joint of the lower extremity. In walking, they act as a free-damping joint in the swing phase, while almost locked during the stance phase. Knee orthosis device are therefore required to assist patients whose knee joint cannot naturally perform their functions.

The first controllable orthosis dedicated to a single joint was designed and patented by Pietro in 1942 (Filippi (1942)). This device was constructed in a simple and compact manner having a light weight which is automatically operated by the natural movements

and postures of the body, establishing a full freedom movement about the knee when required. One of the importance of control associated to exoskeleton was addressed in (Aguirre-Ollinger, Colgate, Peshkin, Goswami *et al.* (2012)). This work is centred on developing a control strategy that will increase the natural frequency of the lower limb and consequently reduce the metabolic energy consumption during walking via inertia compensation. The validation of this control principle was done using a stationary mounted exoskeleton that could assist the flexion and extension of the knee. Trials by subjects established a possible recovery of their natural frequency and an increase in their selected angular velocity.

In (Kim, Yu, Jeong, Heo and Kwon (2013)), a powered knee orthosis equipped with two artificial pneumatic actuators was proposed to assist and enhance muscular activities of lower limbs. The primary function of this actuator is to support the knee extension movement through the muscular stiffness force (MSF) sensor signal. This sensor signal relates to the users' motion intention. Experimental studies were carried out by twenty healthy subjects. These participants were made to utilise the powered knee orthosis during sit-to-stand (STS) and squat motion for a period of 10 times each. To identify the knee orthosis effectiveness, the subjects' lower limb muscular activities with and without the orthosis were measured. Results obtained ascertain that the device will be beneficial to weaken elder people when carrying out their daily activities. Knee joint orthotic devices have considerable amount of designs to assist patients with knee joint disorder.

The control of a lower limb orthosis applied to the knee joint for rehabilitation purposes was presented in (Rifai, Hassani, Mohammed and Amirat (2011)). A bounded control torque was applied in real-time using the EICOSI orthosis. Experiments were conducted on a twenty-seven (27) years old healthy subject, with weight of 90Kg and height of 1.87m in order to test the efficiency of the control law. Results showed a good convergence of

subject knee movement to the predefined trajectory in a considerable time. A controlled knee-joint orthosis designed to restore movements of the human lower limbs; particularly the flexion/extension of the knee joint, is proposed in (Mefoued, Mohammed and Amirat (2011)). A twenty-nine (29) years old healthy patient with weight of 75Kg and height of 1.76m was used to practically validate the control law. The control method utilised was based on High Order Sliding Mode Control (HOSMC) strategy. Comparison with classical PID controllers to test the proposed control law robustness was performed. HOSMC prove to have a more preferred performance.



(Lewis and Ferris (2011)), (Rifai, Hassani, Mohammed and Amirat (2011)) & (Blaya, Herr *et al.* (2004))

Figure 2.7: Hip exoskeleton (Left), Knee exoskeleton (Middle) - EICOSI orthosis & MIT AAFO (Right).

Ankle joints are related to the stance-phase ground propulsion which requires pressure to be exerted on the ground surface. Any disorder about this joint contributes to a deformed gait pattern in humans. Robotic lower limb exoskeletons with regard to ankle joints are surveyed here.

A variable-impedance control applied to an active ankle-foot orthoses (AAFO) in an attempt to reduce the dominant complications of drop-foot gait among persons who have had stroke, sclerosis or cerebral palsy was developed by the MIT Bio-mechatronics Group (Blaya, Herr *et al.* (2004)). This was achieved through the application of biomimetic torsional spring control during plantar flexion control while adjusting the orthotic joint

stiffness to provide a better foot clearance. Positive remarks were gathered from patients who participated in the clinical trials of the device. It could be deduced from the trials that actively adjusting joint impedance reduces the occurrence of slap foot and allows greater powered plantar flexion.

In (Hitt, Sugar, Fleeger *et al.* (2007)), a Powered Ankle Foot Orthosis (PAFO) which utilises a robotic tendon (actuator) via a motor to correctly position a tuned spring in the gait pattern is proposed. The motive was to help people suffering paralysis from stroke. References for the motor position was realised by an adjustable gait pattern. Two healthy subjects participated in this study, and the result presented showed that the control method assisted the users in a safe way.

Other works on ankle-foot orthosis could be found in (Takemura, Onodera, Ming and Mizoguchi (2012)) and (Kim, Kim, Kang, Jeong and Kwon (2010)) to mention a few. Takemura proposed a wearable Stewart platform-type ankle-foot orthosis designed for the purpose of rehabilitation and also as a walking assistive device. The device is made up of six (6) linear actuators mounted between two plates fixed on the leg plate and foot plate. Ankle position and torque control are based on robot kinematic model. Motion measurement and motion reproduction performance of the assistive device were verified using five (5) subjects. Results obtained validated the aim of the device. Alternatively, Kim designed an AFO with one (1) DoF. The actuation of this device is achieved by a pneumatic actuator. This device was built to assist and enhance the muscular activity of elderly subjects. Emphases were laid on the ankle plantar flexion motion. The signal required for actuation is that of a soleus muscle. This is measured using the MSF sensor. For validation experiments, ten (10) elderly adults were used. Measurements were taken while the subjects were executing plantar flexion motion with and without the AFO, with and without feed-forward control and analysed. The result established the effectiveness of the AFO with feed-forward control, due to the decrease in muscular

torque peak value realised in all subjects.

2.6 Conclusion

Mathematical models may be classified as; dynamical equations, statistical models, differential equations, or game theoretic models. This categorisation is not exhaustive because it leaves out certain forms like; category theory ([Spivak and Kent \(2012\)](#)). However, dynamical and differential equations are those mostly used to represent the behaviour of biomechanical systems. This can be deduced from the analyses of the modelling concept used in CPGs and lower limb exoskeleton detailed in this chapter.

Assistive strategies in robotic lower limb exoskeleton may be achieved using two (2) types of methodologies. These methodologies are; motion intention detection and targeted task attainment ([Yan, Cempini, Oddo and Vitiello \(2015\)](#)). In motion intention detection, the control processes are often divided into a series of different phases. The detection and prediction of these phases are realised by the exoskeleton sensory system such as; joint angle sensors, accelerometers, foot pressure sensors e.t.c or rather detected using direct method such as; EMG or muscle stiffness. Targeted task attainment refers to the use of predefined trajectory control in conjunction with the human-exoskeleton model. This method is mostly used for persons suffering from paraplegia and those with severe lower limb disorder. This thesis adopts this methodology for its proposed assistive and rehabilitation protocol design.

This work considers the use of AFO for the estimation of the joint trajectories about the knee and ankle joints with assistive torques generated about each joints. Nonlinear control methods will also be used to illustrate this claim. The level of human contribution will be realised via observer-based design principles. The supposed exoskeleton will be actuated at the knee and ankle joints for subjects in seated position, while for walking,

the exoskeleton will have four (4) actuated joints (hip and knee joints of both legs).

CHAPTER 3. Analysis of Knee- Ankle Orthosis Modelling: An Inverse Dynamics Approach using Adaptive Coupled Oscillators

3.1 Introduction

In this study, an inverse dynamics approach by means of adaptive coupled oscillators is used in the modelling and control of a lower limb orthosis applied at the knee and ankle joint levels in a sitting position. This design is aimed at providing assistance and rehabilitative measures to humans with lower limb disorders and as such presents a platform for which their mobility performance can be improved. Adaptive oscillators are known to have the capability of learning high level parameters of sinusoidal, quasi-sinusoidal or non-sinusoidal signals (amplitude, frequency and offset). However, the later signal (non-sinusoidal) considered in this paper requires a number of oscillators in parallel to replicate the moving joint regarding filtering via adaptive oscillator. This was first acknowledged in ([Large \(2000\)](#)). In ([Righetti, Buchli and Ijspeert \(2005\)](#)), a model of AFO was used to design an adaptive CPG, which was intended to adapt its parameters

in order to learn the frequency of any periodic driving signal. This mechanism was extended to a large class of oscillators in (Righetti, Buchli and Ijspeert (2009)), while also highlighting a variety of different practical applications of the mechanism in robotics. (Ronsse, Vitiello, Lenzi, Van Den Kieboom, Carrozza and Ijspeert (2010)) proposed the first assistance method for simple rhythmic movement at the elbow of a subject using a single adaptive oscillator. To demonstrate the relevance of the above method on walking, an oscillator-based model-free approach designed for the assistance was investigated in (Ronsse *et al.* (2011)). The work in (Ronsse, Vitiello, Lenzi, Van Den Kieboom, Carrozza and Ijspeert (2010)) concentrated on the use of a sinusoidal periodic movement about a single DoF; although this was addressed in (Ronsse *et al.* (2011)), the idea of a model-free approach negates the purpose of this work. Assistance was only demonstrated at the hips joint and rehabilitation was not considered.

This work aims at demonstrating the possibility of practically assisting and rehabilitating patients with lower-limb disabilities at all the joints concurrently. To achieve this, the dynamic model of each limb is independently assumed and non-sinusoidal trajectories are formulated to provide the rhythmic movement pattern. The mechanical coupling between them is compensated for by the AFO-Controller. The formulation of the rehabilitation protocols is envisaged at the knee and ankle for simplicity purpose, and was based on the choice of the physiological parameter used in the simulation. This does provide an avenue for which new rehabilitation protocols could be established. A state of inactivity of the human muscles in the form of disturbance is also introduced.

3.2 Knee-Ankle Orthosis System

In this work, a Shank-Foot CAD model as shown in Fig. 3.1 which depicts the knee-ankle orthosis is considered. The CAD model is assumed to incorporate the parameters

of the orthosis and the user's lower limb (shank-foot to be precise). The model takes into account the flexion/extension of the knee about the revolute joint a and the plantar-flexion/dorsal-flexion of the ankle about b , assuming the motions are performed in a sagittal plane with the subject in a sitting position. The physiological parameters of the subject's shank and foot link of a single leg, are those accounted for in this model. The movements of the knee-ankle orthosis are in the range; $0rad \leq \theta \leq 2.35rad$ for the knee and $0rad \leq \theta \leq 0.87rad$ for the ankle; where $0rad$ relates to the full knee extension, $2.35rad$ is the maximum flexion of the knee and $1.57rad$ corresponds to the rest position of the knee. Furthermore, $0rad$, as regard the ankle movements corresponds to the rest position of the ankle, $0.35rad$ is the maximal ankle dorsal-flexion, while $0.87rad$ denotes the maximal ankle plantar-flexion. The assisted joint positions are required to be measured, so as to determine the human torques required. It should be noted that the system is considered to reflect a controlled concurrent movement about its axis. These establish periodic motions of the joints. Given that the system is mechanically coupled via the joints, the movements are said to be coupled and thus achieved by CPG as discussed in Section 3.3. This is done to guarantee a global movement about the joints, since the dynamic model of the shank-foot is treated as a decoupled system. Based on this, the periodic motion is said to assume the dynamics of a damped simple pendulum for each link.

3.3 CPG Design

In this section the model of the CPG used to provide assistance to the knee-ankle orthosis is described. The design of the CPG using adaptive oscillators and hence the tuning of the adaptive oscillator for the filtering of a two (2) degree of freedom (DoF) along a non-sinusoidal trajectory are described.

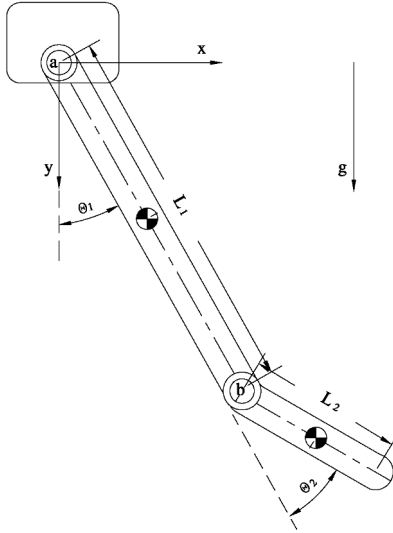


Figure 3.1: Shank-Foot Model.

3.3.1 Adaptive Frequency Oscillator (AFO)

The adaptive frequency Hopf oscillator was first developed in (Righetti, Buchli and Ijspeert (2005)) and (Righetti, Buchli and Ijspeert (2009)). For the purpose of simplicity, the augmented phase oscillator given in ((Righetti, Buchli and Ijspeert, 2009; Rinderknecht, Delaloye, Crespi, Ronsse and Ijspeert, 2011)) is adopted for the design of the CPGs used for the rhythmic movements needed to be achieved in this study. The augmented phase oscillator is written as

$$\begin{aligned}\dot{\phi} &= \omega + \nu F(t) \cos \phi \\ \dot{\omega} &= \nu F(t) \sin \phi\end{aligned}\tag{3.1}$$

where ϕ is the phase of the oscillator and ν represents the learning parameter that determines the speed of the phase synchronisation to $F(t)$ and must be greater than 0; $\nu > 0$. $F(t)$ is the periodic input signal to which the oscillator will adapt its frequency while ω controls the frequency of the oscillations, adapted to the periodic input signal $F(t)$.

3.3.2 Coupled AFO

The principle of coupled oscillator is used to define a precise way of learning any periodic input signal. This is in particular used to learn non-sinusoidal periodic signals since most human movements are not usually sinusoidal. This coupling scheme which is more than just a dynamic Fourier series decomposition of non-sinusoidal periodic signal, was first proposed in (Righetti and Ijspeert (2006)) and later modified using augmented phase oscillator in (Ronsse, Koopman, Vitiello, Lenzi, De Rossi, van den Kieboom, van Asseldonk, Carrozza, van der Kooij and Ijspeert (2011)). This may be expressed as

$$\begin{aligned}
 \dot{\phi}_i &= i\omega + \nu F(t)\cos\phi_i \\
 \dot{\omega} &= \nu F(t)\cos\phi_1 \\
 \dot{\alpha}_i &= \eta F(t)\sin\phi_i \\
 F(t) &= \theta - \hat{\theta} \\
 \hat{\theta} &= \sum_{i=0}^N \alpha_i \sin\phi_i
 \end{aligned} \tag{3.2}$$

- where i represents the number of oscillators in parallel corresponding to the non-sinusoidal periodic signal and N the total number of oscillators.
- α_i is the amplitude associated to the main frequency ω .
- $F(t)$ is the periodic input signal to which the oscillator will adapt its frequency.
- while θ signifies the non-sinusoidal periodic signal.
- $\hat{\theta}$ is the sum of filtered outputs of each oscillator and η is the amplitude integrator gain.

Note that only the main frequency ω will be adapted to $F(t)$.

Furthermore, the CPG corresponds to one DoF, therefore, for two DoF based on the knee-ankle orthosis two CPGs are required. Three oscillators relate to one CPG. This

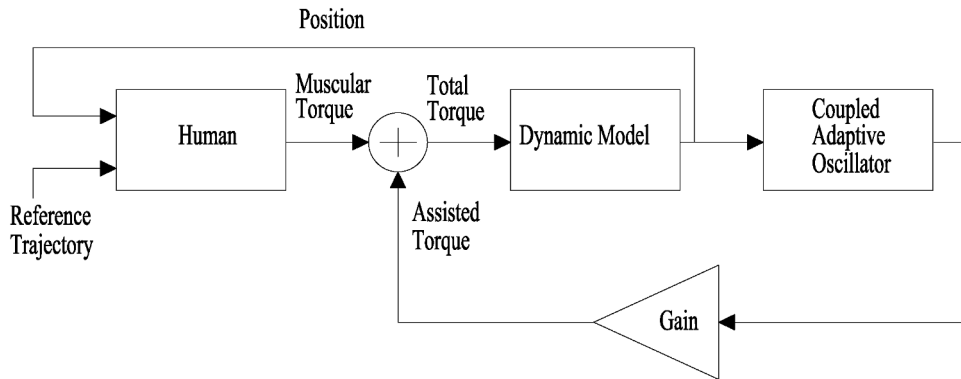


Figure 3.2: Block diagram of the human knee and ankle + orthosis.

is in conjunction with the assumed non-sinusoidal trajectories of the knee and ankle respectively. Consequently, in this model, $N = 3$.

3.4 Mathematical Model

In this section, the building blocks of the entire system are described. The blocks include: the dynamic model, coupled AFO (which includes the signal estimator and the torque estimator) and the human torque. Fig. 3.2 shows the block diagram of the combined system (human knee and ankle + orthosis).

3.4.1 Dynamic Model

The knee and ankle rhythmic movement of the human lower limb generates two trajectories and therefore the system is modelled as two DoF. These rhythmic movements are characterised as movements similar to that of a damped pendulum dynamics. The purpose of this has been explained in Section 3.2. Hence the dynamic model for the knee and the ankle can be mathematically written as:

$$\ddot{\theta}_j = I_j^{-1} \left(-m_j g l_j \sin \theta_j - b_j \dot{\theta}_j + \tau_j \right) \quad (3.3)$$

- where j is the number of joints which corresponds to two for this particular model with $j = 1$ corresponding to the knee and $j = 2$ corresponding to the ankle.
- I_j is the inertia of the shank/foot.
- m_j is the mass of the shank/foot.
- l_j is the equivalent length of the shank/foot, which corresponds to the movement about the knee and ankle joint.
- b_j represents the damping constants of the shank/foot movement about knee/ankle joints.
- g signifies the gravitational force.
- $\ddot{\theta}_j, \dot{\theta}_j, \theta_j$ denotes the knee/ankle angular acceleration, velocity and position respectively.
- τ_j is the total torques applied to the knee and ankle respectively.

The dynamic model block simply retrieves the actual angular position by integrating Eq. 3.3 for each joint level. The generalised coordinate that represents the actual angular position for the knee and ankle may therefore be represented as

$$\theta = [\theta_1 \quad \theta_2]^T \quad (3.4)$$

3.4.2 Coupled AFO (Joints Coupling)

The coupling of adaptive frequency oscillators to reproduce non-sinusoidal periodic signal for a single joint was explained in subsection 3.3.1. However, the simultaneous rhythmic movement of the knee and ankle joints requires coupling between each CPG that represents each joint. The choice of coupling used could differ, as demonstrated

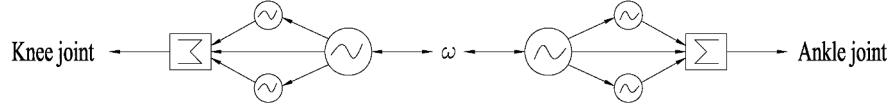


Figure 3.3: Structure of CPG coupling.

in ((Righetti and Ijspeert, 2006; Ronsse, Koopman, Vitiello, Lenzi, De Rossi, van den Kieboom, van Asseldonk, Carrozza, van der Kooij and Ijspeert, 2011)) respectively.

This study adopts the global coupling procedures which require a common variable belonging to each CPG controlled by each CPG. Fig. 3.3 presents a pictorial diagram of the coupling of the CPG with the frequency being the common variable needed to be controlled. The equation of the CPG that incorporates the global coupling between each joint may be written as:

$$\begin{aligned}
 \dot{\phi}_i &= i\omega + \nu F_j(t) \cos \phi_i \\
 \dot{\omega} &= \left(\nu \sum_{j=1}^G F_j(t) \cos \phi_{1,j} \right) / G \\
 \dot{\alpha}_i &= \eta F_j(t) \sin \phi_i
 \end{aligned} \tag{3.5}$$

- where j represents the active joint in question; for which in this particular model $j = 1$ relates to the knee, while $j = 2$ relates to the ankle.
- $F_j(t)$ is the non-sinusoidal periodic signal for each CPG and may be written as $F_j(t) = [F_1(t) \ F_2(t)]^T$.
- ω signifies the frequency and thus initiates the coupling between each CPG.
- G is the total number of joints while other terms are same as defined in Eq. 3.2.

3.4.3 Signal Estimator

The non-sinusoidal input signal $F_j(t)$ of the adaptive oscillator is the difference between the knee-ankle angular positions θ_j and the estimated (learned) signal $\hat{\theta}_j$. This may be

expressed as

$$\begin{aligned} F_j(t) &= \theta_j - \hat{\theta}_j \\ \hat{\theta}_j &= \sum_{i=0}^N \alpha_{i,j} \sin\phi_{i,j} \end{aligned} \quad (3.6)$$

The adaptive oscillator estimate of the velocity and acceleration can be written respectively as in (Rinderknecht, Delaloye, Crespi, Ronsse and Ijspeert (2011)):

$$\begin{aligned} \hat{\dot{\theta}}_j &= \sum_{i=0}^N \alpha_{i,j} \omega \cos\phi_{i,j} \\ \hat{\ddot{\theta}}_j &= - \left(\sum_{i=0}^N \alpha_{i,j} \omega^2 \sin\phi_{i,j} \right) \end{aligned} \quad (3.7)$$

3.4.4 Torque Estimator

The estimated torques is derived from the dynamic model in Eq. 3.3. The value of which is obtained by introducing the estimates from the adaptive oscillators described in Eq. 3.6 & Eq. 3.7. This forms the basis of the AFO control system. The equation may be described as:

$$\hat{\tau}_j = m_j g l_j \sin\hat{\theta}_j - b_j \hat{\dot{\theta}}_j + I_j \hat{\ddot{\theta}}_j \quad (3.8)$$

with each symbol defined as in Eq. 3.3 but represents its estimated version.

3.4.5 Human Torque

The human (muscular) torque applied to the device is determined by the PID controller in conjunction with the reference trajectory for the purpose of simulation and it is thus defined as:

$$\tau_{h,j} = K_{p,j} e_j + K_{i,j} \int e_j dt + K_{d,j} \dot{e}_j \quad (3.9)$$

where e_j is the error signal which is the difference between the reference trajectories and actual angular positions of the knee and ankle and $K_{p,j}$, $K_{i,j}$, $K_{d,j}$ are the proportional, integral and derivative gains of the controller (human torque) about the knee and ankle.

The total torque τ_j is the sum of the human (muscular) torque $\tau_{h,j}$ and the assistive torque $\tau_{e,j}$:

$$\tau_j = \tau_{h,j} + \tau_{e,j} \quad (3.10)$$

with $\tau_{e,j} = \kappa_j \hat{\tau}_j$ where κ_j determines the level of assistance applied at the knee/ankle joint. $\kappa_j = 1$ implies full assistance, $\kappa_j = 0.5$ represents 50% assistance and $\kappa_j = 0$ signifies no assistance.

3.5 Numerical Simulation & Results

Here, the physiological parameters, the non-sinusoidal periodic reference trajectories chosen for the purpose of this simulation and the eventual results of the simulation are highlighted.

3.5.1 Reference Trajectories and Physiological Parameters

The reference trajectories are assumed to be the measured angular position of the knee and ankle and chosen to be within the range of motion specified in Section 3.2; they are given as below respectively:

$$\begin{aligned} \theta_{ref1} &= \frac{\pi}{12}(\sin(2\pi ft) + 0.5\cos(\pi ft) + 2.25\sin(\frac{\pi}{2}ft)) \\ \theta_{ref2} &= \frac{\pi}{90}(\sin(\pi ft) + 0.8\cos(\frac{\pi}{2}ft) + 0.6\sin(\frac{\pi}{4}ft)) \end{aligned} \quad (3.11)$$

with $f = 0.16Hz$

Furthermore, the physiological parameters of the knee-ankle orthosis with respect to the Shank-Foot Model (See Fig. 3.1) are chosen as in Table 3.1.

Note that the value of the inertia is calculated assuming cylindrical links and thus calculated as $I_i = \frac{2}{3}m_iL_i^2$.

The PID controller parameters and Adaptive Oscillator parameters are given as; $K_p = 110, K_i = 5.5, K_d = 2$ are the same for both the knee and ankle PID controllers and

Table 3.1: Physiological Parameters.

Parameters	Units	Values
Shank length (L_1)	m	0.2
Foot length (L_2)	m	0.08
Shank mass (m_1)	kg	2.80
Foot mass (m_2)	kg	1.17
Shank inertia (I_1)	$kg.m^2$	0.075
Foot inertia (I_2)	$kg.m^2$	0.012
gravity (g)	m/s^2	9.8
Shank damping Coefficient (b_1)	Nm/s^2	0.4
Foot damping Coefficient (b_2)	Nm/s^2	0.6

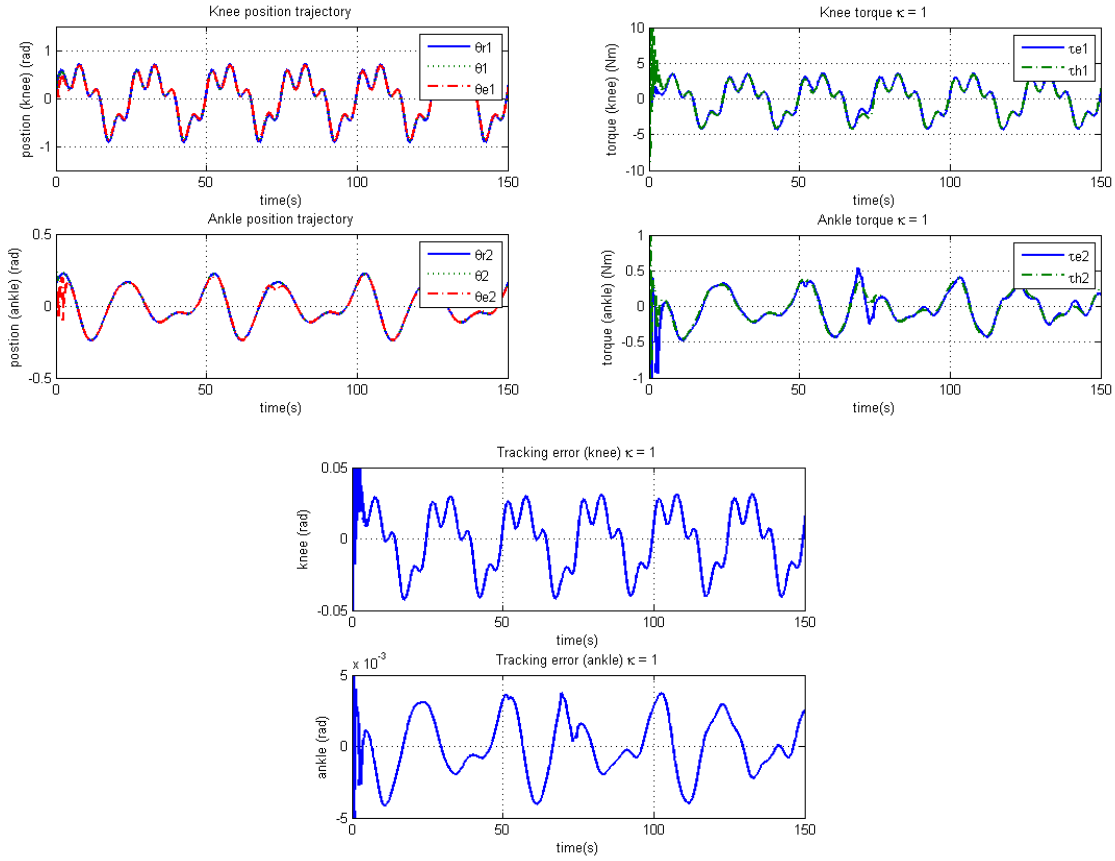
the adaptive oscillator parameters values $\eta = 5, \nu = 25$ are the same for each CPG representing the knee or ankle.

3.5.2 Results

With regards to Section. 3.5, the simulation results are presented in the figures below.

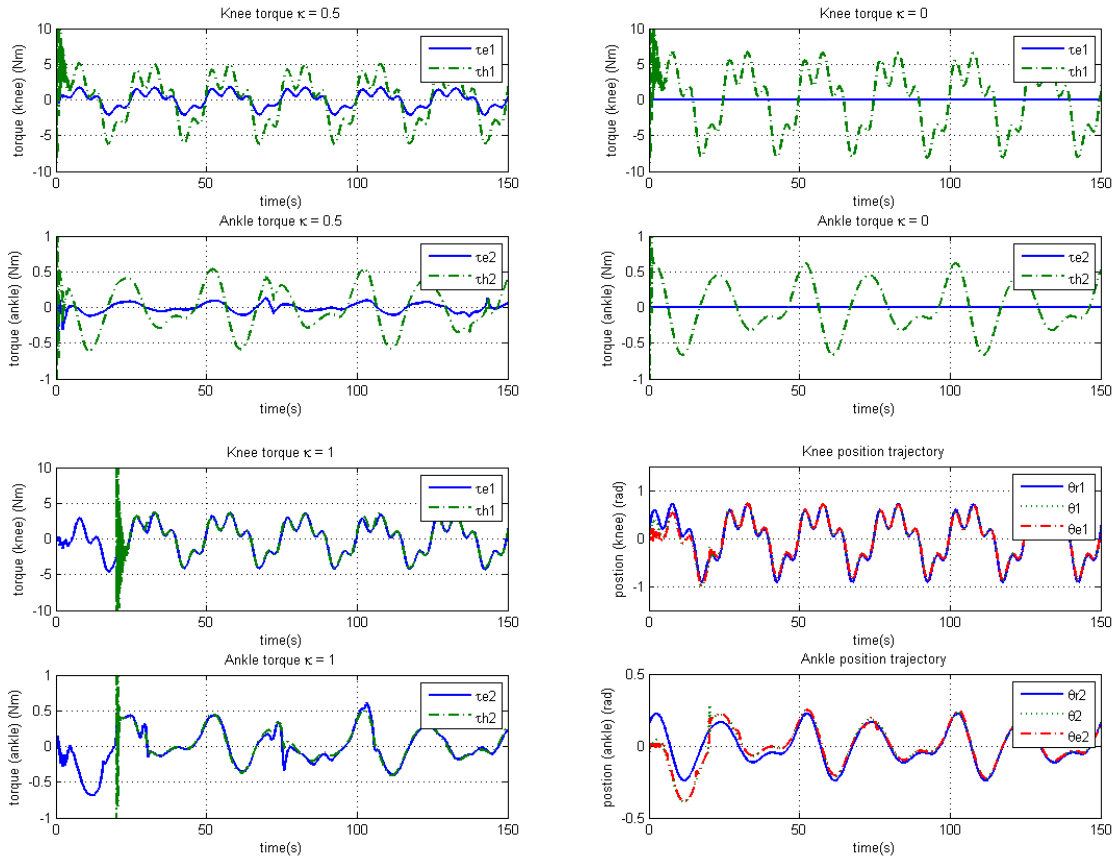
As shown in Fig. 3.4 (Top-Right), the adaptive oscillator was able to achieve phase synchronisation of all three trajectories which include the reference, actual and estimated angular positions (knee and ankle). A considerable replication of the reference trajectories was achieved with little finite time convergence for both positions. This is true for all the conditions which vary from $\kappa = 1$ (full assistance), $\kappa = 0.5$ (50 % assistance) and $\kappa = 0$ (no assistance). By observing Fig. 3.4 (bottom), the tracking errors for the angular positions (knee and ankle) are relatively small with RMS errors value of $0.01012rad$ for the knee position and $0.00308rad$ for the ankle position.

In Fig. 3.4 (Top-Right) and Fig. 3.5 (Top-Left & Top-Right), the level of assistance offered to the subject and the human torque of the subject are plotted vs. time. This is made to verify the effect of the assistance to the subject during a particular training session. It may be perceived from these figures that as the level of assistance decreases from $\kappa = 1$ to $\kappa = 0$, the human torque required to achieve the proposed task increases. The



θ_{r_1}, θ_1 & θ_{e_1} represents the reference, actual and estimated angular position trajectories of the knee respectively, while θ_{r_2}, θ_2 & θ_{e_2} signifies the reference, actual and estimated angular position trajectories of the ankle in the same order. This is same for Fig. 3.5 (Top-Right): Human (muscular) torque and assistive torque simulation of knee and ankle $\kappa = 1$. τ_{e_1} & τ_{h_1} defines the assistive torque and human torque for the knee respectively while τ_{e_2} & τ_{h_2} is same as regard the ankle. This is same for Fig. 3.5 (torque figures only), but having different assistive torques. The tracking error (Fig. 3.4 (Bottom)) is a measure of how close the assistive torque follows the human torque of which it is benchmarked, based on the difference between the actual trajectory and the reference trajectory. Note that, the assistive torque is seen as the torque generated by the exoskeleton, hence in full assistance, it is expected that the assistive torque is equal to the human torque since the patient is assumed to be passive at $\kappa = 1$. This allows an equal amount of torque in comparison to the PID generated human torque.

Figure 3.4: Top-Left: Position trajectory of knee and ankle with adaptive oscillator synchronisation. Top-Right: Assistive and Human torque. Bottom: Bottom: Tracking error result of knee and ankle with adaptive oscillator synchronisation.



It shows the interval of applied disturbance in human torque which is between 0 – 20s.

Figure 3.5: Top-Left: Human (muscular) torque and assistive torque simulation of knee and ankle $\kappa = 0.5$. Top-Right: Human (muscular) torque and assistive torque simulation of knee and ankle $\kappa = 0$. Bottom-Left: Human and assistive torque simulation of knee and ankle $\kappa = 1$ with disturbance. Bottom-Right: Position trajectory of knee and ankle with adaptive oscillator synchronisation in the presence of disturbance.

orthotic device can therefore fully or partially assist the patient concurrently showing the effect of "assist as needed".

To further authenticate the rendered assistive measures, a disturbance which exemplifies the state of inactivity of the human muscles at the knee and ankle is introduced to the knee-ankle orthotic device (system). Its introduction is made at the early phase of the training session with full assistive measure to compensate for this muscle inactiveness (i.e. at 0 – 20s). In real-life circumstances, it could be viewed as an obstruction to the movement of the shank-foot during the training session.

A significant ripple effect on the trajectories of the positions is observed in Fig. 3.5 (Bottom-Right) at the early stage but all the trajectories achieved phase synchronisation at the end of stipulated training session time. This is due to the full assistance given to the subject by the device. Fig. 3.5 (Bottom-Left)) virtually demonstrates this effect; having observed that the human torque was abnormal or ineffective between 0–20s, and the effect could be perceived in Fig. 3.5 (Bottom-Right), due to the tracking difficulties encountered as a result of the disturbance.

Initial spikes of the PID controller which generates the human torques may be seen in figures which describe the said torque pattern. This may be eliminated by tuning the PID parameters more efficiently. However, this is for simulation purpose only as the practical use will be to measure the angular position of the periodic motions of the shank and foot about the knee and ankle respectively. This parameter is then used to calculate the human torques in conjunction with the eventual assistive torques via the estimation of the position, velocity and acceleration by the AFO. For rehabilitative purpose only, a predefined trajectory as specified in the study will be introduced and tracked by the user via the AFO.

3.6 Conclusions and Future Works

This study proposed a rehabilitation protocol for lower limb disorders about the knee and ankle and also investigates the possibility of assisting the patient with such defects at both joint levels simultaneously. This was achieved by exploiting the rhythmic traits of CPGs for the purpose of developing a new rehabilitation protocol that requires the knee and ankle concurrent movement with the aid of a global coupling. An inverse dynamic model assumed to be a simple damped pendulum dynamics for each link was used to obtain a conceived movement pattern. Using chosen numerical data, the assistive orthotic device was affirmed effective. This was established by mimicking the muscular (human) torque with the aid of a PID controller.

In future works, the author intend to verify this assistive effect in the laboratory and also carry out parametric identification by the use of least square method and regression equations of Zatsiorsky ([Swevers, Ganseman, Tükel, De Schutter and Van Brussel \(1997\)](#)). This will be achieved by sampling the inverse dynamic model along stipulated trajectories of both the knee and ankle ([Khalil and Dombre \(1999\)](#)) or rather using system identification to find the dynamic model of the system at each joint. Furthermore, the final goal will be to implement this control method to specific human gait systems using its inverse dynamic model.

CHAPTER 4. Shank-Foot Trajectory Control: A Forward Dynamics Approach using Computed-Torque Control

4.1 Introduction

Developing wearable exoskeleton requires that, the control method employed, meets certain criteria. These criteria involve the exoskeleton controller capability to compensate for un-modelled dynamics, variations in payloads, friction and disturbance torques, parametric variations and noises accounted in measurement ([Merabet and Gu \(2010\)](#)). By fulfilling these criteria, the safety of the user is somehow guaranteed. Several research works relevant to the control of exoskeleton/orthotic device are well documented in published articles. See Section. [2.5](#). It may be deduced from these works that, to achieve the intended purpose of designing a rehabilitative protocol for subjects with lower limb disabilities, the desired trajectory (gait pattern or joint space trajectory) to be followed and a suitable control method to guarantee a fair trajectory tracking of the actuated lower limb exoskeleton/orthosis is paramount. Note that the dynamics of the

system represents an integral part of the overall rehabilitative system and determines the number of DoF to be actuated, except for underactuated¹ systems.

Computed-torque control represents a special application of feedback linearisation of nonlinear systems and has been used extensively in most robotic system due to its robustness (Lewis, Dawson and Abdallah (2003)). In this regard, the computed-torque control may present a platform for the comparison of the torque required by the orthosis based on similar trajectories. In (Williamson (1999a)), an analysis technique aimed at alleviating the difficulty of tuning Matsuoka oscillator was addressed. This method was applied to produce rhythmic commands of the joints of a robotic arm in (Williamson (1999b)), and feedback of the joint motions was used to modify the oscillator behaviour. However, this was implemented on real-system and therefore highlighted only the behaviour of the oscillator as compared to the eventual task of the robotic arm.

In this work, it is intended to demonstrate these features by employing the dynamic equation of motion of a two degrees of freedom system to depict the dynamics of a shank-foot model. The test-bed for which this system is to be experimented is a rigid system and may be equipped with a self-aligning mechanism to cushion the effect of misalignment. Hence, this justifies the assumption that the exoskeleton and the human axes coincide. See Fig. 4.1.

In this chapter a forward dynamic approach for shank-foot trajectory control using the computed-torque control method is proposed. A method for obtaining coordinated dynamic behaviour for a knee-ankle orthosis is also presented. The idea is aimed at providing rehabilitative measures to help patients with lower limb disorders to improve their mobility. This is achieved by designing the desired trajectories for which the shank-foot model follows or rather adapt to in order to achieve this rehabilitative purpose. Hence, two desired trajectories were defined using inverse kinematic transformation and

¹This is a technical term used in robotics and control theory to describe mechanical systems that cannot be commanded to follow arbitrary trajectories in configuration space.

Matsuoka oscillators.

The inverse kinematic transformation method is employed to convert the specified circular trajectory into joint space trajectories for the purpose of control, while the Matsuoka oscillator has no explicit desired trajectory since it is being generated internally by its dynamics. The nonlinear forward dynamics of the Shank-Foot model is derived using Lagrange's equation to describe the two degrees of freedom (DoF) system. Computed-Torque (PID) control method is used for tracking the circular designed trajectory, whereas a simple (PD) control law incorporated into the Computed-Torque is used for the tracking of the internally generated trajectory of the oscillator. Tracking capabilities of both control methods based on each trajectory in the presence of external disturbance and joint friction were analysed using MATLAB/SIMULINK. The results obtained shows a satisfactory performance of the proposed strategy.



Figure 4.1: Exoskeleton "test-bed".

4.2 Shank-Foot Model

The shank-foot is made of a planar two-link model with revolute joints which represent the knee and the ankle (see Fig. 3.1). For clarity purposes, q_1 represents θ_1 and q_2 represents θ_2 . The description of the model is given in Section. 3.2.

4.3 Dynamic Equation of Motion

The general form of the equations of motion is given in (Lewis, Dawson and Abdallah (2003)), but for simplicity it may be reduced as below:

$$M(q)\ddot{q} + N(q, \dot{q}) + \tau_d = \tau \quad (4.1)$$

- where $q \in \mathfrak{R}^n$ is the joint position variable vector.
- $\dot{q} \in \mathfrak{R}^n$ the joint velocity variable vector.
- $\ddot{q} \in \mathfrak{R}^n$ the joint acceleration variable vector.
- $M(q) \in \mathfrak{R}^{n \times n}$ the mass matrix.
- $\tau_d \in \mathfrak{R}^n$ the uncertainty torque vector.
- $\tau \in \mathfrak{R}^n$ the externally applied generalised forces.
- With $N(q, \dot{q}) = C(q, \dot{q})\dot{q} + F(\dot{q}) + G(q)$ which is the nonlinear term and depicted as $C(q, \dot{q}) \in \mathfrak{R}^n$ the Coriolis/centripetal vector, $F(\dot{q}) \in \mathfrak{R}^n$ being the joint friction torque vector and $G(q) \in \mathfrak{R}^n$ the gravity torque vector.
- n simply refers to the dimension of the vectors above, which is two in this case.

Assuming that the mass is distributed along the links of the shank-foot model, the equation of motion is given as below:

Mass matrix:

$$\begin{aligned}
M(q)_{1,1} &= I_1 + I_2 + m_1L_2^2 + 2m_2L_1r_2\cos(q_2) \\
M(q)_{1,2} &= I_2 + m_2L_1r_2\cos(q_2) \\
M(q)_{2,1} &= I_2 + m_2L_1r_2\cos(q_2) \\
M(q)_{2,2} &= I_2
\end{aligned} \tag{4.2}$$

Coriolis/centripetal vector:

$$\begin{aligned}
C(q, \dot{q})_{1,1} &= -2m_2L_1r_2\sin(q_2)\dot{q}_2 + b_1 \\
C(q, \dot{q})_{1,2} &= -m_2L_1r_2\sin(q_2)\dot{q}_2 \\
C(q, \dot{q})_{2,1} &= m_2L_1r_2\sin(q_2)\dot{q}_1 \\
C(q, \dot{q})_{2,2} &= b_2
\end{aligned} \tag{4.3}$$

Gravity vector:

$$\begin{aligned}
G(q)_1 &= (m_1r_1 + m_2L_1)g\sin(q_1) + m_2gr_2\sin(q_1 + q_2) \\
G(q)_2 &= m_2gr_2\sin(q_1 + q_2)
\end{aligned} \tag{4.4}$$

Joint friction torque vector:

$$F_n = v_n\dot{q}_n \tag{4.5}$$

Disturbance torque vector:

$$\tau_{dn} = k_n\text{sgn}(\dot{q}_n) \tag{4.6}$$

where k_n is given as a sine signal in Table. 4.1. Since both actuators are needed the externally applied torque is therefore:

$$\tau_n = 1 \tag{4.7}$$

Note that the generalised torque γ_i is written as:

$$\gamma_n = \tau_n - b_n\dot{q}_n \tag{4.8}$$

Hence, the damping coefficient b_n is included in the Coriolis/centripetal vector equation.

The above dynamic equation of motion was based on Lagrange's method of derivation for mechanical systems.

4.4 Path Generation: Desired & Internally Generated Trajectory

This section defines the task to be performed by the shank-foot (knee-ankle orthosis) model in order to actualise its rehabilitative purpose. It also shows how to convert a given prescribed path from Cartesian space to joint space. Given certain desired points the shank-foot model should pass through, a method used to reconstruct the continuous desired trajectory is shown. It further presents how trajectories are internally generated via the Matsuoka oscillator.

Consider the shank-foot model designed to follow a given cartesian trajectory $p(t) = (x(t), y(t))$ in the (x, y) plane as a function of time as shown in Fig. 4.2. The principle behind this is to enable the user of this knee-ankle orthosis to perform this circular motion repeatedly for the purpose of the rehabilitation of both joints concurrently.

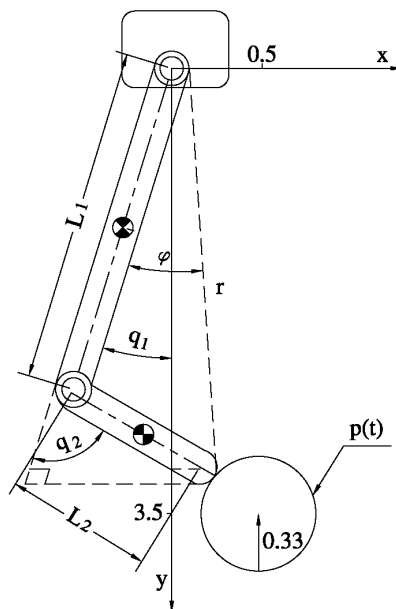


Figure 4.2: Shank-Foot Desired Points.

The lower-limb is controlled by the actuators via angles q_n for $n = 1, 2$, hence it is expected

dient that the cartesian trajectory $(x(t), y(t))$ is converted into a joint space trajectory $(q_1(t), q_2(t))$ for the purpose of control.

The circular path is defined as a function of time (t) as

$$\begin{aligned} x(t) &= 0.5 + 0.33\sin(t) \\ y(t) &= -3.5 - 0.33\cos(t) \end{aligned} \tag{4.9}$$

Calculating this joint space trajectory requires the use of inverse kinematic transformations, considered in (Lewis, Dawson and Abdallah (2003)). The transformation to determine q_2 , q_1 , and ψ in Fig. 4.2 is defined as follows:

$$\begin{aligned} r(t)^2 &= x(t)^2 + y(t)^2 \\ \cos(q_2(t)) &= A = \frac{r(t)^2 - L_1^2 + L_2^2}{2L_1L_2} \\ B &= \pm\sqrt{1 - \cos^2(q_2)} = \pm\sqrt{1 - A^2} \\ q_2 &= \arctan2(B, A) \\ \tan\psi &= \frac{-(L_1 + L_2\cos(q_2))}{L_2\sin(q_2)} \\ \tan(\psi + q_1) &= \frac{y}{x} \\ q_1 &= \arctan2(y, x) = -\arctan2(-(L_1 + L_2\cos(q_2)), L_2\sin(q_2)) \end{aligned} \tag{4.10}$$

Considering the internally generated trajectory, the oscillator employed is a vastly used oscillator (although tuned to suit the behavioural pattern to be established) proposed by Matsuoka in (Matsuoka (1985)). This oscillator has been analysed in Section A.3.

4.5 Computed-Torque Control

The Computed-Torque control is basically referred to as feedback linearisation. It is seen as a standard technique used for the control of non-linear systems. In this section, the concept of the said Computed-Torque control is discussed with the inclusion of the PID and simple PD laws.

4.5.1 Computed-Torque PID Control

With reference to Eq. 4.1, it is expected that the desired trajectory q_d has been defined for the proposed motion, therefore the model based control law is given as in (Lewis, Dawson and Abdallah (2003)):

$$\tau = M(q)(\ddot{q}_d - u) + N(q, \dot{q}) + \tau_d \quad (4.11)$$

with \ddot{q}_d the second derivative of q_d .

Consider a PID feedback loop for the system control design $u \in \mathfrak{R}^n$ (stabilising input); The control law may therefore be written as

$$\tau = M(q)(\ddot{q}_d + K_v \dot{e} + K_i \int e + K_p e) + N(q, \dot{q}) + \tau_d \quad (4.12)$$

where $e \in \mathfrak{R}^n$ is the position error signal $q_d - q$ and $\dot{e} \in \mathfrak{R}^n$ the velocity error signal $\dot{q}_d - \dot{q}$. $K_p \in \mathfrak{R}^n$, $K_i \in \mathfrak{R}^n$, $K_v \in \mathfrak{R}^n$ are the proportional, integral and derivative gains of the controllers.

4.5.2 Computed-Torque simple PD Control

In order to generate this trajectory internally, a Matsuoka oscillator is connected to the shank-foot at the knee and ankle joints (i.e. one oscillator each). The equation of the Matsuoka oscillator may be given by

$$\begin{aligned} \tau_1 \dot{x}_1 &= c - x_1 - \beta v_1 - \gamma y_2 - \sum_j h_j [g_j]^+ \\ \tau_2 \dot{v}_1 &= y_1 - v_1 \\ \tau_1 \dot{x}_2 &= c - x_2 - \beta v_2 - \gamma y_1 - \sum_j h_j [g_j]^- \\ \tau_2 \dot{v}_2 &= y_2 - v_2 \\ y_i = [x_i]^+ &= \max(x_i, 0) \\ y_{out} &= y_1 - y_2 \end{aligned} \quad (4.13)$$

In Eq. 4.13, lines 1–2 represent $neuron_1$ while lines 3–4 represent $neuron_2$. The definition of each parameter are given as follows: β & γ are constants that relates to the external inhibitory input and mutual inhibition of the neurons respectively. Its parameter ranges are defined in (Matsuoka (1985)). c is a tonic parameter which determines the amplitude of the oscillator output while, τ_1 & τ_2 are time constants and they determine the frequency and shape of the output. x_i & v_i are the state variables, where $i = 1, 2$. The inputs to each oscillator are via g_j with a gain of h_j , and are applied as a positive part to one neuron and as a negative part to the other neuron, where j is the number of inputs. y_{out} is the output. Each neuron receives an excitatory tonic input, a mutual inhibition, and an external inhibitory input.

The knee and ankle joint angles $q \in \mathfrak{R}^n$ are used as the input g while the oscillator output $q_d \in \mathfrak{R}^n$ is considered as the internally generated trajectory. This principle ascertain the example used in Section A.3. This was envisaged so as to design a control method using the natural dynamics of the shank-foot. The trajectory may therefore be defined as

$$q_d = y_{out} \quad (4.14)$$

To assure the control of each of the joints, a stabilising input $u \in \mathfrak{R}^n$ (simple PD control law) is used as defined in (Williamson (1999b)):

$$u = k(q_d - q) - b\dot{q} \quad (4.15)$$

where $k \in \mathfrak{R}^n$ is the stiffness of the joint and $b \in \mathfrak{R}^n$ the damping coefficient. The rest of the parameters remain as defined in Eq. 4.5.1. Note that the damping coefficient is not included in the dynamic equation of motion when this stabilising input is used.

The control law that determines the actuated torque is thus written as

$$\tau = M(q)(\ddot{q}_d - k(q_d + q) + b\dot{q}) + N(q, \dot{q}) + \tau_d \quad (4.16)$$

Table 4.1: Physiological Parameters.

Parameters	Units	Values
Shank length (L_1)	m	0.2
Foot length (L_2)	m	0.08
Shank mass (m_1)	kg	2.80
Foot mass (m_2)	kg	1.17
Shank inertia (I_1)	$kg.m^2$	0.075
Foot inertia (I_2)	$kg.m^2$	0.012
gravity (g)	m/s^2	9.8
Shank damping Coefficient b_1	Nm/s^2	0.4
Foot damping Coefficient b_2	Nm/s^2	0.6
Knee joint angle $q_1(0)$ <i>initial condition</i>	rad	0.5
Ankle joint angle $q_2(0)$ <i>initial condition</i>	rad	0.2
Knee joint friction threshold v_1	rad	2.35
Ankle joint friction threshold v_2	rad	0.87
$k_n(\tau_d)$	rad	$5\sin(4\pi t)$

4.6 Numerical Simulations

In this section, the simulations and the eventual results and the proposed task are presented and then discussed. First, the simulations pertaining to the PID control law is analysed, followed by the simple PD law. The assumed physiological parameters for the dynamical model (shank-foot) are given in Table 4.1. Note that the value of the inertia is calculated assuming cylindrical links and thus calculated as $I_{g_i} = I_{z_i} = \frac{2}{3}m_iL_i^2$.

The PID controller parameters are given as below and resultant figures signify the performance of the control law:

- $K_p = 400, K_i = 10$, is the knee and ankle "PI" parameters. This is same for both knee and ankle,
- $K_v = 40, 80$, the respective knee and ankle "D" parameter for the stabilising controllers.

In the case of the PD control, the trajectory is internally generated by the Matsuoka

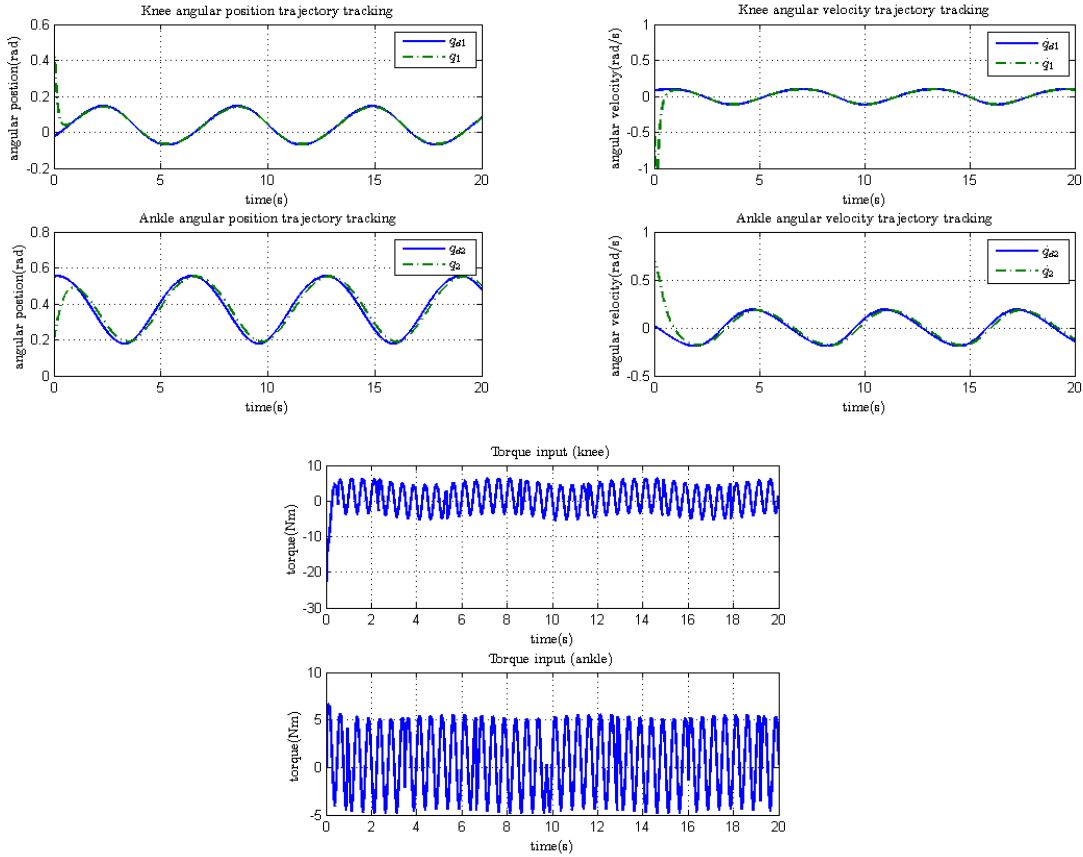


Figure 4.3: Top-Left: Angular position trajectory tracking based on Computed-Torque PID controller. Top-Right: Angular velocity trajectory tracking based on Computed-Torque PID controller. Bottom: Applied torque.

oscillators. Below are the figures which represent the simulation results. Firstly, the parameters for the oscillator and the control law parameters used are as follows.

- $k = 100, 140$, is the respective gain for knee and ankle.
- $b = 0.4, 0.6$ is the damping coefficient of the knee and ankle respectively for the stabilising controllers.
- The parameters for the Matsuoka oscillator are given as follows. Note that the parameters are the same for the oscillator connected to the knee and that connected to the ankle: $\tau_1 = 0.5, \tau_2 = 0.25, c = 0.1, \beta = 2, \gamma = 2$ and $h \leq 0.9$. A ratio of

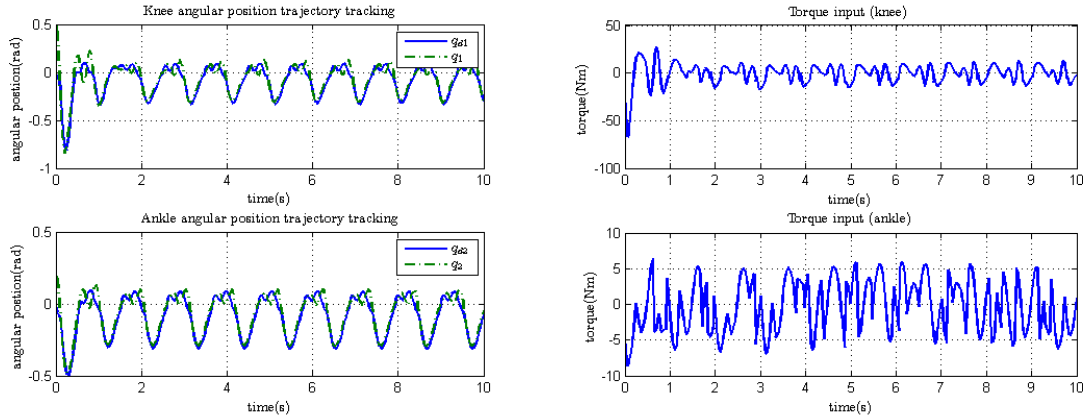


Figure 4.4: Left: Angular position trajectory tracking based on Computed-Torque simple PD controller. Right: Applied Torque

1 : 0.5 was considered for $\tau_1 : \tau_2$ to guarantee a stable oscillation. These parameters were tuned to achieve the expected result.

4.7 Discussion

Simulations were conducted using the shank-foot model to describe the knee-orthosis worn by a subject in a sitting position with flexion/extension at the knee level and plantar-flexion/dorsal-flexion at the ankle level. The simulations are divided into two parts. First, a desired trajectory is developed for the subject, and the computed-Torque PID controller is used to develop the applied torque necessary to track the desired position and velocity. Second, a Matsuoka oscillator is used to develop an internally generated trajectory based on the natural dynamics of the shank-foot. A Computed-Torque simple PD controller was designed to provide the required torque to track the angular position as expected. In both cases a sinusoidal disturbance torque and a joint friction torque were applied to the knee-ankle orthosis to evaluate the robustness of the controllers against perturbations.

Consider tracking the desired trajectory using the Computed-Torque PID controller.

Fig. 4.3 (Top-Left & Top-Right) shows that the controller is able to function as expected, with a high performance with respect to tracking the desired position and velocity trajectories. It took less than a (1) second for it to track the position trajectory, and less than two (2) seconds for it to track the velocity trajectory. The tracking errors of the position and velocity are comparatively very small: with Root-Mean-Square (RMS) values of $RMS_{position} = 0.00089rad$ and $RMS_{position} = 0.00617rad$ for the knee and ankle respectively, and $RMS_{velocity} = 0.00013rad$ $RMS_{velocity} = 0.002459rad$ also for the knee and ankle respectively. With regards to the torque it can be observed in Fig. 4.3 (Bottom) that the applied torque to the knee-ankle orthosis is acceptable for a dynamic system of this nature based on its given parameters.

Consider next tracking the oscillator-generated trajectory using the Computed-Torque simple PD controller. The internally generated trajectory and its tracking capabilities of the position of the knee-ankle orthosis are presented in Fig. 4.4 (Left). The oscillator is able to demonstrate the ability to generate trajectories internally based on the input via the joint angles q_1 & q_2 . It should be noted that the idea behind this is demonstrate this ability. However, the final motion depends solely on the interaction between the oscillator dynamics and the knee-ankle orthosis dynamics. Tuning the oscillator's parameters to achieve the desired final motion is required. The torque applied to the orthosis is also tolerable for this system and can be seen in Fig. 4.4 (Right). In comparison, both torque limits lie within almost the same value.

4.8 Conclusion and Further Works

In this study, a pre-specified trajectory control method for an actuated knee-ankle orthosis has been proposed. The torques were applied at the knee and ankle joint to perform a desired movement pattern termed as a "rehabilitation protocol" to help patients restore their lower limb motor functions. This could be achieved by performing this task repet-

itively until the lower limb is able to function independently. It also explores the use of oscillators to demonstrate the ability of the shank-foot to exhibit natural dynamics when excited at the joint levels. The Matsuoka oscillator was used to generate a specific trajectory for the knee-ankle orthosis in a way; by establishing an interaction between the oscillator and the system itself. It does provide a low gain system as compared to traditional control and eliminates the complexity of planning desired trajectory.

In both cases, the controllers used gave a satisfactory tracking capability and the torque limits may be compared to lie almost within the same limits. This has been used to authenticate the proposed scheme. The controllers also showed a high robustness against external disturbance. It should be noted that measurement noise was not taken into account. This is due to the fact that, measurement noise is inherent in sensor measurements based on the uncertainty that occur within sensors, however filters can be used to eliminate such effects before being fed to the controller. Further works will be solely based on real-life implementation.

CHAPTER 5. Rhythmic Trajectory Design and Control

5.1 Introduction

Mobility disorder caused by SCI or related illnesses in people has been on the increase in recent years ([Chen, Ma, Qin, Gao, Chan, Law, Qin and Liao \(2016\)](#)). To help alleviate the difficulties these people go through, in order to carry out their day to day activities, requires certain robotic devices. Wearable robotic systems such as lower limb exoskeletons do not only provide effective and repetitive gait training, but also reduce the burden of physiotherapists. This is because it allows the integration of the human intelligence with that of the mechanical power of the robot. Among other applications, these devices may be required for gait rehabilitation and human locomotion assistance. Rehabilitation via exoskeletons is of great importance to people with lower limb disorders. For any exoskeleton to perform its required function, it has to be equipped with some form of control mechanism.

Initiating a control mechanism involves generating a reference input signal which is expected to go through the controller in order to produce the control signal necessary to drive the actuators of the exoskeleton. In gait rehabilitation and human locomotion assistance, the wearer depends almost solely on the torque generated by the exoskeleton

device. This is because the joint torque generated by the muscles of the wearer is either infinitesimally small or zero. Generating a reference input (desired motion) signal does not have to be arbitrary since it has to suit the natural envisaged motion (nerve signals) of the wearer developed by the brain. This does give rise to the use of CPGs to produce such signal that is closely related to the nerve signals.

CPG generated signals have in many ways contributed to the design of reference inputs that commensurate with the human movement behaviour. However, most of these signals have been used to stimulate the wearer-exoskeleton at their joint levels without considering the dynamic equation of motion of the wearer-exoskeleton. See Section. 2.4. This may be seen among others in (Righetti and Ijspeert (2006); Dutra, de Pina Filho and Romano (2003); Zielinska, Chew, Kryczka and Jargilo (2009)). This study, therefore utilises CPG-generated signals as input to a motion controller while introducing the dynamic equation of the exoskeleton.

The walking cycle is characterised by a complete step which spans through phases known as DSP-SSP-DSP. CPG-generated walking signal such as that of (Bay and Hemami (1987)) does prove this assumption. See subsection. 5.2.2. Nevertheless, deriving the equations for the various phases of walking such as in (Tzafestas, Raibert and Tzafestas (1996)) may require splitting this CPG-generated signals into phases. This eliminates the purpose of the rhythmic behaviour of wearer-exoskeleton proposed in this study. In this work, the SSP dynamic equation of the wearer-exoskeleton may be used to represent its dynamic behaviour, since the oscillator outputs are mapped out in such a way so as to represent its joint angle profile. See subsection. 5.3.2. To eliminate the discontinuities¹ due to robot-ground collision, the robot-ground contact is not considered.

For this purpose, a well-known robust controller in the form of a computed-torque control is employed to investigate this assumption. Thus, allowing the controller to compensate

¹ This is due to a sudden change in the angular velocities of the joint when the robot touches the ground.

for the un-modelled dynamics. The disturbance torque introduced to the system may serve as an inclusion of the measurement noise. This proposed rehabilitation strategy which is solely based on trajectory tracking control is validated by simulation. This is to achieved both limit cycle walking and sustained local stability.

5.2 CPG Model Design

In this section, the coupled van der Pol oscillators' differential equations used in the generation of the walking trajectory are analysed. In addition, the periodic sequence with the inclusion of the phase transition is discussed.

5.2.1 Coupled van der Pol Oscillators

Here, CPG-generated hip and knee joint angle profiles are synthesised via coupled Van der Pol oscillators. Fig. 5.1 and Fig. 5.3 show the coupling nature and the joint angle trajectories/phase plots respectively. The values of the oscillators parameters used in generating the hip and knee angles for walking are given in Table 5.1.

Table 5.1: Values of Oscillators Parameters

Parameters	Symbol/Values			
Damping Strength	μ_1 2	μ_2 1	μ_3 2	μ_4 1
Amplitude	p_1^2 1	p_2^2 2	p_3^2 1	p_4^2 2
Frequency	g_1^2 17	g_2^2 22	g_3^2 17	g_4^2 22
Offset	ϕ_1 -1	ϕ_2 10	ϕ_3 -1	ϕ_4 10
Coupling Coefficients	λ_{21} -0.2 λ_{13} 0.2	λ_{31} 0.2 λ_{43} -0.2	λ_{12} -0.2 λ_{24} 0.2	λ_{42} 0.2 λ_{34} -0.2

Based on [Bay and Hemami \(1987\)](#) the differential equation representing the bidirectional local coupling of the van der Pol oscillator are given by

$$\begin{aligned}
 \ddot{x}_1 - \mu_1(p_1^2 - x_a^2)\dot{x}_1 + g_1^2 x_a &= \phi_1 \\
 \ddot{x}_2 - \mu_2(p_2^2 - x_b^2)\dot{x}_2 + g_2^2 x_b &= \phi_2 \\
 \ddot{x}_3 - \mu_3(p_3^2 - x_c^2)\dot{x}_3 + g_3^2 x_c &= \phi_3 \\
 \ddot{x}_4 - \mu_4(p_4^2 - x_d^2)\dot{x}_4 + g_4^2 x_d &= \phi_4
 \end{aligned} \tag{5.1}$$

where x_i is the output signal, p_i^2 represents the amplitude, g_i^2 refers to the frequency, ϕ_i the offset parameter, μ_i indicates the nonlinearity and the damping strength while x_{a-d} is the coupling equations and mathematically written as

$$\begin{aligned}
 x_a &= x_1 - \lambda_{21}x_2 - \lambda_{31}x_3 \\
 x_b &= x_2 - \lambda_{12}x_1 - \lambda_{42}x_4 \\
 x_c &= x_3 - \lambda_{13}x_1 - \lambda_{43}x_4 \\
 x_d &= x_4 - \lambda_{24}x_2 - \lambda_{34}x_3
 \end{aligned} \tag{5.2}$$

with λ_{ij} , ($i \neq j$) refers to the coupling coefficient.

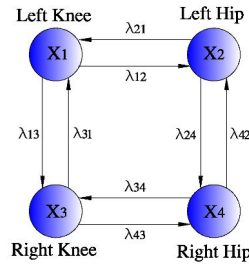


Figure 5.1: Nature of Coupling between the Oscillators

The scaling and shifting equation analysed in [Roy and Demiris \(2005\)](#) is given by

$$\begin{aligned}
 X_1 &= x_1 \cdot 10 - 22 \\
 X_2 &= x_2 \cdot 5 + 30 \\
 X_3 &= x_3 \cdot 10 - 22 \\
 X_4 &= x_4 \cdot 5 + 30
 \end{aligned} \tag{5.3}$$

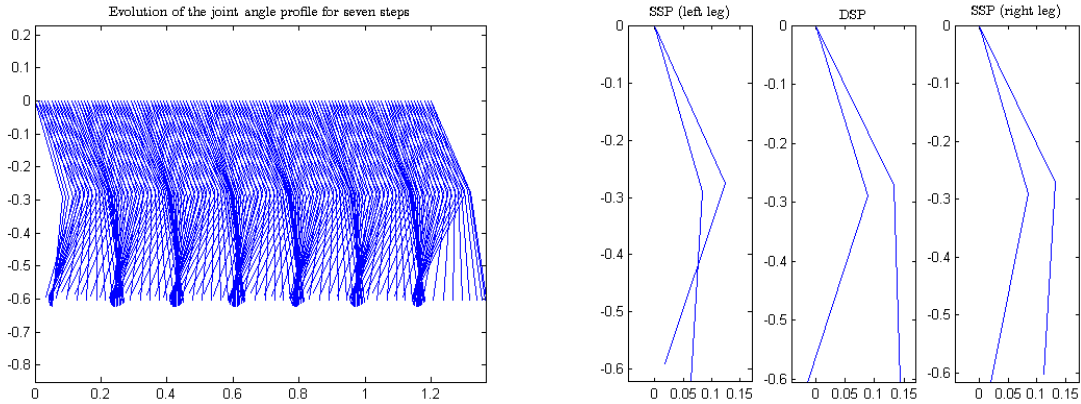


Figure 5.2: Stick diagram of joint angles profile evolution. Left: Fast succession. Right: Phases captured in frames

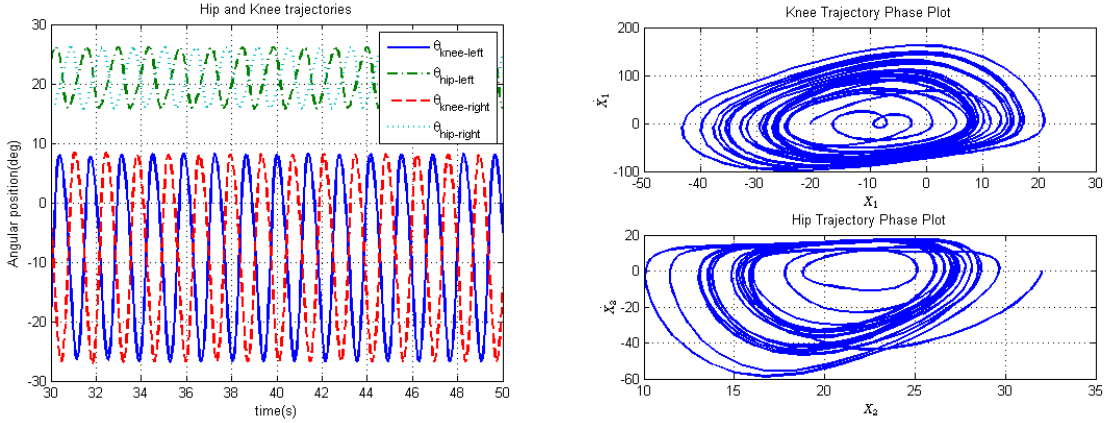
5.2.2 Periodic Sequence

A human gait cycle may be regarded as a complete step or walking cycle. This cycle extends from heel strike to heel strike of one leg and includes the stance and swing phases of both legs. It may be divided into the 'single support phase' (SSP)² and the 'double support phase' (DSP)³. The latter tends to take place at a relatively small time interval.

One of the most interesting features of the rhythmic pattern modelling for joint trajectories using coupled oscillators is the periodic sequence of leg transfers (Zielińska (2009)). The transition between SSP and DSP are thus generated automatically and followed accordingly by the human-exoskeleton (see Fig. 5.2 for an exemplary structure of the walking pattern). Fig. 5.2 (Left) presents the stick diagram of the joint angle profile as it changes from SSP to DSP in fast succession. The joint angle profile represents a continuous change of repeated angular position values with time. It is therefore structured to produce a particular walking pattern which may be defined by the physiotherapist, and should be followed by the human-exoskeleton. This fits the concept of rehabilitative

²This is characterised by one limb moving forward while the other is in contact with the floor.

³This represents the instant when both limbs are in contact with the floor.



The initial conditions used to achieve this plots are: $x_1 = 8.8^\circ$, $x_2 = 22.9^\circ$, $x_3 = -27.0^\circ$, $x_4 = 17.0^\circ$, $\dot{x}_1 = -1.0^\circ/sec$, $\dot{x}_2 = 1.0^\circ/sec$, $\dot{x}_3 = -31.0^\circ/sec$, & $\dot{x}_4 = 43.0^\circ/sec$. Note that the plot only considered steady state values.

Figure 5.3: Hip and Knee trajectories generated via van der Pol oscillators and phase plots.

walking.

Fig. 5.2 (Right) presents the capturing of the robot movement in frames which represent the individual phases. For clarity purposes and for a more visual transition, a small sampling time of $1.2ms$ was introduced. Hence, sampling time connotes $1s$ to represent $1.2ms$ in subsequent figures. Fig. 5.4, demonstrates the transition phases in Fig. 5.2 (Right) using its angular position variation with respect to the sampling time. (See subsection. 5.4.3) for the trajectory mapping as indicated in the figures. Fig. 5.4 (Top-Left) presents a single support phase (SSP) with the left leg as the support leg while the right leg swings forward. Fig. 5.4 (Top-Right) also presents a single support phase (SSP) but this time around it is the opposite, i.e. right leg as support leg while the left leg swings forward. Fig. 5.4 (Bottom) presents the time both feet are on the ground i.e. DSP. Note that variations of angular position are about the joint level and these variations are to the vertical axis.

For simplicity, the hip angular variation is used for the analysis of these phases. In the

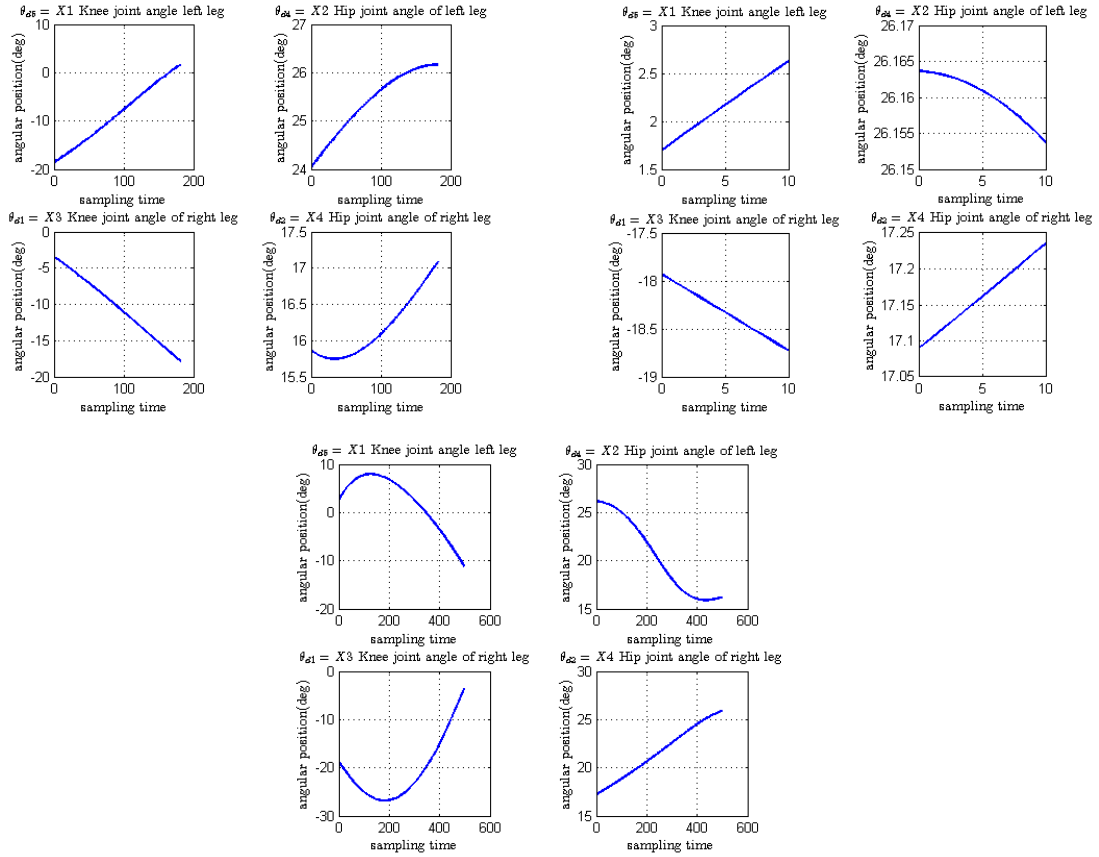


Figure 5.4: Phase transition of the CPG walking gait - *SSP left leg, DSP & SSP right leg*

single support phase (left leg), there seems to be a more rapid increase in the hip angle of the left leg as opposed to the increase in the right leg. For the DSP, angular position variation about the hip joints are very slow and this is evident in Fig. 5.2 (Right). At DSP, humans are not static since there is bound to be an anticipation of the next movement. Finally, in the single support phase (right leg), the same rapid increase as in the previous support phase is seen in the hip angle of the right leg while the left leg hip angular position variation is seen as a decrease. The discrepancies between angular position variation of these phases (SSP left leg & right leg) are as a result of their starting positions.

5.3 Human-Exoskeleton Dynamics

This section addresses the modelling of the human-exoskeleton dynamics conceived as a five-link bipedal system having a single support in a sagittal plane by means of Lagrangian principles. A 2D CAD model of the five-link planar biped model is given in Fig. 5.5. See Fig. 4.1 also for the test-bed envisage for the testing of this study. The CAD model is assumed to incorporate the parameters of the exoskeleton and the user's lower limb in conjunction with the chest attachment. The links consist of the torso (link 3) and two links on each leg which constitute the thigh (link 2 & link 4) and the shank (link 1 & link 5). The links are connected via four actuated brushless motor at the hips and knee joint level and hence modelled as such in the CAD model. This model does not possess ankle joints but feet as being introduced in the real model to help assist its stability during its movement.

5.3.1 Lagrangian equation of motion

The general form of the equations of motion is then arranged as

$$M(\theta)\ddot{\theta} + C(\theta, \dot{\theta}) + G(\theta) = \tau_{\theta} \quad (5.4)$$

where $M(\theta) \in \mathfrak{R}^{n \times n}$ the inertia matrix, $C(\theta, \dot{\theta}) \in \mathfrak{R}^n$ the Coriolis/centripetal vector, $G(\theta) \in \mathfrak{R}^n$ the gravity torque vector and $\tau \in \mathfrak{R}^n$ the externally applied generalised forces. n simply refers to the dimension of the vectors above, which is 5 in this case. The description of the parameters given in Fig. 5.5 are given as below.

- m_i is the mass of link i .
- I_i is the moment of inertia of link i .
- l_i is the length of link i .

- l_{ci} is the distance between the centre of mass (CoM) and the end of link i .
- θ_i is the angle of link i with respect to the vertical, where $i = 1, 2, 3, 4, 5$.
- q_i is the relative angle of link i , where $i = 0, 1, 2, 3, 4$.
- (x, y) is the main coordinate reference system established to have the origin at the point of contact to the ground (i.e at link 1). The x axis are aligned horizontally and y axis are positive in the vertical direction.

Based on the kinematic relationship between the links, the coordinate of the CoM (x_{c_i}, y_{c_i}) of each link i may be given as

$$\begin{aligned}
x_{c_1} &= l_{c1} \sin(\theta_1) \\
y_{c_1} &= l_{c1} \cos(\theta_1) \\
x_{c_2} &= l_1 \sin(\theta_1) + l_{c2} \sin(\theta_2) \\
y_{c_2} &= l_1 \cos(\theta_1) + l_{c2} \cos(\theta_2) \\
x_{c_3} &= l_1 \sin(\theta_1) + l_2 \sin(\theta_2) + l_{c3} \sin(\theta_2) \\
y_{c_3} &= l_1 \cos(\theta_1) + l_2 \cos(\theta_2) + l_{c3} \cos(\theta_2) \\
x_{c_4} &= l_1 \sin(\theta_1) + l_2 \sin(\theta_2) + (l_4 - l_{c4}) \sin(\theta_4) \\
y_{c_4} &= l_1 \cos(\theta_1) + l_2 \cos(\theta_2) - (l_4 - l_{c4}) \cos(\theta_4) \\
x_{c_5} &= l_1 \sin(\theta_1) + l_2 \sin(\theta_2) + l_4 \sin(\theta_4) + (l_5 - l_{c5}) \sin(\theta_5) \\
y_{c_5} &= l_1 \cos(\theta_1) + l_2 \cos(\theta_2) - l_4 \cos(\theta_4) - (l_5 - l_{c5}) \cos(\theta_5)
\end{aligned} \tag{5.5}$$

The velocity of the CoM for each link i may be given as

$$\begin{aligned}
 vc_1 &= \begin{pmatrix} l_{c1}\cos(\theta_1) \\ -l_{c1}\sin(\theta_1) \end{pmatrix} \dot{\theta}_1 \\
 vc_2 &= \begin{pmatrix} l_1\cos(\theta_1) \\ -l_1\sin(\theta_1) \end{pmatrix} \dot{\theta}_1 + \begin{pmatrix} l_{c2}\cos(\theta_2) \\ -l_{c2}\sin(\theta_2) \end{pmatrix} \dot{\theta}_2 \\
 vc_3 &= \begin{pmatrix} l_1\cos(\theta_1) \\ -l_1\sin(\theta_1) \end{pmatrix} \dot{\theta}_1 + \begin{pmatrix} l_{c2}\cos(\theta_2) \\ -l_{c2}\sin(\theta_2) \end{pmatrix} \dot{\theta}_2 + \begin{pmatrix} l_{c3}\cos(\theta_3) \\ -l_{c3}\sin(\theta_3) \end{pmatrix} \dot{\theta}_3 \\
 vc_4 &= \begin{pmatrix} l_1\cos(\theta_1) \\ -l_1\sin(\theta_1) \end{pmatrix} \dot{\theta}_1 + \begin{pmatrix} l_{c2}\cos(\theta_2) \\ -l_{c2}\sin(\theta_2) \end{pmatrix} \dot{\theta}_2 + \begin{pmatrix} (l_4 - l_{c4})\cos(\theta_4) \\ (l_4 - l_{c4})\sin(\theta_4) \end{pmatrix} \dot{\theta}_4 \\
 vc_5 &= \begin{pmatrix} l_1\cos(\theta_1) \\ -l_1\sin(\theta_1) \end{pmatrix} \dot{\theta}_1 + \begin{pmatrix} l_{c2}\cos(\theta_2) \\ -l_{c2}\sin(\theta_2) \end{pmatrix} \dot{\theta}_2 + \begin{pmatrix} (l_4 - l_{c4})\cos(\theta_4) \\ (l_4 - l_{c4})\sin(\theta_4) \end{pmatrix} \dot{\theta}_4 + \begin{pmatrix} (l_5 - l_{c5})\cos(\theta_5) \\ (l_5 - l_{c5})\sin(\theta_5) \end{pmatrix} \dot{\theta}_5
 \end{aligned} \tag{5.6}$$

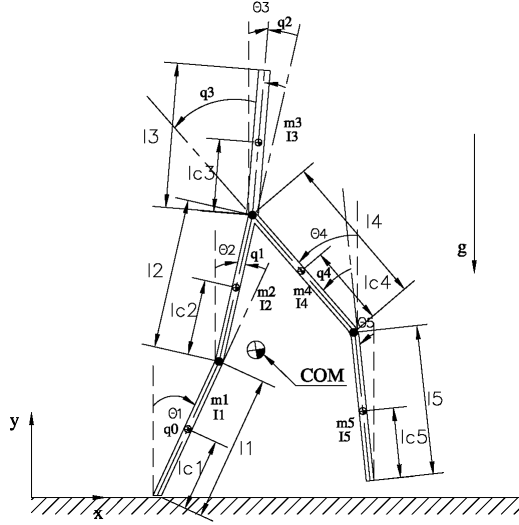


Figure 5.5: Five-Link planar biped model. This is modelled to depict a single support phase.

To derive the equation of motion of a mechanical system using Lagrangian principle it is expedient to consider calculating the Lagrangian of the system defined by the equation

$$\frac{d}{dt} \left(\frac{\partial K}{\partial \dot{\theta}_i} \right) - \frac{\partial K}{\partial \theta_i} + \frac{\partial U}{\partial \theta_i} = \tau_i \tag{5.7}$$

where K is the kinetic energy and U the potential energy. τ_i refers to the applied torque.

The general form of the kinetic energy K and potential energy U are defined as below respectively

$$\begin{aligned} K &= \frac{1}{2}mv^2 \\ U &= mgh \end{aligned} \tag{5.8}$$

where m is mass, v the velocity, g the gravity and h the height with respect to the origin of the system. This is the basic underlying formula for calculating these energies. However certain modifications are needed when computing the links connected to one another. The modification implies that each link is described by its own kinetic and potential energy with regard to its connected link. Hence, K & U are described as a summation of each link.

$$\begin{aligned} K &= \sum_{i=1}^5(K_i) \\ U &= \sum_{i=1}^5(P_i) \end{aligned} \tag{5.9}$$

where $K_i = 0.5m_ivc_i^2 + 0.5I_i\theta_i^2$ and $P_i = m_i g y_{c_i}$. Applying certain dynamic manipulation, the kinetic and potential energies may be derived. Using Eq. 5.7 the equation of motion can then be formulated.

Considering the general form of the Lagrangian equation of motion Eq. 5.4, the equations are derived with the assumption that the left side of the five-link biped model is symmetrical to the right side. This allows the same equation to be used for the left and right leg support phase. Each term may therefore be written as

Inertia matrix ($M(\theta)$)

$$\begin{aligned} M_{11} &= I_1 + l_{1c}^2 m_1 + l_1^2 m_2 + l_1^2 m_3 + l_1^2 m_4 + l_1^2 m_5 \\ M_{12} &= l_1 l_{c2} m_2 \cos(\theta_1 - \theta_2) + l_1 l_2 m_3 \cos(\theta_1 - \theta_2) + l_1 l_2 m_4 \cos(\theta_1 - \theta_2) + l_1 l_2 m_5 \cos(\theta_1 - \theta_2) \\ M_{13} &= l_1 l_{c3} m_3 \cos(\theta_1 - \theta_3) \\ M_{14} &= l_1 l_4 m_4 \cos(\theta_1 + \theta_4) + l_1 l_4 m_5 \cos(\theta_1 + \theta_4) - l_1 l_{c4} m_4 \cos(\theta_1 + \theta_4) \\ M_{15} &= l_1 l_5 m_5 \cos(\theta_1 + \theta_5) - l_1 l_{c5} m_5 \cos(\theta_1 + \theta_5) \end{aligned} \tag{5.10}$$

$$\begin{aligned}
M_{21} &= l_1 l_{c2} m_2 \cos(\theta_1 - \theta_2) + l_1 l_2 m_3 \cos(\theta_1 - \theta_2) + l_1 l_2 m_4 \cos(\theta_1 - \theta_2) + l_1 l_2 m_5 \cos(\theta_1 - \theta_2) \\
M_{22} &= I_2 + l_{c2}^2 m_2 + l_2^2 m_3 + l_2^2 m_4 + l_2^2 m_5 \\
M_{23} &= l_2 l_{c3} m_3 \cos(\theta_2 - \theta_3) \\
M_{24} &= l_2 l_4 m_4 \cos(\theta_2 + \theta_4) - l_2 l_{c4} m_4 \cos(\theta_2 + \theta_4) + l_2 l_4 m_5 \cos(\theta_2 + \theta_4) \\
M_{25} &= l_2 l_5 m_5 \cos(\theta_2 + \theta_5) - l_2 l_{c5} m_5 \cos(\theta_2 + \theta_5)
\end{aligned} \tag{5.11}$$

$$\begin{aligned}
M_{31} &= l_1 l_{c3} m_3 \cos(\theta_1 - \theta_3) \\
M_{32} &= l_2 l_{c3} m_3 \cos(\theta_2 - \theta_3) \\
M_{33} &= I_3 + l_{c3}^2 m_3 \\
M_{34} &= 0 \\
M_{35} &= 0
\end{aligned} \tag{5.12}$$

$$\begin{aligned}
M_{41} &= l_1 l_4 m_4 \cos(\theta_1 + \theta_4) - l_1 l_{c4} m_4 \cos(\theta_1 + \theta_4) + l_1 l_4 m_5 \cos(\theta_1 + \theta_4) \\
M_{42} &= l_2 l_4 m_4 \cos(\theta_2 + \theta_4) - l_2 l_{c4} m_4 \cos(\theta_2 + \theta_4) + l_2 l_4 m_5 \cos(\theta_2 + \theta_4) \\
M_{43} &= 0 \\
M_{44} &= I_4 + l_4^2 m_4 + l_4^2 m_5 + l_{c4}^2 m_4 - 2l_4 l_{c4} m_4 \\
M_{45} &= l_4 l_5 m_5 \cos(\theta_4 - \theta_5) - l_4 l_{c5} m_5 \cos(\theta_4 - \theta_5)
\end{aligned} \tag{5.13}$$

$$\begin{aligned}
M_{51} &= l_1 l_5 m_5 \cos(\theta_1 + \theta_5) - l_1 l_{c5} m_5 \cos(\theta_1 + \theta_5) \\
M_{52} &= l_2 l_5 m_5 \cos(\theta_2 + \theta_5) - l_2 l_{c5} m_5 \cos(\theta_2 + \theta_5) \\
M_{53} &= 0 \\
M_{54} &= l_4 l_5 m_5 \cos(\theta_4 - \theta_5) - l_4 l_{c5} m_5 \cos(\theta_4 - \theta_5) \\
M_{55} &= I_5 + l_5^2 m_5 + l_{c5}^2 m_5 - 2l_5 l_{c5} m_5
\end{aligned} \tag{5.14}$$

Coriolis/centripetal vector ($C(\theta, \dot{\theta})$)

$$C_{11} = 0$$

$$C_{12} = \dot{\theta}_2 l_1 l_{c2} m_2 \sin(\theta_1 - \theta_2) + \dot{\theta}_2 l_1 l_2 m_3 \sin(\theta_1 - \theta_2) + \dot{\theta}_2 l_1 l_2 m_4 \sin(\theta_1 - \theta_2) + \dot{\theta}_2 l_1 l_2 m_5 \sin(\theta_1 - \theta_2)$$

$$C_{13} = \dot{\theta}_3 l_1 l_{c3} m_3 \sin(\theta_1 - \theta_3)$$

$$C_{14} = \dot{\theta}_4 l_1 l_{c4} m_4 \sin(\theta_1 + \theta_4) - \dot{\theta}_4 l_1 l_4 m_4 \sin(\theta_1 + \theta_4) - \dot{\theta}_4 l_1 l_4 m_5 \sin(\theta_1 + \theta_4)$$

$$C_{15} = -\dot{\theta}_5 l_1 l_5 m_5 \sin(\theta_1 + \theta_5) + \dot{\theta}_5 l_1 l_{c5} m_5 \sin(\theta_1 + \theta_5)$$

(5.15)

$$C_{21} = -\dot{\theta}_1 l_1 l_{c2} m_2 \sin(\theta_1 - \theta_2) - \dot{\theta}_1 l_1 l_2 m_3 \sin(\theta_1 - \theta_2) - \dot{\theta}_1 l_1 l_2 m_4 \sin(\theta_1 - \theta_2) - \dot{\theta}_1 l_1 l_2 m_5 \sin(\theta_1 - \theta_2)$$

$$C_{22} = 0$$

$$C_{23} = \dot{\theta}_3 l_2 l_{c3} m_3 \sin(\theta_2 - \theta_3)$$

$$C_{24} = -\dot{\theta}_4 l_2 l_4 m_4 \sin(\theta_2 + \theta_4) - \dot{\theta}_4 l_2 l_4 m_5 \sin(\theta_2 + \theta_4) + \dot{\theta}_4 l_2 l_{c4} m_4 \sin(\theta_2 + \theta_4)$$

$$C_{25} = -\dot{\theta}_5 l_2 l_5 m_5 \sin(\theta_2 + \theta_5) + \dot{\theta}_5 l_2 l_{c5} m_5 \sin(\theta_2 + \theta_5)$$

(5.16)

$$C_{31} = -\dot{\theta}_1 l_1 l_{c3} m_3 \sin(\theta_1 - \theta_3)$$

$$C_{32} = -\dot{\theta}_2 l_2 l_{c3} m_3 \sin(\theta_2 - \theta_3)$$

$$C_{33} = 0$$

$$C_{34} = 0$$

$$C_{35} = 0$$

(5.17)

$$C_{41} = \dot{\theta}_1 l_1 l_{c4} m_4 \sin(\theta_1 + \theta_4) - \dot{\theta}_1 l_1 l_4 m_4 \sin(\theta_1 + \theta_4) - \dot{\theta}_1 l_1 l_4 m_5 \sin(\theta_1 + \theta_4)$$

$$C_{42} = \dot{\theta}_2 l_2 l_{c4} m_4 \sin(\theta_2 + \theta_4) - \dot{\theta}_2 l_2 l_4 m_4 \sin(\theta_2 + \theta_4) - \dot{\theta}_2 l_2 l_4 m_5 \sin(\theta_2 + \theta_4)$$

$$C_{43} = 0$$

$$C_{44} = 0$$

$$C_{45} = \dot{\theta}_5 l_4 l_5 m_5 \sin(\theta_4 - \theta_5) - \dot{\theta}_5 l_4 l_{c5} m_5 \sin(\theta_4 - \theta_5);$$

(5.18)

$$\begin{aligned}
C_{51} &= -\dot{\theta}_1 l_1 l_5 m_5 \sin(\theta_1 + \theta_5) + \dot{\theta}_1 l_1 l_{c5} m_5 \sin(\theta_1 + \theta_5) \\
C_{52} &= -\dot{\theta}_2 l_2 l_5 m_5 \sin(\theta_2 + \theta_5) + \dot{\theta}_2 l_2 l_{c5} m_5 \sin(\theta_2 + \theta_5) \\
C_{53} &= 0 \\
C_{54} &= -\dot{\theta}_4 l_4 l_5 m_5 \sin(\theta_4 - \theta_5) + \dot{\theta}_4 l_4 l_{c5} m_5 \sin(\theta_4 - \theta_5) \\
C_{55} &= 0
\end{aligned} \tag{5.19}$$

Gravity vector ($G(\theta)$)

$$\begin{aligned}
G_1 &= -gl_{c1} m_1 \sin(\theta_1) - gl_1 m_2 \sin(\theta_1) - gl_1 m_3 \sin(\theta_1) - gl_1 m_4 \sin(\theta_1) - gl_1 m_5 \sin(\theta_1) \\
G_2 &= -gl_{c2} m_2 \sin(\theta_2) - gl_2 m_3 \sin(\theta_2) - gl_2 m_4 \sin(\theta_2) - gl_2 m_5 \sin(\theta_2) \\
G_3 &= -gl_{c3} m_3 \sin(\theta_3) \\
G_4 &= gl_4 m_4 \sin(\theta_4) - gl_{c4} m_4 \sin(\theta_4) + gl_4 m_5 \sin(\theta_4) \\
G_5 &= gl_5 m_5 \sin(\theta_5) - gl_{c5} m_5 \sin(\theta_5)
\end{aligned} \tag{5.20}$$

5.3.2 Phase Transition

Walking is characterised by a continuous sequence of phase transition from DSP to SSP. In the single support phase (SSP), the swing leg (left or right) moves forward to make contact with the ground. At that point of contact, which is due to collision with the walking surface, there exists a sudden change in the angular velocity of each joint. This necessitates the computation of the dynamic model of the double support phase or biped in the air to compute the sharp changes in angular velocities at the moment the supporting leg is changed. This occurs after the completion of each step (Tzafestas, Raibert and Tzafestas, 1996; Chan, 2000). Hence a switching matrix and state vectors which specifies the position and velocities immediately after and before the switch is needed (Mu and Wu (2003a)). This may be valid for joint angle profiles that are computed for a single step and repeated at intervals.

This study concentrates on the efficacy of rehabilitative walking for patients with lower limb disorders at the hips and the knee joint level. This is envisaged to be achieved via a wearable robot controlled by CPG. The platform for which this study may be investigated mathematically is by utilising a symmetrical⁴ dynamic model of the SSP, which is used to track the CPG generated trajectories⁵ with a suitable controller. In the light of this, and since these CPG generated trajectories (signals) may actually be used to stimulate the joints, the concept of calculating the angular position coordinates and angular velocities before and after switching is eliminated. This transition is done automatically (see Section 5.2). Nevertheless, in this case, a search algorithm is needed to automatically search for the angular position of the knee with reference to the vertical axis at full extension ($0rad$) in order to initiate switching. Switching refers to relabelling the transformed dynamic equation of the 5-link system i.e. link 1 \leftrightarrow link 5 & link 2 \leftrightarrow link 4 while Link 3 is unchanged. Hence, $q_0 \leftrightarrow q_5$, $q_2 \leftrightarrow q_4$ & q_3 remain the same.

5.4 Exoskeleton control

For the purpose of a fair trajectory tracking of the actuated exoskeleton, the need for a robust control is expedient. Based on this, the joint angles of the exoskeleton are made to track the rhythmic trajectory modelled in section 5.2 using feedback linearisation techniques. This tracking procedure is assumed to be done using a body weight support system on a treadmill. The treadmill reduces the impact on the joints and also allows proper friction between the shoe sole and the ground surface while also guaranteeing a constant ground level. In order to achieve this, Eq. 5.4 is transformed to the relative angles using the relationship in (Tzafestas, Raibert and Tzafestas (1996)).

⁴The same equations could be used for both left and right SSP.

⁵These are continuous rhythmic signals.

5.4.1 Matrix transformation analysis

The relationship between the absolute angles and the relative angles is given by

$$\begin{bmatrix} \theta_1 \\ \theta_2 \\ \theta_3 \\ \theta_4 \\ \theta_5 \end{bmatrix} = \begin{bmatrix} 1 & 0 & 0 & 0 & 0 \\ 1 & -1 & 0 & 0 & 0 \\ 1 & -1 & -1 & 0 & 0 \\ -1 & 1 & 1 & 1 & 0 \\ -1 & 1 & 1 & 1 & -1 \end{bmatrix} \begin{bmatrix} q_0 \\ q_1 \\ q_2 \\ q_3 \\ q_4 \end{bmatrix} \quad (5.21)$$

and

$$\begin{bmatrix} q_0 \\ q_1 \\ q_2 \\ q_3 \\ q_4 \end{bmatrix} = \begin{bmatrix} 1 & 0 & 0 & 0 & 0 \\ 1 & -1 & 0 & 0 & 0 \\ 0 & 1 & -1 & 0 & 0 \\ 0 & 0 & 1 & 1 & 0 \\ 0 & 0 & 0 & 1 & -1 \end{bmatrix} \begin{bmatrix} \theta_1 \\ \theta_2 \\ \theta_3 \\ \theta_4 \\ \theta_5 \end{bmatrix} \quad (5.22)$$

For control purposes it is paramount to transform the τ_θ to τ_q and this is expressed as

$$\begin{bmatrix} \tau_{q0} \\ \tau_{q1} \\ \tau_{q2} \\ \tau_{q3} \\ \tau_{q4} \end{bmatrix} = \begin{bmatrix} 1 & 1 & 1 & -1 & -1 \\ 0 & -1 & -1 & 1 & 1 \\ 0 & 0 & -1 & 1 & 1 \\ 0 & 0 & 0 & 1 & 1 \\ 0 & 0 & 0 & 0 & -1 \end{bmatrix} \begin{bmatrix} \tau_{\theta1} \\ \tau_{\theta2} \\ \tau_{\theta3} \\ \tau_{\theta4} \\ \tau_{\theta5} \end{bmatrix} \quad (5.23)$$

It is these relationship in Eq. 5.21, Eq. 5.22 & Eq. 5.23 that are used to derive the relative angles equation in Lagrangian form as

$$D(q)\ddot{q} + H(q, \dot{q})\dot{q} + G(q) + \tau_d = \tau_q \quad (5.24)$$

where $q \in \mathfrak{R}^n$ is the joint position variable vector, $\dot{q} \in \mathfrak{R}^n$ the joint velocity variable vector, $\ddot{q} \in \mathfrak{R}^n$ the joint acceleration variable vector, $D(q) \in \mathfrak{R}^{n \times n}$ the inertia matrix, $\tau_d \in \mathfrak{R}^n$ the disturbance torque vector and $\tau_q \in \mathfrak{R}^n$ the externally applied generalised forces. With $H(q, \dot{q}) \in \mathfrak{R}^n$ the Coriolis/centripetal vector, and $G(q) \in \mathfrak{R}^n$ the gravity torque vector.

Prior to the transformation from Eq. 5.4 to Eq. 5.24, certain manipulations have to be considered. The terms in $M(\theta)$, $C(\theta, \dot{\theta})$ & $D(\theta)$ are first defined

$$\begin{aligned}
\theta &= [\theta_i]^T, \\
\tau_\theta &= [\tau_{\theta_i}]^T, \\
M(\theta) &= [M_{ij}(\theta)], \\
G(\theta) &= \text{col} [G_i(\theta)], \\
C(\theta, \dot{\theta}) &= \text{col} \left[\sum_{j=1}^5 (j \neq i) c_{ijj} (\dot{\theta}_j)^2 \right], (i, j = 1, 2, \dots, 5).
\end{aligned} \tag{5.25}$$

Therefore using the same relationship as in Eq. 5.23, the equation of motion may be expressed as

$$\begin{aligned}
\tau_{q0} &= A_{11}\ddot{\theta}_1 + A_{12}\ddot{\theta}_2 + A_{13}\ddot{\theta}_3 + A_{14}\ddot{\theta}_4 + A_{15}\ddot{\theta}_5 + H_{q0} + G_{q0} \\
\tau_{q1} &= A_{21}\ddot{\theta}_1 + A_{22}\ddot{\theta}_2 + A_{23}\ddot{\theta}_3 + A_{24}\ddot{\theta}_4 + A_{25}\ddot{\theta}_5 + H_{q1} + G_{q1} \\
\tau_{q2} &= A_{31}\ddot{\theta}_1 + A_{32}\ddot{\theta}_2 + A_{33}\ddot{\theta}_3 + A_{34}\ddot{\theta}_4 + A_{35}\ddot{\theta}_5 + H_{q2} + G_{q2} \\
\tau_{q3} &= A_{41}\ddot{\theta}_1 + A_{42}\ddot{\theta}_2 + A_{43}\ddot{\theta}_3 + A_{44}\ddot{\theta}_4 + A_{45}\ddot{\theta}_5 + H_{q3} + G_{q3} \\
\tau_{q4} &= A_{51}\ddot{\theta}_1 + A_{52}\ddot{\theta}_2 + A_{53}\ddot{\theta}_3 + A_{54}\ddot{\theta}_4 + A_{55}\ddot{\theta}_5 + H_{q4} + G_{q4}
\end{aligned} \tag{5.26}$$

where

$$A_{1j} = M_{1j} + M_{2j} + M_{3j} - M_{4j} - M_{5j}$$

$$A_{2j} = -M_{2j} - M_{3j} + M_{4j} + M_{5j}$$

$$A_{3j} = -M_{3j} + M_{4j} + M_{5j}$$

$$A_{4j} = M_{4j} + M_{5j}$$

$$A_{5j} = -M_{5j}$$

$$H_{q0} = c_1 + c_2 + c_3 - c_4 - c_5$$

$$H_{q1} = -c_2 - c_3 + c_4 + c_5$$

$$H_{q2} = -c_3 + c_4 + c_5$$

$$H_{q3} = c_4 + c_5$$

$$H_{q4} = -c_5$$

$$G_{q0} = G_1 + G_2 + G_3 - G_4 - G_5$$

$$G_{q1} = -G_2 - G_3 + G_4 + G_5$$

$$G_{q2} = -G_3 + G_4 + G_5$$

$$G_{q3} = G_4 + G_5$$

$$G_{q4} = -G_5$$

(5.27)

Eq. 5.24 can therefore be described as

$$\begin{aligned}
D_{i1} &= A_{i1} + A_{i2} + A_{i3} - A_{i4} - A_{i5} \\
D_{i2} &= -A_{i2} - A_{i3} + A_{i4} + A_{i5} \\
D_{i3} &= -A_{i3} + A_{i4} + A_{i5} \\
D_{i4} &= A_{i4} + A_{i5} \\
D_{i5} &= -A_{i5} \\
D(q) &= \left[[D_{i1}]^T, [D_{i2}]^T, [D_{i3}]^T, [D_{i4}]^T, [D_{i5}]^T \right], (i = 1, 2, \dots, 5) \\
H(q, \dot{q}) &= [H_{q0}, H_{q1}, H_{q2}, H_{q3}, H_{q4}]^T \\
G(q) &= [G_{q0}, G_{q1}, G_{q2}, G_{q3}, G_{q4}]^T \\
\tau_q &= [\tau_{q0}, \tau_{q1}, \tau_{q2}, \tau_{q3}, \tau_{q4}]^T
\end{aligned} \tag{5.28}$$

Although τ_{q0} is hypothetically described as being equal to zero, there exists a resistive passive torque at the joint (q_0) which must be compensated for by the controller. $D(q)$ should be positive definite and hence invertible. See appendix. C. The disturbance torque vector may well be given as

Disturbance torque ((τ_d))

$$\tau_{dn} = k_n \text{sgn}(\dot{q}_n) \tag{5.29}$$

k_n is given as a sine signal in Table. 5.2.

5.4.2 Feedback linearisation

Computed-Torque control is basically referred to as feedback linearisation. It is seen as a standard technique used for the control of nonlinear systems. It does so by eliminating the nonlinearities of the biped system dynamics, thereby providing a platform to obtain a simple input-output relation. Fig. 5.6 shows the block diagram of a closed loop control system. The concept of the said Computed-Torque control is discussed below.

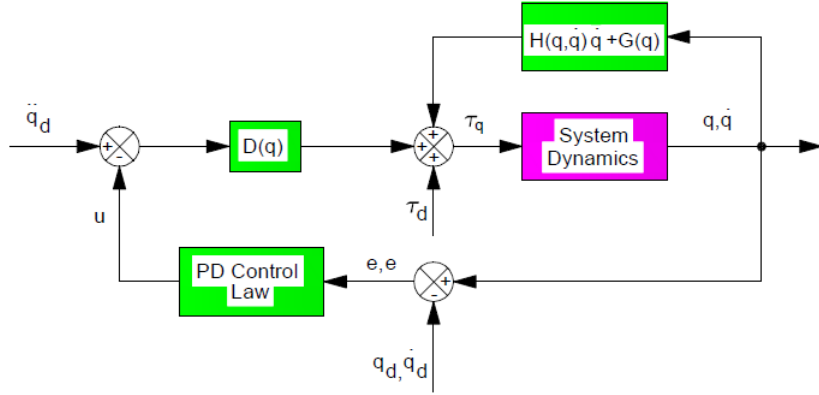


Figure 5.6: Block diagram of a closed loop control system (Computed-Torque Control).

With reference to Eq. 5.24, It is expected that the desired trajectory q_d has been defined for the proposed coordinated motion, therefore the control torque is given as in (Lewis, Dawson and Abdallah (2003)):

$$\tau_q = D(q)(\ddot{q}_d - u) + H(q, \dot{q}) + G(q) + \tau_d \quad (5.30)$$

The rest of the parameters are given as in Eq. 5.24. For this system control design $u \in \mathfrak{R}^n$ is defined as a PD control law (stabilising input). The stabilising control law may therefore be written as

$$u = -(K_d \dot{e} + K_p e) \quad (5.31)$$

where $e \in \mathfrak{R}^n$ is the position error signal $q_d - q$ and $\dot{e} \in \mathfrak{R}^n$ the velocity error signal $\dot{q}_d - \dot{q}$. $K_p \in \mathfrak{R}^{n \times n}$, and $K_d \in \mathfrak{R}^{n \times n}$ are the proportional and derivative gains of the controllers. These gains are termed to be diagonal matrices and are positive definite. Comparing Eq. 5.24 and Eq. 5.30, gives

$$\ddot{q} = \ddot{q}_d - u \quad (5.32)$$

Substituting Eq. 5.32 into Eq. 5.31 gives the closed loop equation of the error dynamics given by

$$\ddot{e} = K_d \dot{e} + K_p e \quad (5.33)$$

The closed loop equation (Eq. 5.33) defines the error between the actual joint angle profiles (relative angles) and the desired joint angle profiles. This forms the basis of the feedback linearisation. It may be observed that $e \rightarrow 0$, as $t \rightarrow \infty$, the gain matrices K_p & K_d are selected sufficiently large to ensure critical damping and given by

$$\begin{aligned} K_p &= \text{diag}[\omega_n^2] \\ K_d &= \text{diag}[2\omega_n] \end{aligned} \tag{5.34}$$

where ω_n is the natural frequency of the closed loop system. Assuming the controller is robust enough to compensate for the un-modelled parameters of the actual system due to the simplification of the dynamic equation of the exoskeleton based on the DoF, Eq. 5.32 provides the assertion that the nonlinear terms will be completely eliminated (Chan (2000)).

5.4.3 Desired trajectory mapping

The oscillator outputs X_3, X_4, X_2 & X_1 in Eq. 5.3 give the absolute angles ⁶ of link 1, link 2, link 4 and link 5 respectively (see Fig. 5.5). The coupling of the oscillator is actualised in such a way that the angles generated are with respect to the vertical axis. It therefore implies that; $X_3 \leftrightarrow \theta_{d1}, X_4 \leftrightarrow \theta_{d2}, X_2 \leftrightarrow \theta_{d4}$ & $X_1 \leftrightarrow \theta_{d5}$. The desired absolute angle for link 3 is assumed to be zero. For clarity purposes, the transformation of θ_d to q_d may be derived from the relationship in Eq. 5.22.

5.5 Numerical simulation

In this section, the simulation conducted using the five-link biped model to describe a full-exoskeleton worn by a subject in an upright position with flexion/extension at the hip and knee level was presented. The physiological parameters for the dynamical model are given in table 5.2 below as in (Aphiratsakun, Chairungsarpsook and Parnichkun (2010)).

⁶The angular orientation of a body segment with respect to a fixed line of reference.

Table 5.2: Physiological Parameters

Parameters	Units	Values
$l_{1,5}$	m	0.37
$l_{2,4}$	m	0.52
l_3	m	0.75
$l_{c1,c5}$	m	0.19
$l_{c2,c4}$	m	0.26
l_{c3}	m	0.38
$m_{1,5}$	kg	3.02
$m_{2,4}$	kg	6.50
m_3	m	44.07
$I_{1,5}$	$kg.m^2$	0.28
$I_{2,4}$	$kg.m^2$	1.17
I_3	$kg.m^2$	16.53
g	m/s^2	9.8
$k_n(\tau_d)$	rad	$5\sin(4\pi t)$

Note that, the value of the inertia is calculated, assuming cylindrical links. The parameters are considered for a person with weight of $65kg$. Exoskeleton parameters are also inclusive. Note also that sensor noise is not taken into account and only disturbance torque are considered. Filters such as Kalman filter can be used to cushion this effect.

5.5.1 Simulation results

The PD controller parameters are given as below and resultant figures signify the performance of the control law: $K_p = 484$ & $K_d = 44$ are the PD gains for the controller; for which ω_n is chosen as $22rad/s$. The choice of the value of ω_n parameters is related to the realisation of the best tracking results about this value. Choosing the gains of the system is based on first linearising the system about certain chosen values along the desired trajectory. Linear quadratic optimal control method is then used to arrive at gains that closely fit the feedback linearisation controller gain. However, this is then manually tuned using the concept described in subsection 5.4.2.

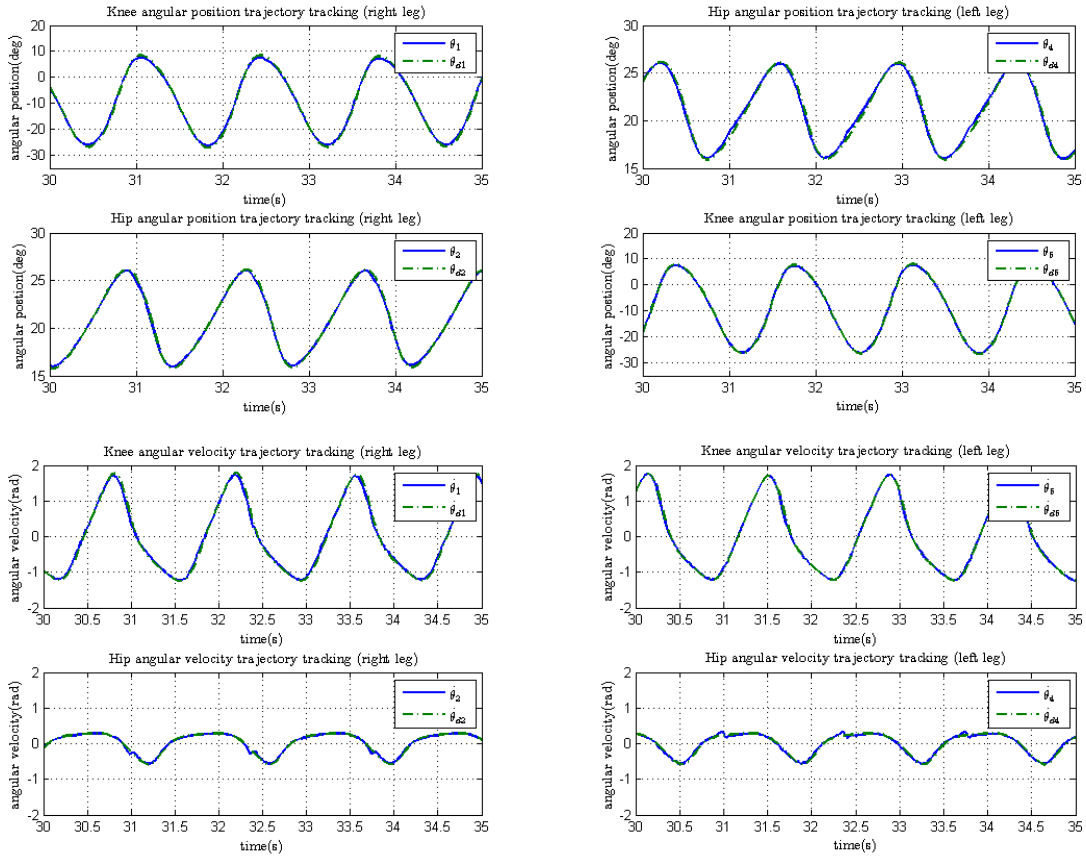


Figure 5.7: Hip and Knee angular position and velocity trajectory tracking for both legs.

5.5.2 Analysis of results

Fig. 5.7 presents the tracking results of the desired angular position and angular velocity trajectories of the hips and knees. The dash-dotted line represents the desired joint angle profiles while the continuous line represents the actual joint angle profiles. Results show that the controller is able to function as expected, with high performance in the tracking of the desired angular position and angular velocity trajectories respectively. This establishes a rehabilitation protocol capable of assisting patients with lower limb disorders regain their motor functions. The tracking errors of the angular position are comparatively very small, with Root-Mean-Square (RMS) values of the angular position being $0.001737rad$ and $0.001692rad$ for the respective left and right knee and $0.004245rad$

and $0.00117rad$ for the respective left and right hip respectively. The desired trajectories θ_{di} from the oscillator output tend to develop a momentary variation in the frequency of the joint angle profile at the beginning of its generation, but stabilises after a period of time of about 30s; therefore only the steady state values are considered for tracking purposes.

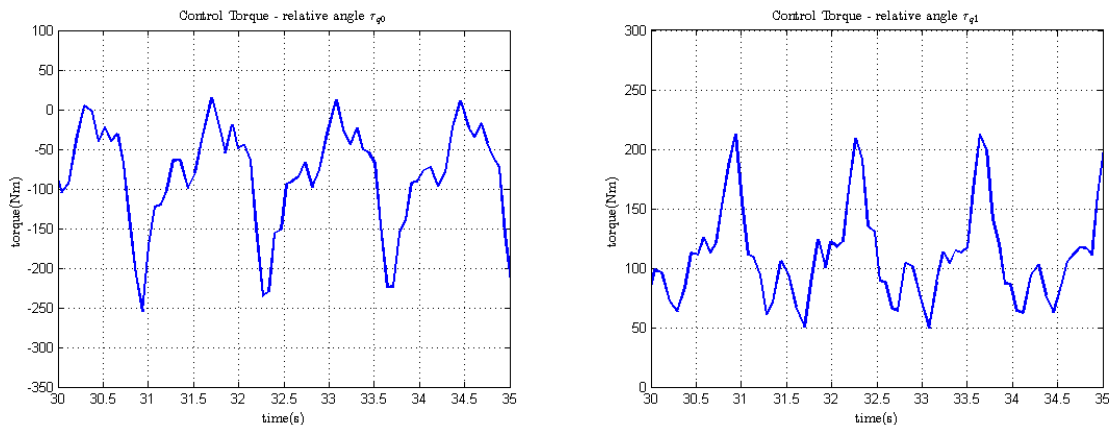


Figure 5.8: Control Torque τ_{q0} & τ_{q1} .

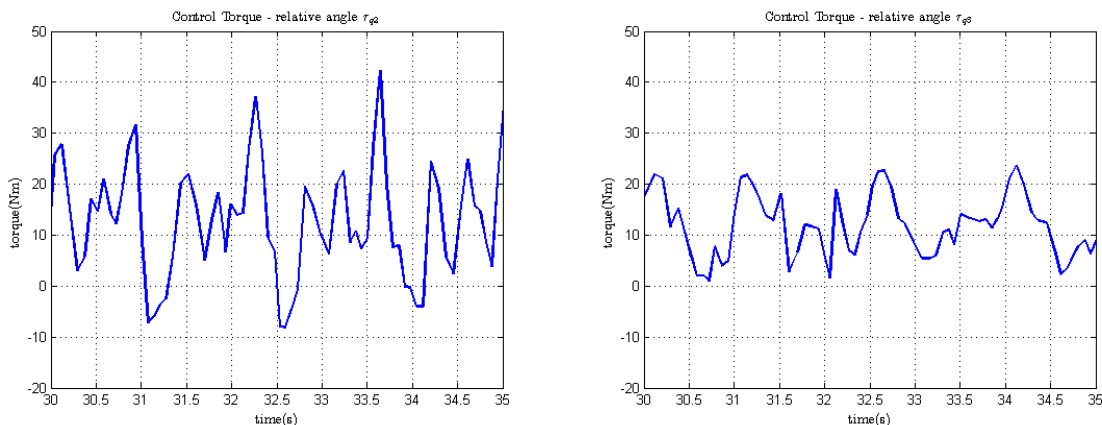


Figure 5.9: Control Torque τ_{q2} & τ_{q3} .

In Figures 5.8, 5.9 and 5.10, the control torques applied to the joints of the five-link biped exoskeleton were presented. Results show a reasonable range of torque values for a system of this nature. This may be observed when compared to the values obtained in (Mu and Wu (2003a)). Also based on (Chan (2000)) & (Mu and Wu (2003a)), it is

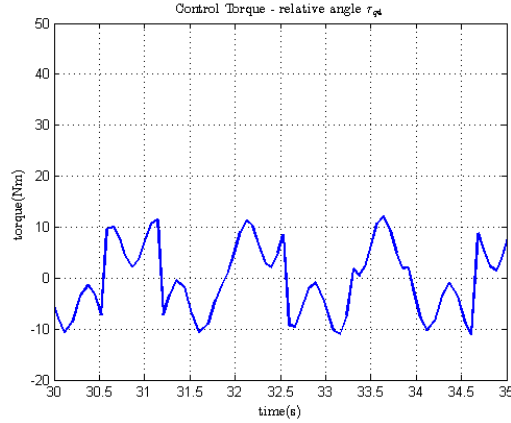


Figure 5.10: Control Torque τ_{q4} .

expected that the control torque τ_{q0} at the joint q_0 is largest and the control torque τ_{q4} at q_4 is least. It should be noted that the joint q_0 is not actuated but rather performs the role of providing support to the biped system. Hence, the control torque τ_{q0} is a passive torque and does occur due to the frictional effect that exist between the ground and the foot. The large torque value of τ_{q0} depends on this frictional effect and the weight of the body. The actuated joints are q_1, q_2, q_3 & q_4 . However, for the purpose of simulation, the controller has to compensate for the envisaged passive torque about q_0 .

5.6 Conclusion and Future works

In this study, the control of a lower limb exoskeleton having four actuated joints situated at both hips and knees joints level has been addressed. In a bid to achieve this, a rhythmic movement which takes the form of a normal walking gait for humans using CPG is designed and applied as the desired trajectory of a five-link biped system. To demonstrate this principle via computer simulations, the dynamic equation of the biped system for the single support phase (SSP) was derived using Lagrangian principles and transformed to its relative angles form. The control law used guarantees proper rehabilitation measures for persons with partial or complete lower limb disorders and

paraplegics since the user is completely passive during the training sessions. It is also robust enough to ensure stability of the wearer in the presence of a disturbance torque τ_d . The validation was achieved by simulation in order to provide a platform for which the real system could be compared.

The formulation of the desired trajectory eliminates the switching of roles for the legs since it is achieved automatically by the joint angle profile (see Fig. 5.2). However, a suitable search algorithm is needed to know when the knee angular position is at full extension so as to relabel the links for the purpose of using the same equation throughout the entire cycle. This also eradicates the consideration of the ground-foot impact when the foot makes ground contact. However, this might be a limitation because ground reaction forces may have an influence on the joints i.e. adding more force on the joints during the transition. A considerable measure to compensate for this effect will be to provide the biped system with a body weight support system to minimise ground reaction forces. In the real-life system, this may be actualised via force sensors connected at the foot of the exoskeleton to help detect the weight during transition. Angular sensors may be also be used to measure the angular position.

In the further works, the proposed control measure is envisaged to be tested by an exoskeleton to validate its authenticity in real-time, thereby taking into consideration the wearer's muscles' effort for the purpose of assisting when needed. The actual control torque and current values of the brushless actuators will then be recorded for each joint during these sessions. Prior to this study, relevant accessories needed to perform real-time experiments on the exoskeleton were purchased and assembled, but are not fully functional. Another limitation of this desired trajectory generation is that it limits the ability to select initial conditions that identify the double support phase (DSP) and the duration of the SSP may well be difficult to identify. Nevertheless, the use of numerical methods to approximate the joint angle profile could remedy this situation. This will

also be considered in further works.

CHAPTER 6. Bounded Control of an Actuated Lower Limb Orthosis

6.1 Introduction

Bounded control literally refers to the control of a system within certain bounded variables. This type of control method seeks to define certain limits that correspond to the physical limit of the variable in question. The variables often considered are those of the amplitude of the actuators. This is to avoid the possibility of an irreversible damage to the actuator (see subsection 1.3.4). This concept was used in (Guerrero-Castellanos, Marchand, Hably, Lesecq and Delamare (2011)) and adequately described in (Flikop (2004)). (Rifai, Hassani, Mohammed and Amirat (2011)), proposed a bounded control method based on nested saturations for the rehabilitation of the knee joint. By "nested saturation" it is meant that the actuator is subjected to magnitude and rate saturation simultaneously (Bateman and Lin (2003)). This does not only allow maintaining the bounded inputs of the control torque, but also provide an efficient convergence of the position and velocity of the physical system.

This work is an attempt to generalise the methodology in (Rifai, Hassani, Mohammed and Amirat (2011)) and propose the same for the rehabilitation of individuals with hip, knee or ankle impairment. In order to accomplish this task, two applications are

considered. The first application seeks to drive the knee-ankle orthosis to follow a predefined rehabilitation trajectory with and without human contribution. To verify the level of contribution of the human the system may allow, a high gain observer is designed for this purpose. Although high gain observers as been extensively used for the recovery of states such as in (Wang (2003)), in this work, the recovered states are employed to verify the level of human contribution. The stability of the closed-loop system without human contribution is verified using Lyapunov-based analysis. The convergence of the error between the states of the wearer-exoskeleton and that of the high gain observer is also analysed using Lyapunov stability theory.

In the second application, the system is used to drive a full-body exoskeleton with four actuated joints in its lower limb (Hips and Knees) to follow a CPG-based human gait. The CPG-based human gait is modified using polynomial functions to allow the selection of initial conditions for the human-exoskeleton. Simulation and the eventual results were obtained via MATLAB/SIMULINK. The performance of the system is discussed accordingly.

6.2 Observer-based Bounded Control of an Actuated Lower Limb orthosis

In this section, the first application is considered. Hence, an observer-based bounded control is employed for the rehabilitation and assistance of a patient with lower limb with complete and partial disorder. A high gain observer is used in the estimation of the angular position and angular velocities which is in turn applied for the estimation of the joint torques. The level of human contribution is a feedback of a fraction of the estimated joint torque. This is to meet the demands for a bounded human torque: *i.e.*, $\tau_h \leq N_{2,n} \leq N_{1,n}$. The fraction fed back as the human torque is determined by the value of

proportional constant κ . This helps varying the proportion of the human torque input in percentage (see subsection 1.3.7). Simulations are performed in MATLAB/SIMULINK to verify the proposed control law. Results obtained guarantee a fair trajectory tracking of the physiotherapist trajectory. For the analysis of the knee-ankle orthosis model see subsection 4.2. Also, the structure of the model is shown in Fig. 3.1. Note that in this case, θ_1 & θ_2 are represented by q_1 & q_2 respectively.

6.2.1 Mathematical Description of the Knee-Ankle Orthosis

The section presents the dynamic model of the orthosis and its state space description.

6.2.1.1 Dynamic Model

The dynamic model of the system may be derived by the Euler-Lagrange principle and written as (Lewis, Dawson and Abdallah (2003)):

$$M(q)\ddot{q} + C(q, \dot{q})\dot{q} + G(q) = \tau \quad (6.1)$$

For the purpose of this study, the friction torque, disturbance torque and the human torque are included; therefore Eq. 6.1 may be modified to give

$$M(q)\ddot{q} + C(q, \dot{q})\dot{q} + G(q) + F(\dot{q}) + \tau_d = \tau + \tau_h \quad (6.2)$$

- where $q \in \mathfrak{R}^n$ is a vector of angular positions, and are assumed available by measurement.
- $M(q) \in \mathfrak{R}^{n \times n}$ is the inertia matrix of the links, while $\tau \in \mathfrak{R}^n$ is the control torque, which serves as the control inputs of the system.
- $C(q, \dot{q})\dot{q} \in \mathfrak{R}^n$ is the vector of the Coriolis and centripetal torque, and $G(q) \in \mathfrak{R}^n$ is the gravitational torque.

- The matrices associated with $M(q) \in \mathfrak{R}^{n \times n}$, $C(q, \dot{q})\dot{q}$ and $G(q) \in \mathfrak{R}^n$ have been derived in Section. 4.3.
- $\tau_h \in \mathfrak{R}^n$ is the human torque, which allows the investigation of the passive and active mode of the wearer. i.e. $\tau_h = 0$ implies no human effort and $\tau_h \neq 0$ implies the presence of human effort.
- τ_d is the disturbance torque, which may be due to measurement noise and was represented by the equation below: See Table. 4.1.

$$\tau_d = k_n \text{sgn}(\dot{q}) \quad (6.3)$$

k_n is a sine signal as previously given.

The human torque τ_h are stated as

$$\tau_h = \kappa \hat{\tau} \quad (6.4)$$

where κ is the variable factor of the level of contribution of the human, and $\hat{\tau}$ is the estimated torque.

For simplicity the friction torque $F(\dot{q})$ is written in the form above, but may be represented as

$$F(\dot{q}) = F_v \dot{q} + F_d \text{sign}(\dot{q}) \quad (6.5)$$

where $F_v = \text{diag}[v_n]$ is the viscous friction torque and $F_d = \text{diag}[d_n]$ is the dynamic friction torque and v_n and d_n are vector quantities associated to their respective torques. $\text{sign}(\cdot)$ is a Signum function.

For clarity purposes, the human and exoskeleton system dynamics may be defined as being summed up in Eq. (6.2). Hence, they may be regarded as $i \in [1, 2]$, which stands for the respective human and exoskeleton components, i.e. $M(q) = \sum_{i=1}^2 M_i(q)$, $C(q, \dot{q}) = C_i(q, \dot{q})$, $G(q) = G_i(q)$, $F_v = F_{v_i}$ and $F_d = F_{d_i}$. From Eq. (6.5), it should be noted that

the dynamic friction is balanced so as to make the exoskeleton most transparent to the wearer. The gravity torque is also balanced since the exoskeleton is usually used for rehabilitation purpose.

6.2.1.2 State Space Description

To describe the nonlinear state space form of Eq. 6.2, the human torque τ_h is neglected. This is because it is a fraction of an estimate of the control torque. Since the matrix $M(q)$ is positive definite, it is invertible. Hence, the Eq. 6.2 may be written as

$$\ddot{q} = M(q)^{-1}(\tau - C(q, \dot{q})\dot{q} - G(q) - F(\dot{q}) - \tau_d) \quad (6.6)$$

The nonlinear state space form of the dynamic model Eq. (6.1) is given by

$$\dot{x} = f(x) + g(x)\tau \quad (6.7)$$

where the state vector $x : x_1 = [q_1 \quad q_2]^T$ & $x_2 = [\dot{q}_1 \quad \dot{q}_2]^T$. The functions $f(x)$ & $g(x)$ are assumed to be continuously differentiable a sufficient number of times.

6.2.2 High Gain Observer Structure and Estimation

In wearable robotic systems coordinates may be precisely measured by an encoder for each joint. However, velocity measurement obtained via tachometers are easily perturbed by noises. These constraints may be overcome by employing an observer for state estimation. The high gain observer is employed for this purpose. Prior to defining the observer dynamics it is necessary to reorganise the state space model of system in Eq. 6.7 as

$$\begin{bmatrix} \dot{x}_1 = x_2 \\ \dot{x}_2 = f(x) + g(x)\tau = \phi(x_1, x_2, t) \\ y = x_1 \end{bmatrix} \quad (6.8)$$

where y is the measurable position vector.

The state observer is based on the application of high gains, for the system to estimate the angular positions and velocities. The observer takes in state-space is given by:

$$\begin{bmatrix} \dot{\hat{x}}_1 = \hat{x}_2 - \frac{1}{\mu} H_p (y - \hat{x}_1) \\ \dot{\hat{x}}_2 = \phi(x_1, x_2, t) - \frac{1}{\mu^2} H_v (y - \hat{x}_1) \end{bmatrix} \quad (6.9)$$

with \hat{x}_1 , \hat{x}_2 denoting the generalised positions and velocities, i.e, \hat{x}_1 is the estimation of the joint angular position $[q_1 \ q_2]$ and \hat{x}_2 is the estimation of the joint angular velocities $[\dot{q}_1 \ \dot{q}_2]$ and $\hat{x} = \begin{bmatrix} \hat{x}_1^T & \hat{x}_2^T \end{bmatrix}^T$. μ is a scalar parameter chosen with the limit; $0 < \mu < 1$ while H_p and H_v are the two constant observer gain which has the form:

$$\begin{aligned} H_p &= \text{diag}[h_{pn}] \\ H_v &= \text{diag}[h_{vn}] \end{aligned} \quad (6.10)$$

6.2.2.1 Observer Error Dynamics

The observer error dynamics between the knee-ankle orthosis and the high gain observer may be given by:

$$\begin{bmatrix} \dot{\tilde{x}}_1 = \tilde{x}_2 - \frac{1}{\mu} H_p (y - \tilde{x}_1) \\ \dot{\tilde{x}}_2 = \phi(x_1, x_2, t) - \frac{1}{\mu^2} H_v (y - \tilde{x}_1) \end{bmatrix} \quad (6.11)$$

where $\tilde{x}_1 = x_1 - \hat{x}_1$ and $\tilde{x}_2 = x_2 - \hat{x}_2$. $\tilde{x} = \begin{bmatrix} \tilde{x}_1^T & \tilde{x}_2^T \end{bmatrix}^T$ is the error between the system states and the observer states.

For the purpose of the convergence analysis, the error is transformed into a more convenient form as

$$\begin{aligned} \tilde{e}_1 &= \tilde{x}_1 \\ \tilde{e}_2 &= \mu \tilde{x}_2 \\ \tilde{e} &= \begin{bmatrix} \tilde{e}_1^T & \tilde{e}_2^T \end{bmatrix}^T \end{aligned} \quad (6.12)$$

Based on the new transformation the error dynamics may be rewritten as

$$\mu \dot{\tilde{e}} = H\tilde{e} + \mu^2 W \phi(x_1, x_2, t) \quad (6.13)$$

where $H = \begin{bmatrix} -H_p & I_{2 \times 2} \\ -H_v & 0_{2 \times 2} \end{bmatrix}$, and $W = \begin{bmatrix} 0_{2 \times 2} \\ I_{2 \times 2} \end{bmatrix}$.

6.2.2.2 Convergence Analysis

For clarity, the Lyapunov-based approach in (Wang (2003)) is employed to ascertain the error convergence of the orthosis states and the high gain observer.

Definition 6.2.1. - Define the upper bound for the terms $M(q), C(q, \dot{q}), G(q), F_v \dot{q} + F_d \dot{q}$ & τ_d , in Eq. 6.2, as: $\|M(q)\| \leq \lambda_0$, $\|C(q, \dot{q})\| \leq \lambda_1 \|\dot{q}\|^2$, $\|G(q)\| \leq \lambda_2$, $\|F_v \dot{q} + F_d \dot{q}\| \leq v \|\dot{q}\| + d_1$ and $\|\tau_d\| \leq d_2$. $\|\cdot\|$ is a any appropriate norm and λ_i are positive non-zero constants; where $0 < \lambda_i < \infty, \forall i$, and all these properties are applicable $\forall q, e \in \mathfrak{R}^2$ with $\|\tilde{e}\| < \infty$.

With regard to these definitions, the condition for which the error of the nonlinear error dynamics converge to zero may be found.

Proposition 1. - *Considering the dynamic of the system composed of the wearer and the exoskeleton given in Eq. 6.2, with $\tau_h = 0$.*

Proof. Consider the quadratic Lyapunov function V for the error dynamics in Eq. 6.13 to be:

$$V = \tilde{e}^T P \tilde{e}. \quad (6.14)$$

where P is the solution to the Lyapunov equation $H^T P + P H = -I$ of a linear system. P is a positive definite matrix and it is independent of μ .

The derivative of V is then given by:

$$\dot{V} = \dot{\tilde{e}}^T P \tilde{e} + \tilde{e}^T P \dot{\tilde{e}}. \quad (6.15)$$

substituting Eq. 6.13 in \dot{V} gives:

$$\begin{aligned}
& \left(\frac{1}{\mu} H \tilde{e} + \mu W \phi \right)^T P \tilde{e} + \tilde{e}^T P \left(\frac{1}{\mu} H \tilde{e} + \mu W \phi \right). \\
& = \frac{1}{\mu} \tilde{e}^T (H^T P + P H) \tilde{e} + 2\mu \phi^T W^T P \tilde{e}. \\
& = -\frac{1}{\mu} \|\tilde{e}\|^2 + 2\mu \phi^T W^T P \tilde{e}.
\end{aligned} \tag{6.16}$$

where ϕ is the vector function of the states x_1 and x_2 .

Based on Eq. 6.16, the inequality below may be obtained:

$$\dot{V} \leq -\frac{1}{\mu} \|\tilde{e}\|^2 + 2\mu \|PW\phi(x_1, x_2, t)\| \|\tilde{e}\|. \tag{6.17}$$

Define the upper bounded term and a set for the least upper bound as:

$$\psi(t) = \|PW\phi(x_1, x_2, t)\| \ \& \ c_T = \sup_{t \in [0, T]} \psi(t) \tag{6.18}$$

Since $\phi(x_1, x_2, t)$ may be defined as the acceleration of the orthotic device (See Eq. 6.8), it is therefore upper bounded based on def. 6.2.1 and shows that $\psi(t)$ is upper bounded and c_T exists. P and W are constant matrices.

Assumption 1. - Assume that $c_T = \sup_{t \in [0, T]} \psi(t)$ exists for any finite value $T > 0$.

From Eq. 6.17, it follows that:

$$\begin{aligned}
\dot{V} & \leq -\frac{1}{\mu} \|\tilde{e}\|^2 + \frac{1}{\mu} K_e(\mu, c_T) \|\tilde{e}\|, \forall t \in [0, T] \\
& = \frac{1}{\mu} (K_e(\mu, c_T) - \|\tilde{e}\|) \|\tilde{e}\|
\end{aligned} \tag{6.19}$$

where $K_e(\mu, c_T) = 2\mu^2 c_T$. K_e is a value determined by μ and c_T . This value remains unchanged when the observer of the orthosis is designed. From Eq. 6.19, it may be deduced that if $\|\tilde{e}\| > K_e(\mu, c_T)$, then $\dot{V} < 0, \forall t \in [0, T]$. Also based on Eq. 6.18, it may be seen that different cases could arise.

Assumption 2. - Assume that $c_T < \infty$.

Then it means that $\|\tilde{e}(t_0)\| \leq K_e(\mu, c_T)$. Therefore, it may be deduced that $\|\tilde{e}\| \leq K_e(\mu, c_T), \forall t \in [0, T]$. The reason is that, once $\|\tilde{e}(t_1)\| > K_e(\mu, c_T)$, then the derivative $\dot{V} < 0$, and therefore the norm of the error $\|\tilde{e}\|$ diminish. By choosing small enough values of μ , the errors between the states of the system and the observer state can be kept small for any finite T .

Assumption 3. - *Also assume that $\psi(t) \leq \eta$.*

where η represents the bounded range of $[0, \infty)$. Hence, $c = \sup_{t \in [0, \infty)} \psi(t) < \infty$. It may be also seen that if $\|\tilde{e}\| \leq K_e(\mu, c)$, then $\|\tilde{e}(t)\| \leq K_e(\mu, c), \forall t \in \eta$. Also if $\|\tilde{e}(t_0)\| > K_e(\mu, c)$, causes the derivative $\dot{V} < 0$ which inturn diminish $\|\tilde{e}(t)\|$. Therefore, there exists a finite value $t_\mu > 0$ such that $\|\tilde{e}(t)\| \leq K_e(\mu, c) \forall t > t_\mu$.

From the transformed error coordinate in Eq. 6.12, it may be deduced that for $\mu < 1, \|\tilde{x}\| \leq \frac{1}{\mu} \|\tilde{e}\|$. Hence if $\|\tilde{e}\| \leq K_e(\mu, c_T)$, then $\|\tilde{x}\| \leq K_x(\mu, c_T)$, where $K_x(\mu, c_T) = 2\mu c_T$. For any finite value of T , $K_x(\mu, c_T)$ may be made small by making μ small enough. The obtained error convergence proves that the state of the orthosis can be observed by the high gain observer in Eq. 6.9. Therefore the torque may be estimated based on the recovered states. \square

6.2.3 Control Law

The formulation of the control law is based on considering the safety of the wearer. It must therefore be sufficiently robust for the stability of the human-orthosis system when the user is passive or active. The proposed control law is based on (Rifai, Hasani, Mohammed and Amirat (2011)). However the generalisation of the control law is considered in this study and it is modified as

$$\tau = sat_{N_1, n} [K_d \dot{\epsilon} + sat_{N_2, n}(K_p \epsilon)] + M(q)\ddot{q}_d + C(q, \dot{q})\dot{q}_d + G(q) + F_v \dot{q} + F_d sign(\dot{q}) \quad (6.20)$$

- where $\epsilon \in \mathfrak{R}^n = q_d - q$ is a vector of the angular position error.
- $\dot{\epsilon} \in \mathfrak{R}^n = \dot{q}_d - \dot{q}$ is the vector of the angular velocity error.
- $\ddot{\epsilon} \in \mathfrak{R}^n = \ddot{q}_d - \ddot{q}$ is the vector of the angular acceleration error.
- $q_d \in \mathfrak{R}^n, \dot{q}_d \in \mathfrak{R}^n$ and $\ddot{q}_d \in \mathfrak{R}^n$ signifies the desired joint angular position, angular velocity and angular acceleration respectively.
- $K_d = \text{diag}[k_{dn}]$ is the derivative gain while $K_p = \text{diag}[k_{pn}]$ is the proportional gain.
 $n = 1, 2$.

The definition of the saturation function is given below.

6.2.4 Saturation Function

The saturation function $\text{sat}_{N_{i,n}}(x_n)$ is defined as

$$\text{sat}_{N_{i,n}} = \min(N_{i,n}, \max(-N_{i,n}, x_n)), \forall x_n \in \mathfrak{R}^n \quad (6.21)$$

where $\pm N_{i,n}$ represent the saturation bounds. This bounded interval (point) is chosen such that $N_{1,n} > 2N_{2,n}$. The saturation of the control law allows the actuator of the exoskeleton to avoid saturation, thereby maintaining the linearity of the actuator and avoiding the hysteresis cycles which may result in irreversible damages. This guarantees the stability of the closed loop trajectories. High value control law demands high power and may expose the user to risk.

6.2.5 Closed Loop System

The dynamics of the closed loop system are achieved by substituting Eq. (6.5) into Eq. (6.2) and then substituting the eventual equation into Eq. (6.20). The resulting

equation is given by

$$M(q)\ddot{\epsilon} = -\text{sat}_{N_{1,n}} [K_d\dot{\epsilon} + \text{sat}_{N_{2,n}}(K_p\epsilon)] - C(q, \dot{q})\dot{\epsilon} - \tau_h \quad (6.22)$$

Note that τ_d is not included in the closed loop system equation for the purpose of the proof.

6.2.6 Stability Analysis

Here, the closed loop stability of the entire system (orthotic device and controller) is verified. A completely passive mode (i.e $\tau_h = 0$) for the user is considered. Passive mode refers to a user exerting no muscular torque that may interfere with the orthosis trajectory, as specified by the physiotherapist. The stability for the system's equilibrium point is proven. For the purpose of this proof consider $N_{i,n} \in \mathfrak{R}^n$.

Proposition 2. - *Also consider the wearer-exoskeleton dynamics defined by Eq. 6.2, with $\tau_h = 0$.*

Assumption 4. - *Assume that the derivatives of the desired angle (\dot{q}_d , \ddot{q}_d & $q_d^{(3)}$) are bounded and known.*

Then the equilibrium point $x_e = [\epsilon^T \quad \dot{\epsilon}^T]^T = 0 \in \mathfrak{R}^{2n}$ of the closed loop system (Eq. 6.22) is asymptotically stable.

Proof. Let $K_p|\epsilon| > N_{2,n}$ and $K_d|\dot{\epsilon}| > N_{1,n} - N_{2,n} > N_{2,n}$. Defining the positive definite Lyapunov function V_1 to be:

$$V_1 = \frac{1}{2}\dot{\epsilon}^T M(q)\dot{\epsilon} \quad (6.23)$$

The derivative of \dot{V}_1 is given by

$$\dot{V}_1 = \dot{\epsilon}^T M(q)\ddot{\epsilon} + \frac{1}{2}\dot{\epsilon}^T \dot{M}(q)\dot{\epsilon}. \quad (6.24)$$

Substituting (6.22) into (6.24): \dot{V}_1 becomes

$$\begin{aligned} \dot{V}_1 = & -\dot{\epsilon}^T (\text{sat}_{N_1,n} [K_d \dot{\epsilon} + \text{sat}_{N_2,n}(K_p \epsilon)] - C(q, \dot{q}) \dot{\epsilon} \\ & - \tau_h) + \frac{1}{2} \dot{\epsilon}^T \dot{M}(q) \dot{\epsilon}. \end{aligned} \quad (6.25)$$

If $\tau_h = 0$, the derivative \dot{V}_1 results into

$$\begin{aligned} \dot{V}_1 = & -\dot{\epsilon}^T \text{sat}_{N_1,n} [K_d \dot{\epsilon} + \text{sat}_{N_2,n}(K_p \epsilon)] - \dot{\epsilon}^T C(q, \dot{q}) \dot{\epsilon} \\ & + \frac{1}{2} \dot{\epsilon}^T \dot{M}(q) \dot{\epsilon} \end{aligned} \quad (6.26)$$

By factorisation, (6.26) may be given by

$$\begin{aligned} \dot{V}_1 = & -\dot{\epsilon}^T \text{sat}_{N_1,n} [K_d \dot{\epsilon} + \text{sat}_{N_2,n}(K_p \epsilon)] + \frac{1}{2} \dot{\epsilon}^T (\dot{M}(q) \\ & - 2C(q, \dot{q})) \dot{\epsilon} \end{aligned} \quad (6.27)$$

The matrices $\dot{M}(q)$ and $C(q, \dot{q})$ are dependant, as the following relation is satisfied by the second term in (6.27) therefore, $\dot{\epsilon}^T S \dot{\epsilon} = \frac{1}{2} \dot{\epsilon}^T (\dot{M}(q) - 2C(q, \dot{q})) \dot{\epsilon} = 0$. where S is skew symmetric. Then (6.27) becomes

$$\dot{V}_1 = -\dot{\epsilon}^T \text{sat}_{N_1,n} [K_d \dot{\epsilon} + \text{sat}_{N_2,n}(K_p \epsilon)]. \quad (6.28)$$

If $|K_d \dot{\epsilon}| > N_{2,n}$; by observation $\dot{\epsilon}$ and $K_d \dot{\epsilon} + \text{sat}_{N_2,n}(K_p \epsilon)$ have same sign and certainly $|K_d \dot{\epsilon} + \text{sat}_{N_2,n}(K_p \epsilon)| > 0$. With regards to this, \dot{V}_1 can be reduced to

$$\dot{V}_1 = -\lambda |\dot{\epsilon}^T|_{N_1,n} \leq 0. \quad (6.29)$$

It may therefore be assumed that as $|\dot{\epsilon}^T|$ decreases \dot{V}_1 decreases also. Note that λ is any positive value to derive the inequality for checking the negativeness of \dot{V}_1 . However based on this, no conclusion can be reached with regard to its asymptotic stability. To establish this, a second Lyapunov function is chosen considering a velocity reference signal and the filtered tracking error.

Definition 6.2.2. - Define the velocity reference signal as $\dot{q}_r = \dot{q}_d - \Gamma \epsilon$, and the filtered error as $s = \dot{q}_r - \dot{q} = \dot{\epsilon} - \Gamma \epsilon$, $\Gamma = \text{diag}[\gamma_i] > 0$. Hence, $\dot{s} = \ddot{q}_r - \ddot{q} = \ddot{\epsilon} - \Gamma \dot{\epsilon}$.

Based on the above def. (6.2.2), the following equation holds

$$M(q)[\dot{s} + k_1 s] + C(q, \dot{q})s = M(q)[\ddot{q}_r - k_1 s] + C(q, \dot{q})\dot{q}_r - [M(q)\ddot{q} + C(q, \dot{q})\dot{q}] \quad (6.30)$$

where $M(q)k_1 \geq 0$ and commutative. $k_1 = \text{diag}[\alpha] \geq 0$. Substituting (6.2) into (6.30) yields

$$M(q)[\dot{s} + k_1 s] + C(q, \dot{q})s = M(q)[\ddot{q}_r - k_1 s] + C(q, \dot{q})\dot{q}_r - [\tau + \tau_h - G(q) - F_v \dot{q} - F_d \text{sign}(\dot{q})] \quad (6.31)$$

Assumption 5. - From (6.20), consider an equivalence controller of the form

$$\tau = \text{sat}_{N_1, n} [K_d \dot{s} + \text{sat}_{N_2, n} (K_p s)] + M(q)[\ddot{q}_r - k_2 s] + C(q, \dot{q})\dot{q}_r + G(q) + F_v \dot{q} + F_d \text{sign}(\dot{q}) \quad (6.32)$$

where k_2 is of the same form as k_1 .

Introducing (6.32) into (6.31) results in the closed loop system with regard to the def. (6.2.2).

$$M(q)\dot{s} = -Ks - \text{sat}_{N_1, n} [K_d \dot{s} + \text{sat}_{N_2, n} (K_p s)] - C(q, \dot{q})s \quad (6.33)$$

where $K = M(q)(2k_1 - k_2)$

Consider the Lyapunov function

$$V_2 = \frac{1}{2} s^T M(q) s \quad (6.34)$$

The derivative of the V_2 may be given as

$$\dot{V}_2 = s^T M(q) \dot{s} + \frac{1}{2} s^T \dot{M}(q) s \quad (6.35)$$

Substituting (6.33) into (6.35) results into

$$\dot{V}_2 = -s^T K s - s^T \text{sat}_{N_1, n} [K_d \dot{s} + \text{sat}_{N_2, n} (K_p s)] + \frac{1}{2} s^T (\dot{M}(q) - 2C(q, \dot{q})) s \quad (6.36)$$

$\frac{1}{2}s^T(\dot{M}(q) - 2C(q, \dot{q}))s = 0$ based on the skew symmetric properties as previously stated.

The derivative of V_2 therefore becomes

$$\dot{V}_2 = -s^T K s - s^T \text{sat}_{N_1, n} [K_d \dot{s} + \text{sat}_{N_2, n}(K_p s)] \quad (6.37)$$

using the same principle as in (6.28), \dot{V}_2 can be reduced to

$$\dot{V}_2 = -s^T K s - \lambda |s^T|_{N_1, n} \leq 0 \quad (6.38)$$

λ is same as previously defined.

This then leads to $-\dot{V}_2(0) \leq \dot{V}_2(t)$. Consequently, the boundedness of \dot{s} , s and \dot{e} subsequently leads to $e \rightarrow 0$ as $t \rightarrow \infty$. Based on the above choice of different Lyapunov function (V_1 & V_2), the need for the mastrov theorem for conclusion of asymptotic stability is eliminated. For further undersatnding see (Khalil and Grizzle (1996)).

□

6.2.7 Orthosis Control

The orthosis control with human-in-the-loop requires three building blocks; the dynamics of the human-orthosis (or rather wearer-exoskeleton) the controller and the observer/-torque estimator (see Fig. 6.1.). The dynamics of the human-orthosis has been discussed in subsection 6.2.1 and the controller (control law) has also been presented in subsection. 6.2.3. Here, the mathematical equation for the torque estimator and the reference inputs are presented.

The physiotherapist trajectories for the knee and ankle are chosen to fit within the limit of their range of motions and are given by

$$\begin{aligned} q_1 &= \frac{3\pi}{2} \sin\left(\frac{2\pi}{3}t\right) \\ q_2 &= \frac{\pi}{6} \sin\left(\frac{\pi}{2}t\right) \end{aligned} \quad (6.39)$$

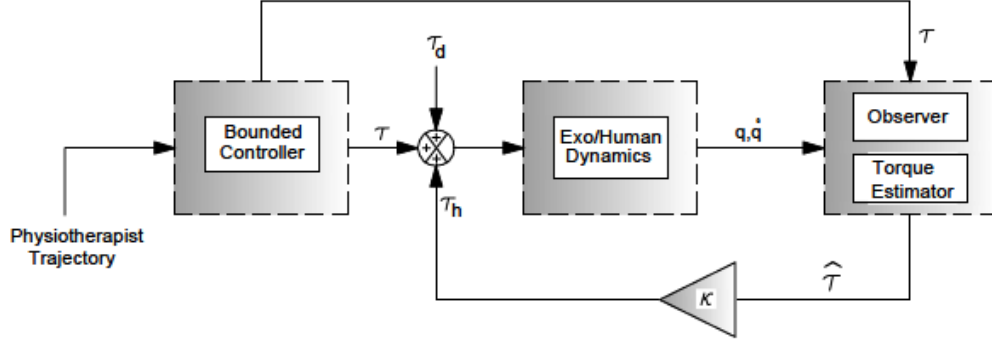


Figure 6.1: Block diagram of the Observer-Based Controller.

Furthermore, the high gain observer used for the estimation of the angular positions and velocities is analysed in subsection. 6.2.2. The estimation of the torque is derived from these values based on the equation

$$\hat{\tau} = M(\hat{q})\hat{\ddot{q}} + C(\hat{q}, \hat{\dot{q}})\hat{\dot{q}} + G(\hat{q}) + F_v\hat{\dot{q}} + F_d\text{sign}(\hat{\dot{q}}) \quad (6.40)$$

where all the parameters in the equation are same as that in Eq. 6.2 but represents the estimated version.

6.2.8 Simulations Results

The physiological parameters used are those of Table 4.1, with the exception of the d_n & v_n . Hence, an arbitrary value of $d_n = 2.35\text{rad}$ & $v_n = 0.87\text{rad}$ were chosen for the purpose of simulation. For this bounded control law, it is desired that the maximal motor torque is 15Nm for both joint torques. The saturation bounds $N_{1,1}$ and $N_{1,2}$ are chosen to be 7.6Nm for both joints, whereas $N_{2,1}$ and $N_{2,2}$ are chosen to be $\frac{7.6}{2.1}\text{Nm}$ for both joints as well. The controller gains for K_p are 15.218×10^2 and 9.450×10^2 for the knee and ankle joints and K_d are 0.284×10^3 and 0.672×10^3 for the respective joints. The observer gains $h_{v1} = 15.5$, $h_{v2} = 14.2$, $h_{p1} = 10.5$ and $h_{p2} = 12.5$. While μ is set to 0.01. The gains of the system controller are manually tuned to find the best fit. This is same for the observer gain. Due to the presence of control chattering activity

induced by the saturation function, the control gains required to ensure a good tracking performance somehow increase. This justifies the high gains needed for this controller.

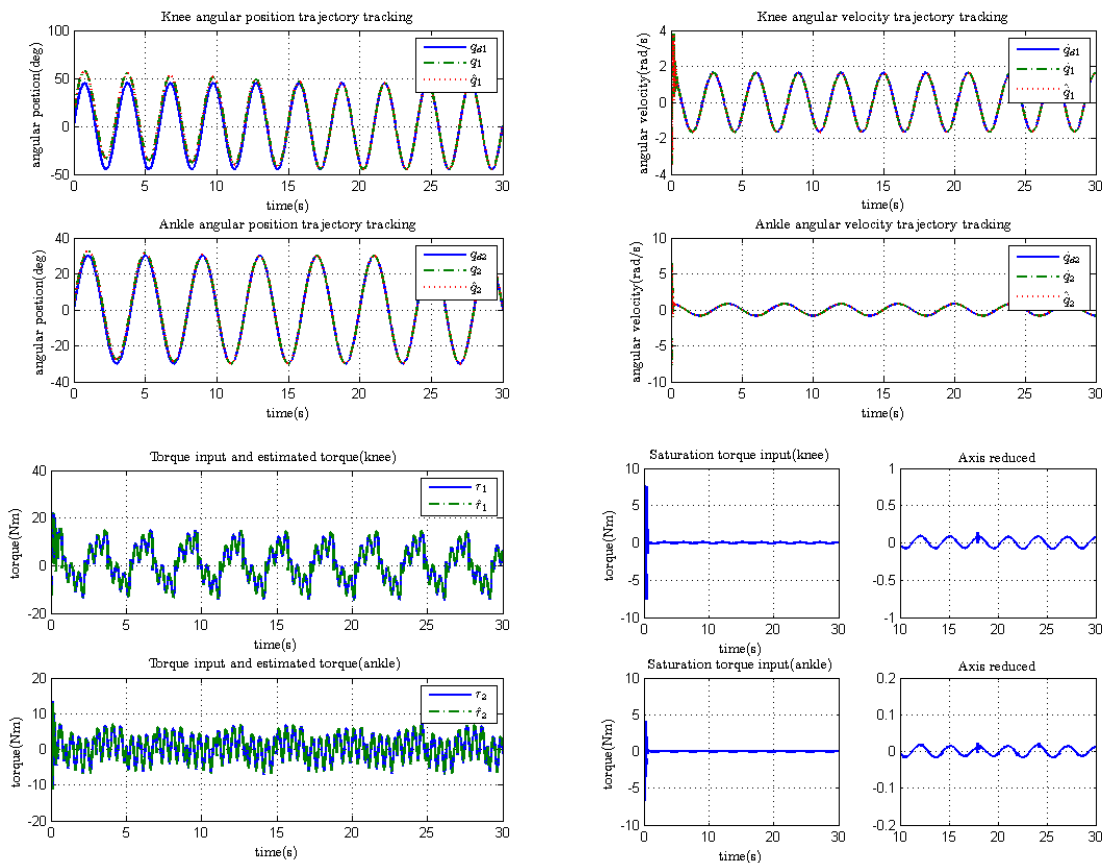


Figure 6.2: Top-Left: Knee-Ankle position trajectory tracking. Top-Right: Knee-Ankle velocity trajectory tracking. Bottom-Left: Knee-Ankle torque input and estimated torque. Bottom-Right: Knee-Ankle saturation torque input. For $\tau_h = 0$.

Four simulations were performed; where the desired trajectory is expected to be tracked by the wearer. In the first case, the wearer is completely passive (complete motor function disorder), i.e., $\tau_h = 0$, (see Fig. 6.2). The controller is seen to perform the task of making the user completely track the desired angular position and velocity trajectories, at a considerable time. The torque input is within the limits of $15Nm$ and the saturation torque input are small enough to initiate the limits set by the saturation bounds and avoid the saturation of the actuators. The observer's ability to correctly estimate the position and velocity trajectories is also guaranteed.

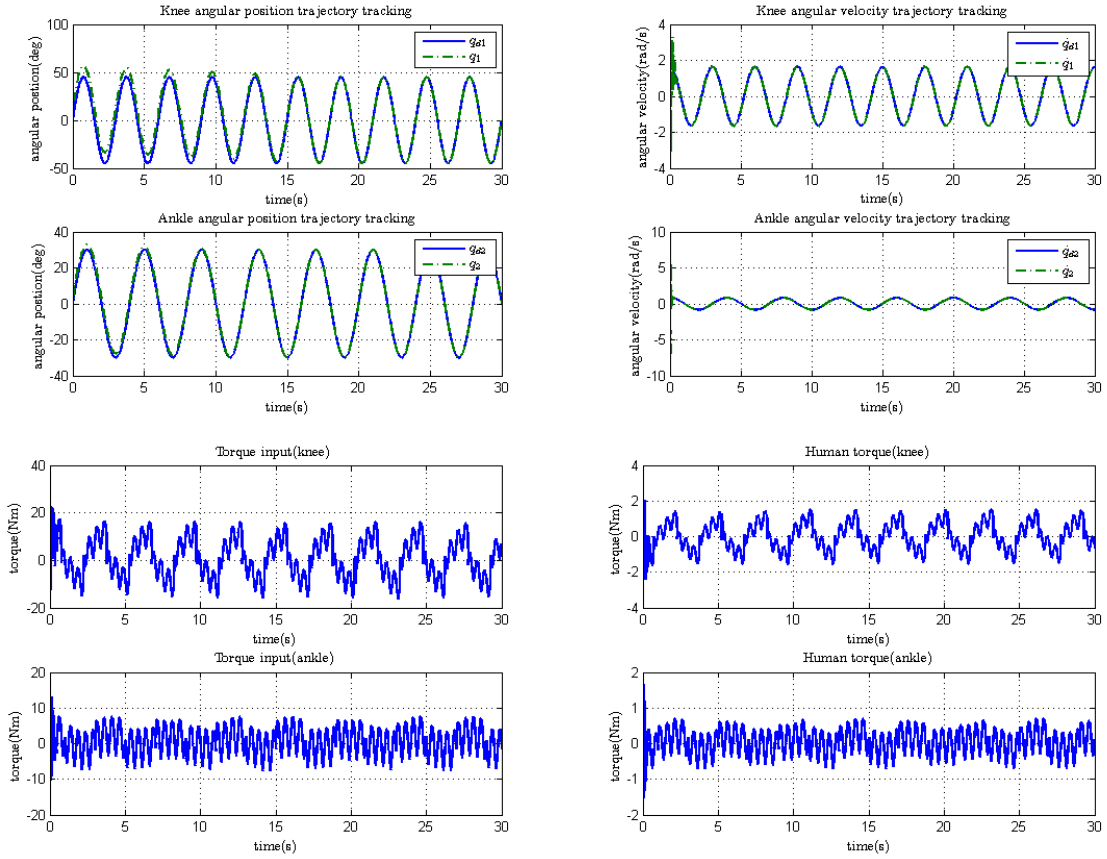


Figure 6.3: Top-Left: Knee-Ankle position trajectory tracking. Top-Right: Knee-Ankle velocity trajectory tracking. Bottom-Left: Knee-Ankle torque input. Bottom-Right: Knee-Ankle human torque input (resistive torque). For $\tau_h \neq 0, \kappa = 0.1$.

In the second and third cases, simulations that show the wearer, providing a percentage of the human torque used in resisting the orthosis control ability to track the desired angular position and velocity trajectories are presented (see Fig. 6.3 & Fig. 6.4). In both cases, the human torque $\tau_h \neq 0$, and it's a percentage of the estimated torque given by $\tau_h = \kappa \hat{\tau}$, where $\kappa = 0.1$ & 0.2 , i.e., 10% & 20% of the torque inputs. The angular position and velocity trajectory tracking are likewise accomplished and the control torque inputs have a higher value. The higher the resistive torque, the higher is the control torque value. This is because the controller has to produce more torque to overcome the resistance of the wearer. The resistive human torque is achieved by inverting a fraction of the estimated torque. This may be seen in Fig. 6.3 & 6.4 (Bottom-Right). However,

since it is within a specified limit, the torque input should not be allowed to overcome the specified limit to avoid saturation. Although the maximal torque is somewhat exceeded by a small percentage, a considerable tolerance actuator value in the physical system could compensate for this. Beyond these limits, saturation occurs. The main interest is to ensure that the wearer safety is still guaranteed.

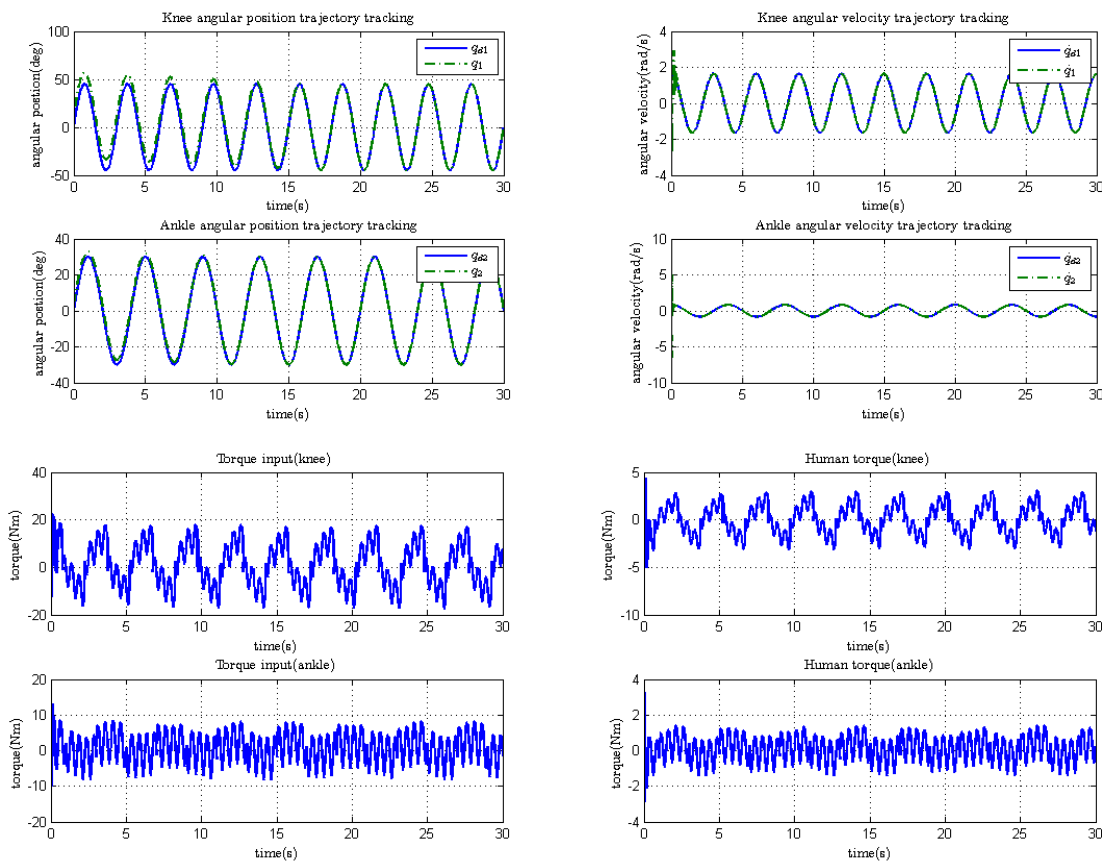


Figure 6.4: Top-Left: Knee-Ankle position trajectory tracking. Top-Right: Knee-Ankle velocity trajectory tracking. Bottom-Left: Knee-Ankle torque input. Bottom-Right: Knee-Ankle human torque input (resistive torque). For $\tau_h \neq 0, \kappa = 0.2$.

In the fourth case, an assistant, human torque provided by the wearer to assist the orthosis control in order to track the desired angular position and velocity trajectories is verified. (see Fig. 6.5). The assistive human torque ($\tau_h \neq 0$) provided, is 10% percentage of the estimated torque. The angular position and velocity trajectory tracking are guaranteed as required, but the control torque inputs have a smaller value. This is

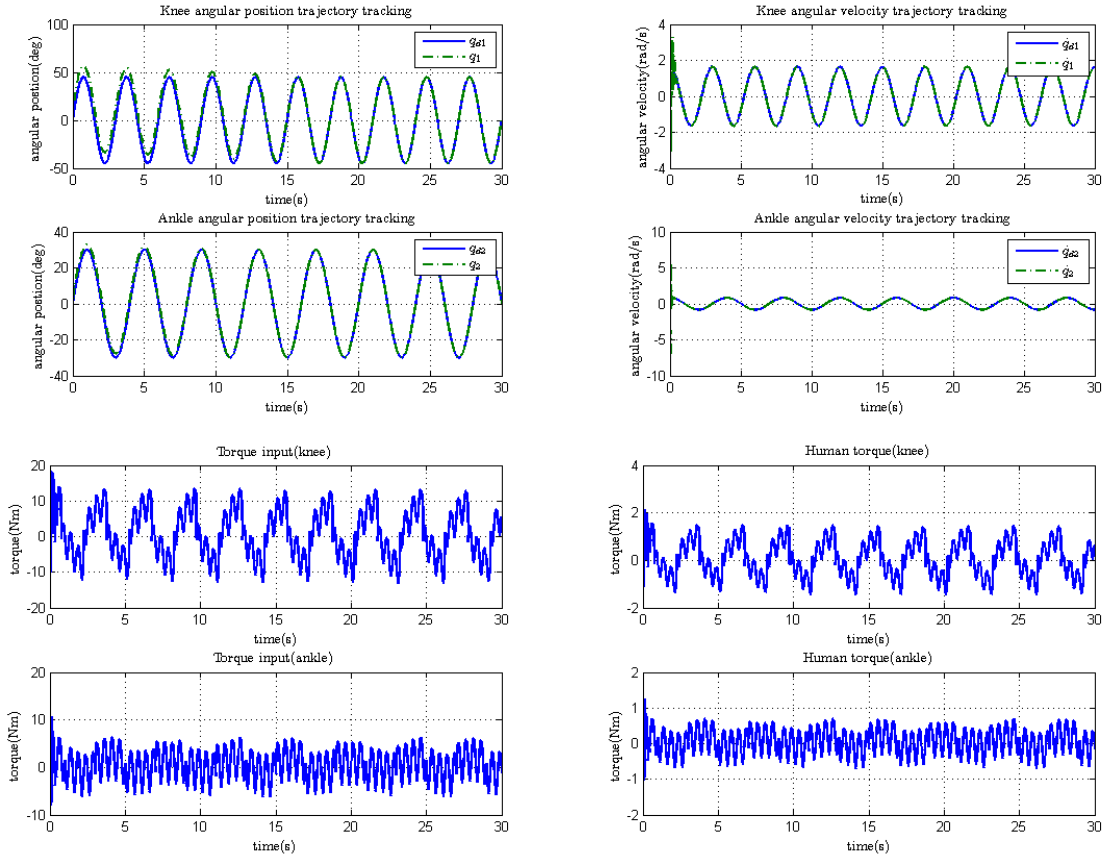


Figure 6.5: Top-Left: Knee-Ankle position trajectory tracking. Top-Right: Knee-Ankle velocity trajectory tracking. Bottom-Left: Knee-Ankle torque input. Bottom-Right: Knee-Ankle human torque input (assistive torque). For $\tau_h \neq 0, \kappa = 0.1$.

due to the assistance provided by the wearer. The assistive human torque is achieved by inputting a fraction of the estimated torque directly in contrast to the resistive torque applied. This may be seen in Fig. 6.5 (Bottom-Right). It should be noted that the second, third and fourth cases exemplifies a partial motor function disorder.

6.2.9 Conclusion and Future Work

Developing an exoskeleton device needs a well-designed control system so as to ensure the wearer is not further injured by the device. It is therefore necessary that the controller is robust enough to actualise its capability. In this study, a bounded nonlinear feedback

controller in conjunction with a high gain observer is proposed for the rehabilitation of the user and the determination of the level of contribution a wearer can offer for a specific exoskeleton. The level of contribution helps demonstrate the partial motor function disorder i.e. the user may be able to exact a certain amount of human torque. This was tested via MATLAB/SIMULINK simulations for a knee-ankle orthosis model. Simulation results obtained help to establish this fact. In addition to the controller robustness, its ability to avoid the saturation of the actuators has been verified. Note that the wearer is in a sitting position.

In future works, the controller is expected to be tested in the laboratory. It is expected that parametric identification is first carried out before it is tested in real time.

6.3 Bounded Control of a Full Exoskeleton Device with 4 Degree of Freedom

6.3.1 Introduction

In order to accomplish the task in this section as discussed in Section 6.1, the rhythmic trajectory designed in Chapter. 5 is used as the desired trajectory to be tracked by the wearer-exoskeleton considered as a five-link biped system. However, a certain modification was employed. This modification is an effort to remedy the limitations associated with CPG-generated human gaits using Van der Pol oscillators. Limitations such as choosing specified initial conditions for the robotic (exoskeleton) movements provides a difficult task for knowing when the human is at DSP or SSP. The modification involves the use of time polynomial function to approximate the CPG joint angle profile generated to determine the desired trajectory. This trajectory is meant to be tracked by the wearer-exoskeleton under the influence of a bounded controller (see subsection 1.3.4).

The control torque is envisaged to ensure a proper trajectory following of the wearer-exoskeleton for the flexion/extension movements of the hip and knee within the range of motion (ROM) associated with walking.

6.3.2 Trajectory Design

Here, an extraction of the joint angle numerical values from the CPG-generated trajectories in Section 5.2 are used to determine the joint angle profile that corresponds to a one step movement. This is done by selecting a fixed-step ode3 solver option size with an unconstrained periodic sample time of $1.2ms$ in order to visibly see the CPG signal transition.

Based on Eq. 5.1 and Eq. 5.2, numerical methods such as time polynomial functions were used to develop a one step trajectory by identifying the corresponding numerical values. The polynomial functions that represent each joint angle profile are given as

$$\begin{aligned}
 \theta_{d1} &= a_0 + a_1t + a_2t^2 - a_3t^3 - a_4t^4 \\
 \theta_{d2} &= -b_0 - b_1t - b_2t^2 + b_3t^3 - b_4t^4 - b_5t^5 \\
 \theta_{d3} &= 0 \\
 \theta_{d4} &= -c_0 + c_1t + c_2t^2 - c_3t^3 + c_4t^4 - c_5t^5 \\
 \theta_{d5} &= d_0 + d_1t + d_2t^2 - d_3t^3 + d_4t^4 - d_5t^5
 \end{aligned} \tag{6.41}$$

where each coefficient is a measure of the gait characteristics of a period (T). The duration is defined by: $0 \leq t \leq T$. T is the time step for the SSP period before switching. θ_{di} represents the desired trajectory for a single step and i signifies each link of the exoskeleton (*This will be discussed later*). Note that since the polynomial functions were derived from the oscillator output, there is a need to map the joint angles to fit the five-link biped system joint angles. The resulting physical joint angles are plotted in Fig. 6.6 (Left). The evolution of the joint angle profile is also presented in

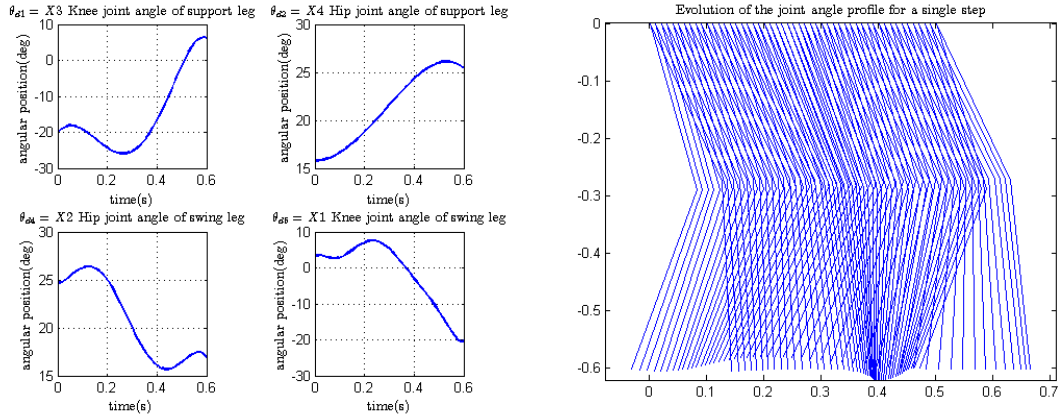


Figure 6.6: Left: Physical joint angles. Right: Joint angle profile evolution for a single step (skick diagram).

Fig. 6.6 (Right). Note that; $X_3 \leftrightarrow \theta_{d1}$, $X_4 \leftrightarrow \theta_{d2}$, $X_2 \leftrightarrow \theta_{d4}$ & $X_1 \leftrightarrow \theta_{d5}$ are referred to as the absolute angles.

6.3.3 Human-Exoskeleton Dynamics

The theory behind the human-exoskeleton dynamics, its CAD model, mathematical formulation and eventual Lagrangian equation of motion are given in Section. 5.3.

6.3.4 Exoskeleton control

The problem formulation lies in the exoskeleton user's ability to track the desired trajectory designed in subsection. 6.3.2 using a bounded feedback controller. In order to achieve this, the absolute angles are first transformed to the relative angles (see subsection 5.4.1).

The human-exoskeleton dynamics in a sagittal plane (friction torque included for this application) may then be given as

$$D(q)\ddot{q} + H(q, \dot{q})\dot{q} + G(q) + F_v\dot{q} + F_d\text{sign}(\dot{q}) + \tau_d = \tau_q \quad (6.42)$$

- where $q \in \mathfrak{R}^n$ is the joint relative position variable vector.
- $\dot{q} \in \mathfrak{R}^n$ the joint relative velocity variable vector.
- $\ddot{q} \in \mathfrak{R}^n$ the joint relative acceleration variable vector.
- $D(q) \in \mathfrak{R}^{n \times n}$ the mass matrix.
- $\tau_d \in \mathfrak{R}^n$ the uncertainty torque vector.
- $\tau_q \in \mathfrak{R}^n$ the externally applied generalised forces.
- $H(q, \dot{q}) \in \mathfrak{R}^n$ the Coriolis/centripetal vector.
- $G(q) \in \mathfrak{R}^n$ the gravity torque vector. $F_v = \text{diag}[v_n]$ is the viscous friction torque and $F_d = \text{diag}[d_n]$ is the dynamic friction torque.
- $\text{sign}(\cdot)$ is a Signum function.
- τ_d is the disturbance torque.

For simplicity the friction torque may be written as

$$F(\dot{q}) = F_v \dot{q} + F_d \text{sign}(\dot{q}) \quad (6.43)$$

- where $F_v = \text{diag}[v_n]$ is the viscous friction torque.
- $F_d = \text{diag}[d_n]$ is the dynamic friction torque.
- v_i and d_i are vector quantities associated to their respective torques. $\text{sign}(\cdot)$ is a Signum function.

Note that the human-exoskeleton dynamics may be defined as being summed up in Eq. (6.42). i.e. $D(q) = \sum_{n=1}^2 D_i(q)$, $H(q, \dot{q}) = H_i(q, \dot{q})$, $G(q) = G_i(q)$, $F_v = F_{v_i}$ and $F_d =$

F_{d_i} . Hence, $i \in [1, 2]$, representing the respective human and exoskeleton components.

The disturbance torque is represented by:

$$\tau_{dn} = k_n \text{sgn}(\dot{q}_n) \quad (6.44)$$

k_n is a sine signal as previously given.

6.3.4.1 Control Law

The proposed control law is adapted version of (Rifai, Hassani, Mohammed and Amirat (2011)). For clarity and symbol variation the equation for the control law is given as

$$\tau_q = \text{sat}_{N_1, n} [K_d \dot{\epsilon} + \text{sat}_{N_2, n} (K_p \epsilon)] + D(q) \ddot{q}_d + H(q, \dot{q}) \dot{q}_d + G(q) + F_v(\dot{q}) + F_d \text{sign}(\dot{q}) \quad (6.45)$$

- where $\epsilon \in \mathfrak{R}^n = q_d - q$ is a vector of the angular position error.
- $\dot{\epsilon} \in \mathfrak{R}^n = \dot{q}_d - \dot{q}$ is the vector of the angular velocity error.
- $\ddot{\epsilon} \in \mathfrak{R}^n = \ddot{q}_d - \ddot{q}$ is the vector of the angular acceleration error.
- $q_d \in \mathfrak{R}^n, \dot{q}_d \in \mathfrak{R}^n$ and $\ddot{q}_d \in \mathfrak{R}^n$ signifies the desired joint angular position, angular velocity and angular acceleration respectively.
- $K_d = \text{diag}[k_{dn}]$ is the derivative gain while $K_p = \text{diag}[k_{pn}]$ is the proportional gain.
- $n = 1, 2, 3, 4, 5$ represents the number of links of the robot.

The definition of the saturation function is given in subsection 6.2.4.

6.3.5 Numerical simulation

Here, simulations conducted using the five-link biped model to describe a full-exoskeleton worn by a subject in an upright position with flexion/extension at the hip and knee

level is presented. The physiological parameters for the dynamical model are given in Table 5.2 with the exception of the d_n & v_n . Note that the value of the inertia is calculated assuming cylindrical links and the parameters are considered for a person with a weight of $65kg$ (Aphiratsakun, Chairungsarpsook and Parnichkun (2010)) with the parameters of the exoskeleton inclusive.

6.3.5.1 Simulation Parameters

The controller parameters k_{pi} & k_{di} were found to be 5.4809×10^3 , 5.4809×10^3 , 1.1537×10^3 , 2.1031×10^3 , 2.9351×10^3 , & 0.02×10^3 , 0.129×10^3 , 0.9304×10^3 , 0.0032×10^3 , 0.2728×10^3 respectively. Due to the presence of control chattering activity induced by the saturation function, the control gains required to ensure a good tracking performance somewhat increase. This justifies the high gains needed for this controller. Furthermore, for an arbitrary choice of $200Nm$ for the maximal torque output; $N_{1,n} = 100Nm$ & $N_{2,n} = \frac{100}{2.1}Nm$. d_n & v_n are 5.50 & 0.90 respectively. The Initial condition of the relative angles: $q_0 = -20.1051^\circ$, $q_1 = -35.8614^\circ$, $q_2 = 24.6085^\circ$, $q_3 = 24.6085^\circ$, $q_4 = 21.6349$ and initial velocities $\dot{q}_0 = 0.0688rad/s$, $\dot{q}_1 = 0.680rad/s$, $\dot{q}_2 = 0.0028rad/s$, $\dot{q}_3 = 0.0028rad/s$ & $\dot{q}_4 = -0.0530rad/s$. The choice of these values is based on choosing an initial condition close to the values of the starting point of the wearer-exoskeleton desired relative position trajectory.

6.3.5.2 Discussion

Fig. 6.7& 6.8 present the relative angles tracking in conjunction with the driving torques. It can be observed that the user with the aid of the controller was able to track the one step gait properly. *Tracking the relative angle signifies tracking the absolute angles.* Utilising bounded control helps define certain limits that correspond to the physical limit of the actuator's amplitude. Defining such limits must conform technically with

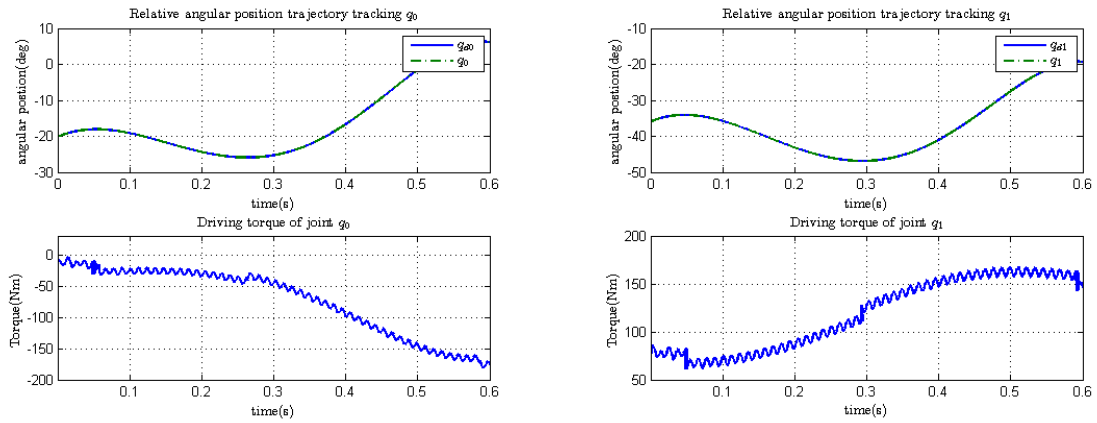


Figure 6.7: Top: Relative angular position tracking. Bottom: Driving torque output. q_0 & q_1

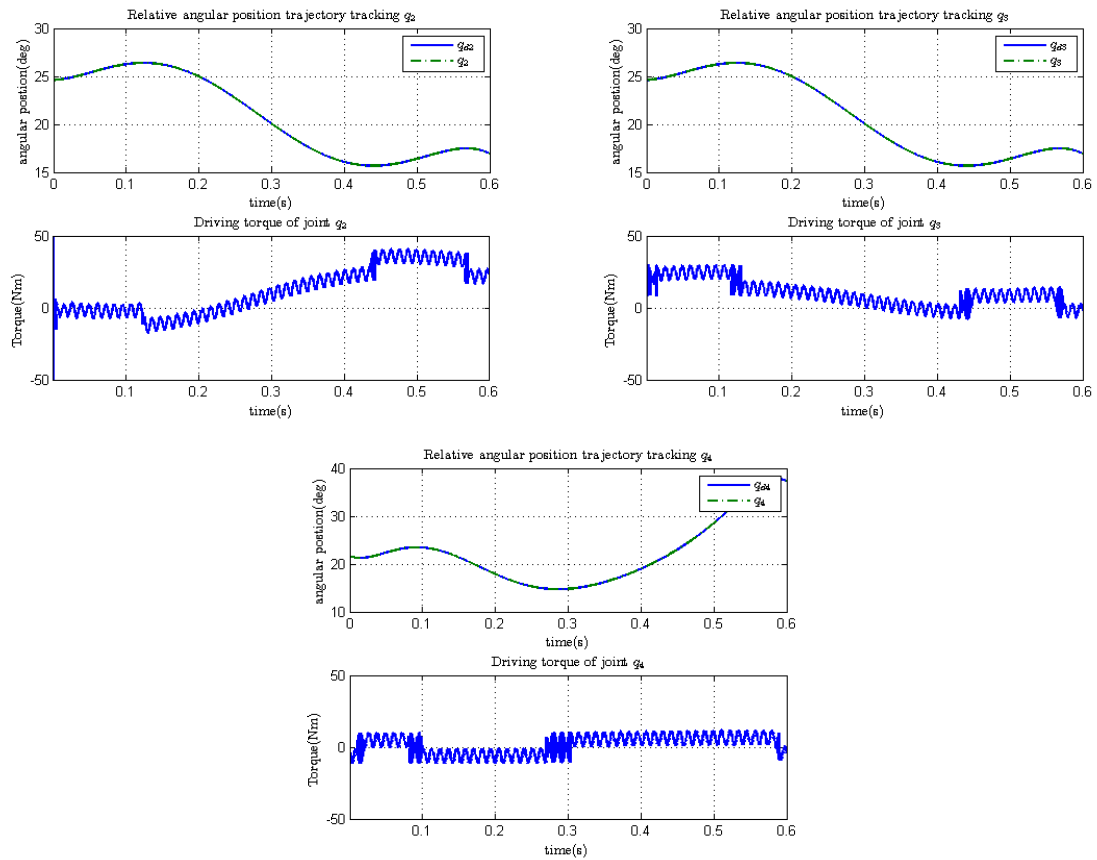


Figure 6.8: Top: Relative angular position tracking. Bottom: Driving torque output. q_2, q_3 & q_4

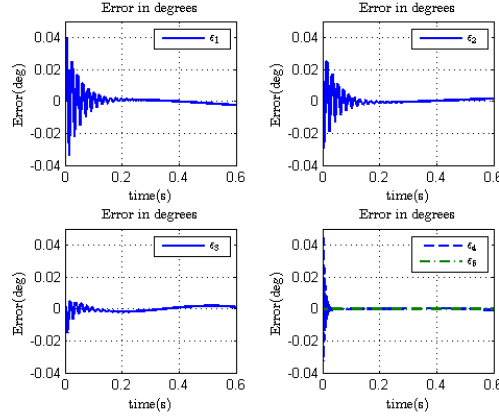


Figure 6.9: Error in degrees.

what is achievable. This has been defined based on (Mu and Wu (2003a)). The driving torques are seen not to have exceeded the maximal torque as envisaged. Based on (Chan, 2000; Mu and Wu, 2003a), it is expected that the control torque τ_{q_0} about the joint q_0 is largest and the control torque τ_{q_4} about q_4 is least. Note that the joint q_0 is not actuated but rather performs the role of providing support to the biped system. Hence, the control torque τ_{q_0} is a passive torque and does occur due to the frictional effect that exist between the ground and the foot. The large torque value of τ_{q_0} depends on this frictional effect and the weight of the body. τ_{q_1} & τ_{q_4} relate to the driving torque of the support leg knee joint q_1 and the driving torque of the swing leg knee joint q_4 respectively, while τ_{q_2} & τ_{q_3} relate to the driving torque of the support leg hip joint q_2 and the driving torque of the swing leg knee joint q_3 respectively. However, for the purpose of simulation, the controller has to compensate for the envisaged passive torque about q_0 . In addition, Fig. 6.9 presents the error (ϵ) of the system, defined in Eq. 6.45. The error values are very small and that show the very close tracking of the desired trajectories. With this the user is guaranteed proper safety.

6.3.6 Conclusion and Further Works

In this study, a five-link biped robotic system was used to depict the dynamics of a full-exoskeleton system having 4 actuated joints. A nonlinear bounded controller generalised to accommodate $n - DoF$ was used to track the desired gait. The gait was considered to be only for a one step movement. The proposed model may be applied to biped walking, (SSP only). It does not entail the DSP. However, continuous walking could be achieved by switching both legs (Tzafestas, Raibert and Tzafestas (1996)). This results in a minor discontinuity and will require calculating the velocity of the swing leg impact. Based on this, further works will entail switching both legs at the end of each swing motion with reduced velocity to reduce the impact force. The system controller has been proven to guarantee asymptotic stability. Applications relating to rehabilitation will further be carried out in the laboratory.

6.4 Conclusion

This work covers the development of rehabilitation protocols, and the determination of the level of human contribution (assisting or resisting) an orthotic device can accommodate. The maximal physical limit of an actuator is also considered. To achieve this goal, computer simulations via MATLAB/SIMULINK were made. Two applications were considered for this purpose: the knee-ankle orthosis control and the full-exoskeleton control. For the knee-ankle orthosis, a bounded nonlinear controller in conjunction with a high gain observer were employed while only the bounded nonlinear feedback controller was used for the full-exoskeleton control. The effectiveness of the control law was established and the stability analysis of the control law was also derived for the knee-ankle orthosis. The convergence analysis of the error between the states of the orthotic device and that of the observer states was also verified.

CHAPTER 7. Conclusion, Future Works & Recommendation

7.1 Introduction

This chapter integrates the various issues discussed in this thesis, while identifying the theoretical and practical importance and implications of the entire study. It also restates the problem statement and the sub-problem of this study. The limitations and possible directions in future research are highlighted.

7.1.1 Conclusion

This study was set out to theoretically develop actuated lower limb exoskeletons/orthosis using mathematical principles for the rehabilitation and assistance to patients with lower limb complaints. These mathematical principles entail the modelling of the robotic device (wearer-exoskeleton) and the formulation of the control strategies used to actualise the intended motive. Control strategies employed are those of CPGs (AFO to be specific), computed torque control and bounded control with nested saturation. The methodology used is centred on targeted task attainment and applied to gait rehabilitation and human locomotion assistance. This therefore necessitates the modelling of the motion task proposed to be performed by the device wearer. Modelling motion

(movement) task requires taking into consideration the human movement pattern which includes its range of motion (ROM). Most of the applications used in this thesis are based on trajectory tracking control; therefore in real-life application, angular position sensors such as potentiometer may well be sufficient for measuring the relation between the reference position and the actual position which is then fed to the controller for proper tracking. To develop this robotic device a number of sub-problems which require the attention of this thesis arise. These sub-problems are stated below:

- The use of CPG-generated trajectories for the stimulation of joint for the purpose of human locomotion has gained enormous publicity and used by researchers in this field of study. However, the modalities this procedure entails and the rationale behind the use of various types of oscillators for modelling these CPGs remains a problem to be investigated.
- The coupling of nonlinear oscillators for the excitation of joints on real-systems have most often been done using virtual simulation software. How this physical system does interact with the CPGs remain vague since the mathematical dynamic equation of motion of these physical systems is not often considered.
- Robotic-based rehabilitation approach is more advantageous compared to the manual rehabilitation approach. This is because it saves excessive time and energy wasted by a physiotherapist. The problem of designing practical, achievable rehabilitative procedures that can help recuperate the motor function of human at the different joint levels simultaneously need to be addressed.
- Classical PD and PID control methods have consistently been used in the control of lower limb exoskeleton/orthoses. Nonetheless, most of these control methods are not robust enough against model uncertainties and disturbance. This may pose a high risk to the user of such exoskeleton because of the increase in power

and consequently high torques these exoskeletons may require. This therefore necessitates the use of a suitable controller that could guarantee the safety of the wearer's/user.

- Control methods such as neuro-fuzzy approaches are an intuitive type of control methods, and may not guarantee the stability of the system. For systems such as exoskeleton which worn by humans require some level of reliability. The stability proof of the system may therefore be by a form of assurance that system could perform as expected.
- As a way of further ensuring the stability of the wear-exoskeleton, synthesising a complete gait cycle for a particular biped physical system with tangible gait characteristics remain paramount. Currently the trend of modelling joint profile has shifted from the advanced ZMP method to the “limit cycle walking” paradigm, due to its stability attributes. The use of methods such as oscillator-based gait modelling for synthesising gait cycle for the purpose of gait rehabilitation may provide the stability required. This is based on its stable limit cycle behaviour.
- The use of CPG-generated signals via oscillators for walking in humans case provides a platform for which the rhythmic walking behaviour of humans could be investigated. Although, this may well be appropriate for the stimulation of humans at a joint level, when used as a reference input for motion targeted task, certain complications arise. In the generation of such movement there exists a transient period before the steady values. The problem of choosing initial conditions for the system physical system and the identification of the phases associated with walking need to be addressed.
- Finally, it has been noted that robotic therapy is most successful when the wearer is involved in the therapeutic exercise. The use of EMG has been a practical way

of detecting and classifying the wearer intention in the form of a torque. This does come with a challenge which may be associated to the sensor location and its sensitivity to noise. In order to help cushion this effect, it is therefore expedient to devise another way of determining the extent of human contribution. This will help test the capability of the robotic device to assist the patient when needed without exceeding its capacity.

In order to solve the sub-problems itemised above, this thesis has been able to furnish a standard documentation for the description of the research topic and above all provide some answers to the identified problems. This documentation is structured into chapters concise enough for comprehensive reading.

Chapter 1 justifies the proposed research topic. It basically provides in-depth knowledge concerning the conceptual idea of the design studies. Key aspects such as the problem statements, hypotheses and contribution of the study and the thesis outline were detailed.

In chapter 2, a detailed review of lower limb exoskeletons describing the rehabilitative and assistive strategies available is provided. Modelling concepts of human lower limbs, CPGs, human gait and control strategies are also documented.

Chapter 3 sets the tune for the design of robotic exoskeleton. CPG-based method was used for rehabilitation and assistance purposes. In this chapter, the problem of practically stimulating the joints of real systems without considering the dynamics equation of motion of multi-joint systems were addressed. It also further clearly defines the coupling strategy for an adaptive oscillator. The possibility of providing assistance simultaneously for multi-joint level was also addressed. The Hopf AFO was used as the fundamental unit for CPG-based method. Note that this method may effectively suit motion intention detection since it based on inverse dynamic approach, however for the purpose of the mathematical study, the need for mimicking a practical scenario is needed by conceiving

a targeted task attainment. Simulations were performed and results were presented to prove the efficiency of the techniques used.

Chapter 3 brought about a certain difficulty. This difficulty is associated with correctly modelling the inverse dynamics of a system with multiple DoF. To overcome this difficulty, the forward dynamic approach was used to design a rehabilitation protocol that could perform the task of improving the motor functions of humans with lower limb difficulties about multi-joints concurrently in chapter 4. This approach is made possible because the wearer-orthosis considered is that of a rigid system. Simulation results obtained established a practicable knowledge of the proposed idea. To compare the torque required by each joint for a predefined task and that of a naturally envisaged task within the range of motion (ROM) of a knee-ankle movement, Matsuoka oscillators were used to excite each joint level and tuned to internally generate the trajectories of humans about each joint level, thereby exploring the natural dynamics of the wearer-orthosis dynamics. Simulation results further established the fact that the movement of humans could be generated via CPGs and controlled within its ROM. Control strategies used are based on computed torque control. The rehabilitative method envisaged in chapter 3 and 4 are applicable to patients in a sitting position.

Having considered users in sitting position, it becomes necessary to assume a rehabilitative walking scenario. Chapter 5 considers this aspect. Chapter 5 proposed a rhythmic trajectory design and control for rehabilitative walking in patients with lower limb disorders at the hip and knee joint level. The rhythmic trajectory was based on van der pol oscillators. It is envisaged that the joint profiles generated are close to those of humans. To investigate this rehabilitative procedure a five-link biped system was used (a rigid system is still envisaged). Although only the SSP of five-link wearer-exoskeleton device was used for the entire phase of the gait cycle, the principle lies in the stimulation of the wearer-exoskeleton at each joint level. It is therefore assumed that since the CPG-

generated gait cycle can be effectively followed by the wearer-exoskeleton dynamics, the need for the switching of each phase is not required. Nevertheless, the relabelling of each link is required at the point where the knee is at full extension.

In chapter 6, a bounded control strategy was introduced for rehabilitation purposes. This was applied to both sitting and walking scenarios. In the sitting scenario, the knee-ankle orthotic device was considered. To test the capacity and capability of this device, assistance and resistance to the robotic device were provided using a high gain observer to recover the states of the system and feed them back as the human torque to depict the human contribution. Simulation results obtained have proven the efficacy of this method. To establish the convergence of the error of the observer states and the wearer-orthosis states, a convergence analysis using Lyapunov stability theory was performed. The controller used entails a saturation bound which does ensure that the physical limits of the actuator are not exceeded. Hence, the problem of increased power and high torque is eliminated. The stability of the generalised bounded control law was also proven.

In the walking scenario, the dynamic equation of the SSP of a five-link biped system was used. This was to remedy the already known limitation of the CPG-generated walking trajectory via coupled Van der Pol oscillators. Hence, a single step gait was designed using polynomial functions, to interpolate the steady state joint angle profile so as to be able to choose initial conditions for the rehabilitative walking exercise. Results obtained were presented to ascertain the effectiveness of the control method.

7.1.2 Further Works

There has been a growing development of orthoses and exoskeleton device within the last two decades. This is not farfetched, since the population of aging people and lower limb disorders in patients are increasing rapidly. However, there remains a challenge in the

development of robotic exoskeletons that could assist the user naturally and efficiently. This therefore requires more sensitive intelligent systems. Assistive strategies are verified using various motion tasks as given in this thesis, but there is a need to verify this strategy using two or more continuous tasks on the same device. Not many researchers have been able to work on this aspect. The safety of the exoskeleton wearer has always been said to be paramount. Nonetheless, a clear method which assures this at the assistive level remains to be investigated.

Concerning this study, a sitting and walking task was provided for rehabilitation and assistive purposes. For the walking task, both legs were considered to possess the same disability. It will be interesting to consider a functional leg and a partly functional one. The need to test this on different terrains in contrast to leveled terrains will also be a good research area. The leg impact to the ground is not analysed in this work and the eventual switching of both legs are left out. For the single step gait designed, it will be necessary to verify this assumption in further works.

7.1.3 Recommendation

In the field of rehabilitation and assistive robotics, the methods used include motion intention detection, pre-specified targeted task and the eventual validations with human-in-the loop. Analysing these methods efficiently requires both theoretical and practical means. Nevertheless, since these methods are more practical, theoretical model designs are needed for experimental purposes.

7.2 Conclusion

Basically, the aim of this research was to develop functional mathematical models and control methods for actualisation of rehabilitation and assistive protocols. These models

are intended to be practically implemented in the laboratory. The principle behind this is to contribute technologically to humanity in this area of study. The problem statement and sub problems have been summarised for the purpose of clarity. The answers provided are embedded in the chapters of this thesis. This has been carefully highlighted to clearly show the contribution of this work. The thesis limitations are also detailed in this chapter and the preceding ones. This has also prompted the identification of specific research areas for further studies given in this chapter. These research areas are not restricted to the limitations of this work, but include the larger concept of robotic lower limb exoskeleton.

Bibliography

- Acebrón, J.A., Bonilla, L.L., Vicente, C.J.P., Ritort, F. & Spigler, R. 2005. *The Kuramoto model: A simple paradigm for synchronization phenomena*. *Reviews of modern physics*, 77(1), 137.
- Acosta-Marquez, C. & Bradley, D.A. 2005. *The analysis, design and implementation of a model of an exoskeleton to support mobility*. In: *Rehabilitation Robotics, 2005. ICORR 2005. 9th International Conference on*. IEEE, 99–102.
- Aguirre-Ollinger, G. 2013. *Learning muscle activation patterns via nonlinear oscillators: application to lower-limb assistance*. In: *Intelligent Robots and Systems (IROS), 2013 IEEE/RSJ International Conference on*. IEEE, 1182–1189.
- Aguirre-Ollinger, G., Colgate, J.E., Peshkin, M., Goswami, A. *et al.* 2012. *Inertia compensation control of a one-degree-of-freedom exoskeleton for lower-limb assistance: initial experiments*. *Neural Systems and Rehabilitation Engineering, IEEE Transactions on*, 20(1), 68–77.
- Ajayi, M.O., Djouani, K. & Hamam, Y. 2014. *Shank-foot trajectory control: A forward dynamics approach using computed-torque control*. In: *Humanoid Robots (Humanoids), 2014 14th IEEE-RAS International Conference on*. IEEE, 652–657.
- Aoustin, Y. 2015. *Walking Gait of a Biped with a Wearable Walking Assist Device*. *International Journal of Humanoid Robotics*, 1550018.

- Aphiratsakun, N., Chairungsarpsook, K. & Parnichkun, M. 2010. *ZMP based gait generation of AIT's Leg Exoskeleton*. In: *Computer and Automation Engineering (ICCAE), 2010 The 2nd International Conference on*, vol. 5. IEEE, 886–890.
- Banala, S.K., Kim, S.H., Agrawal, S.K. & Scholz, J.P. 2009. *Robot assisted gait training with active leg exoskeleton (ALEX)*. *Neural Systems and Rehabilitation Engineering, IEEE Transactions on*, 17(1), 2–8.
- Basmajian, J.V. 1962. *Muscles Alive. Their Functions Revealed by Electromyography*. *Academic Medicine*, 37(8), 802.
- Bateman, A. & Lin, Z. 2003. *An analysis and design method for linear systems under nested saturation*. *Systems & control letters*, 48(1), 41–52.
- Bay, J.S. & Hemami, H. 1987. *Modeling of a neural pattern generator with coupled nonlinear oscillators*. *Biomedical Engineering, IEEE Transactions on*, (4), 297–306.
- Behnke, S. 2006. *Online trajectory generation for omnidirectional biped walking*. In: *Robotics and Automation, 2006. ICRA 2006. Proceedings 2006 IEEE International Conference on*. IEEE, 1597–1603.
- Blaya, J., Herr, H. *et al.* 2004. *Adaptive control of a variable-impedance ankle-foot orthosis to assist drop-foot gait*. *Neural Systems and Rehabilitation Engineering, IEEE Transactions on*, 12(1), 24–31.
- Braune, W. & Fischer, O. 1895. *Der Gang des Menschen: I. Theil: Versuche am unbelasteten und belasteten Menschen*, vol. 1. BS Hirzel.
- Brown, T.G. 1911. *The intrinsic factors in the act of progression in the mammal*. *Proceedings of the Royal Society of London. Series B, containing papers of a biological character*, 308–319.

- Brown, T.G. 1914. *On the nature of the fundamental activity of the nervous centres; together with an analysis of the conditioning of rhythmic activity in progression, and a theory of the evolution of function in the nervous system.* *The Journal of Physiology*, 48(1), 18.
- Buchanan, J.T. 1992. *Neural network simulations of coupled locomotor oscillators in the lamprey spinal cord.* *Biological cybernetics*, 66(4), 367–374.
- Buchli, J. & Ijspeert, A.J. 2004. *Distributed central pattern generator model for robotics application based on phase sensitivity analysis.* In: *Biologically Inspired Approaches to Advanced Information Technology.* Springer, 333–349.
- Cabodevila, G. & Abba, G. 1997. *Quasi optimal gait for a biped robot using genetic algorithm.* In: *Systems, Man, and Cybernetics, 1997. Computational Cybernetics and Simulation., 1997 IEEE International Conference on*, vol. 4. IEEE, 3960–3965.
- Cai, L.L., Fong, A.J., Otoshi, C.K., Liang, Y., Burdick, J.W., Roy, R.R. & Edgerton, V.R. 2006. *Implications of assist-as-needed robotic step training after a complete spinal cord injury on intrinsic strategies of motor learning.* *The Journal of neuroscience*, 26(41), 10564–10568.
- Chan, C.Y.A. 2000. *Dynamic modeling, control and simulation of a planar five-link bipedal walking system.*
- Charalambous, C.P. 2014. *The Major Determinants in Normal and Pathological Gait.* In: *Classic Papers in Orthopaedics.* Springer, 403–405.
- Chen, B., Ma, H., Qin, L.Y., Gao, F., Chan, K.M., Law, S.W., Qin, L. & Liao, W.H. 2016. *Recent developments and challenges of lower extremity exoskeletons.* *Journal of Orthopaedic Translation*, 5, 26–37.

- Chittajallu, S. & Kohrt, K. 1996. *FORM2D—a mathematical model of the knee. Mathematical and computer modelling*, 24(9), 91–101.
- Close, J. & Todd, F. 1959. *The phasic activity of the muscles of the lower extremity. I Bone and Joint Surg 41-A: 189*, 208.
- Cohen, A.H., Holmes, P.J. & Rand, R.H. 1982. *The nature of the coupling between segmental oscillators of the lamprey spinal generator for locomotion: a mathematical model. Journal of mathematical biology*, 13(3), 345–369.
- Collins, J.J. & Richmond, S.A. 1994. *Hard-wired central pattern generators for quadrupedal locomotion. Biological Cybernetics*, 71(5), 375–385.
- Colombo, G., Wirz, M., Dietz, V. et al. 2001. *Driven gait orthosis for improvement of locomotor training in paraplegic patients. Spinal Cord*, 39(5), 252–255.
- Colombo, G., Jorg, M. & Dietz, V. 2000. *Driven gait orthosis to do locomotor training of paraplegic patients. In: Engineering in Medicine and Biology Society, 2000. Proceedings of the 22nd Annual International Conference of the IEEE*, vol. 4. IEEE, 3159–3163.
- Conradt, J. & Varshavskaya, P. 2003. *Distributed central pattern generator control for a serpentine robot. In: Proceedings of the International Conference on Artificial Neural Networks (ICANN)*. 338–341.
- Crespi, A. & Ijspeert, A.J. 2008. *Online optimization of swimming and crawling in an amphibious snake robot. Robotics, IEEE Transactions on*, 24(1), 75–87.
- Daniels, B.C. 2005. *Synchronization of globally coupled nonlinear oscillators: the rich behavior of the Kuramoto model. Ohio Wesleyan Physics Dept., Essay*, 7(2).
- de Pina Filho, A.C., Dutra, M.S. & Raptopoulos, L.S. 2005. *Modeling of a bipedal robot using mutually coupled Rayleigh oscillators. Biological cybernetics*, 92(1), 1–7.

- de Pina Filho, A.C., Santos, L. & Dutra, M.S. 2006. *Modelling of Bipedal Robots Using Coupled Nonlinear Oscillators*.
- Dellon, B. & Matsuoka, Y. 2007. *Prosthetics, exoskeletons, and rehabilitation*. *IEEE Robotics and Automation magazine*, 14(1), 30.
- Díaz, I., Gil, J.J. & Sánchez, E. 2011. *Lower-limb robotic rehabilitation: literature review and challenges*. *Journal of Robotics*, 2011.
- Do Nascimento, B.G., Vimieiro, C.B.S., Nagem, D.A.P. & Pinotti, M. 2008. *Hip orthosis powered by pneumatic artificial muscle: voluntary activation in absence of myoelectrical signal*. *Artificial organs*, 32(4), 317–322.
- Dollar, A.M. & Herr, H. 2008. *Lower extremity exoskeletons and active orthoses: challenges and state-of-the-art*. *Robotics, IEEE Transactions on*, 24(1), 144–158.
- Drake, R., Vogl, A.W. & Mitchell, A.W. 2014. *Gray's anatomy for students*. Elsevier Health Sciences.
- Dutra, M.S., de Pina Filho, A.C. & Romano, V.F. 2003. *Modeling of a bipedal locomotor using coupled nonlinear oscillators of Van der Pol*. *Biological Cybernetics*, 88(4), 286–292.
- Eberhart, H.D., Inman, V., Saunders, J., Levens, A., Bresler, B. & McCowan, T. 1947. *Fundamental studies of human locomotion and other information relating to design of artificial limbs*. *Report to the National Research Council*.
- Edgerton, V.R. & Roy, R.R. 2009. *Robotic training and spinal cord plasticity*. *Brain research bulletin*, 78(1), 4–12.
- Ekeberg, Ö. 1993. *A combined neuronal and mechanical model of fish swimming*. *Biological cybernetics*, 69(5-6), 363–374.

- Esquenazi, A., Talaty, M., Packel, A. & Saulino, M. 2012. *The ReWalk powered exoskeleton to restore ambulatory function to individuals with thoracic-level motor-complete spinal cord injury*. *American Journal of Physical Medicine & Rehabilitation*, 91(11), 911–921.
- Ferrati, F., Bortoletto, R. & Pagello, E. 2013. *Virtual modelling of a real exoskeleton constrained to a human musculoskeletal model*. In: *Biomimetic and Biohybrid Systems*. Springer, 96–107.
- Ferris, D.P. & Lewis, C.L. 2009. *Robotic lower limb exoskeletons using proportional myoelectric control*. In: *Engineering in Medicine and Biology Society, 2009. EMBC 2009. Annual International Conference of the IEEE*. IEEE, 2119–2124.
- Ferris, D.P., Sawicki, G.S. & Daley, M.A. 2007. *A physiologist’s perspective on robotic exoskeletons for human locomotion*. *International Journal of Humanoid Robotics*, 4(03), 507–528.
- Ferris, D.P., Sawicki, G.S. & Domingo, A. 2005. *Powered lower limb orthoses for gait rehabilitation*. *Topics in spinal cord injury rehabilitation*, 11(2), 34.
- Field-Fote, E.C. 2000. *Spinal cord control of movement: implications for locomotor rehabilitation following spinal cord injury*. *Physical Therapy*, 80(5), 477–484.
- Filippi, P. 1942. *Device for the automatic control of the articulation of the knee applicable to a prosthesis of the thigh*. US Patent 2,305,291.
- FitzHugh, R. 1961. *Impulses and physiological states in theoretical models of nerve membrane*. *Biophysical journal*, 1(6), 445.
- Flikop, Z. 2004. *Bounded Input Bounded Predefined Control Bounded Output*. *arXiv preprint cs/0411015*.

- Furusho, J. & Masubuchi, M. 1986. *Control of a dynamical biped locomotion system for steady walking*. *Journal of Dynamic Systems, Measurement, and Control*, 108(2), 111–118.
- Gilbert, K.E. 1966. *EXOSKELETON PROTOTYPE PROJECT*.. Tech. rep., DTIC Document.
- Guerrero-Castellanos, J., Marchand, N., Hably, A., Lesecq, S. & Delamare, J. 2011. *Bounded attitude control of rigid bodies: Real-time experimentation to a quadrotor mini-helicopter*. *Control Engineering Practice*, 19(8), 790–797.
- Guglielmelli, E., Johnson, M.J. & Shibata, T. 2009. *Guest editorial special issue on rehabilitation robotics*. *Robotics, IEEE Transactions on*, 25(3), 477–480.
- Guizzo, E. & Goldstein, H. 2005. *The rise of the body bots [robotic exoskeletons]*. *Spectrum, IEEE*, 42(10), 50–56.
- Guttman, R., Feldman, L. & Jäkbsson, E. 1980. *Frequency entrainment of squid axon membrane*. *The Journal of membrane biology*, 56(1), 9–18.
- Habib, M.K., Liu, G.L., Watanabe, K. & Izumi, K. 2007. *Bipedal locomotion control via cpgs with coupled nonlinear oscillators*. In: *Mechatronics, ICM2007 4th IEEE International Conference on*. IEEE, 1–6.
- Hassani, W., Mohammed, S. & Amirat, Y. 2013. *Real-Time EMG Driven Lower Limb Actuated Orthosis for Assistance As Needed Movement Strategy*.. In: *Robotics: Science and Systems*. Citeseer.
- Hein, D., Hild, M. & Berger, R. 2008. *Evolution of biped walking using neural oscillators and physical simulation*. In: *RoboCup 2007: Robot Soccer World Cup XI*. Springer, 433–440.

- Hellgren, J., Grillner, S. & Lansner, A. 1992. *Computer simulation of the segmental neural network generating locomotion in lamprey by using populations of network interneurons. Biological cybernetics*, 68(1), 1–13.
- Heralić, A., Wolff, K. & Wahde, M. 2007. *Central pattern generators for gait generation in bipedal robots. Humanoid Robots—New Developments*, 285–304.
- Herr, H. 2009. *Exoskeletons and orthoses: classification, design challenges and future directions. Journal of neuroengineering and rehabilitation*, 6, 21.
- Hesse, S., Schmidt, H., Werner, C. & Bardeleben, A. 2003. *Upper and lower extremity robotic devices for rehabilitation and for studying motor control. Current opinion in neurology*, 16(6), 705–710.
- Hitt, J.K., Sugar, T., Fleeger, J. *et al.* 2007. *Control of a regenerative braking powered ankle foot orthosis. In: Rehabilitation robotics, 2007. ICORR 2007. IEEE 10th international conference on. IEEE*, 28–34.
- Hobbelen, D.G. 2008. *Limit cycle walking*. TU Delft, Delft University of Technology.
- Hogan, N., Krebs, H.I., Rohrer, B., Palazzolo, J.J., Dipietro, L., Fasoli, S.E., Stein, J., Hughes, R., Frontera, W.R., Lynch, D. *et al.* 2006. *Motions or muscles? Some behavioral factors underlying robotic assistance of motor recovery. Journal of rehabilitation research and development*, 43(5), 605.
- Hooper, S.L. 2000. *Central pattern generators. Current Biology*, 10(5), R176–R179.
- Hoy, M.G., Zajac, F.E. & Gordon, M.E. 1990. *A musculoskeletal model of the human lower extremity: the effect of muscle, tendon, and moment arm on the moment-angle relationship of musculotendon actuators at the hip, knee, and ankle. Journal of biomechanics*, 23(2), 157–169.

- Hristic, D., Vukobratovic, M. & Timotijevic, M. 1981. *New model of autonomous 'active suit' for dystrophic patients*. In: *Proceedings of the International Symposium on External Control of Human Extremities*. 33–42.
- Huang, Q., Yokoi, K., Kajita, S., Kaneko, K., Arai, H., Koyachi, N. & Tanie, K. 2001. *Planning walking patterns for a biped robot*. *Robotics and Automation, IEEE Transactions on*, 17(3), 280–289.
- Hurmuzlu, Y. 1993. *Dynamics of bipedal gait: Part I—Objective functions and the contact event of a planar five-link biped*. *Journal of Applied Mechanics*, 60(2), 331–336.
- Ijspeert, A.J. 2008. *Central pattern generators for locomotion control in animals and robots: a review*. *Neural Networks*, 21(4), 642–653.
- Ijspeert, A.J. & Crespi, A. 2007. *Online trajectory generation in an amphibious snake robot using a lamprey-like central pattern generator model*. In: *IEEE International Conference on Robotics and Automation, 2007*. IEEE, 262–268.
- Ijspeert, A.J., Crespi, A. & Cabelguen, J.M. 2005. *Simulation and robotics studies of salamander locomotion*. *Neuroinformatics*, 3(3), 171–195.
- Ijspeert, A.J., Crespi, A., Ryczko, D. & Cabelguen, J.M. 2007. *From swimming to walking with a salamander robot driven by a spinal cord model*. *science*, 315(5817), 1416–1420.
- Ijspeert, A.J., Hallam, J. & Willshaw, D. 1999. *Evolving swimming controllers for a simulated lamprey with inspiration from neurobiology*. *Adaptive Behavior*, 7(2), 151–172.
- Ikehara, T., Nagamura, K., Ushida, T., Tanaka, E., Saegusa, S., Kojima, S. & Yuge, L. 2011. *Development of closed-fitting-type walking assistance device for legs and*

- evaluation of muscle activity*. In: *Rehabilitation Robotics (ICORR), 2011 IEEE International Conference on*. IEEE, 1–7.
- Inada, H. & Ishii, K. 2004. *Bipedal walk using a central pattern generator*. In: *international congress Series*, vol. 1269. Elsevier, 185–188.
- Inman, V.T., Eberhart, H.D. *et al.* 1953. *The major determinants in normal and pathological gait*. *The journal of bone & joint surgery*, 35(3), 543–558.
- Inoue, K., Ma, S. & Jin, C. 2004. *Neural oscillator network-based controller for meandering locomotion of snake-like robots*. In: *Robotics and Automation, 2004. Proceedings. ICRA '04. 2004 IEEE International Conference on*, vol. 5. IEEE, 5064–5069.
- Israel, J.F., Campbell, D.D., Kahn, J.H. & Hornby, T.G. 2006. *Metabolic costs and muscle activity patterns during robotic-and therapist-assisted treadmill walking in individuals with incomplete spinal cord injury*. *Physical therapy*, 86(11), 1466–1478.
- Ivashko, D.G., Prilutsky, B.I., Markin, S., Chapin, J.K. & Rybak, I.A. 2003. *Modeling the spinal cord neural circuitry controlling cat hindlimb movement during locomotion*. *Neurocomputing*, 52, 621–629.
- Jackson, E.A. 1992. *Perspectives of nonlinear dynamics*, vol. 1. CUP Archive.
- Kassim, M.H., Zainal, N. & Arshad, M.R. 2008. *Central Pattern Generator in Bio-inspired Robot: Simulation using MATLAB*.
- Kato 1983. *Biped Walking Robot*. In: *Proceeding of 6th World Congress on Theory of Machines and Mechanisms*. 22–32.
- Kazerooni, H., Racine, J.L., Huang, L. & Steger, R. 2005. *On the control of the berkeley lower extremity exoskeleton (BLEEX)*. In: *Robotics and Automation, 2005. ICRA 2005. Proceedings of the 2005 IEEE International Conference on*. IEEE, 4353–4360.

- Khalil, H.K. & Grizzle, J. 1996. *Nonlinear systems*, vol. 3. Prentice hall New Jersey.
- Khalil, W. & Dombre, E. 1999. *Modélisation, identification et commande des robots*. Hermès science publ.
- Khang, G. & Zajac, F.E. 1989. *Paraplegic standing controlled by functional neuromuscular stimulation. i. computer model and control-system design*. *Biomedical Engineering, IEEE Transactions on*, 36(9), 873–884.
- Kiguchi, K., Iwami, K., Yasuda, M., Watanabe, K. & Fukuda, T. 2003. *An exoskeletal robot for human shoulder joint motion assist*. *Mechatronics, IEEE/ASME Transactions on*, 8(1), 125–135.
- Kiguchi, K., Tanaka, T. & Fukuda, T. 2004. *Neuro-fuzzy control of a robotic exoskeleton with EMG signals*. *Fuzzy Systems, IEEE Transactions on*, 12(4), 481–490.
- Kim, K., Kim, J.J., Kang, S.R., Jeong, G.Y. & Kwon, T.K. 2010. *Analysis of the assistance characteristics for the plantarflexion torque in elderly adults wearing the powered ankle exoskeleton*. In: *Control Automation and Systems (ICCAS), 2010 International Conference on*. IEEE, 576–579.
- Kim, K., Yu, C.H., Jeong, G.Y., Heo, M. & Kwon, T.K. 2013. *Analysis of the assistance characteristics for the knee extension motion of knee orthosis using muscular stiffness force feedback*. *Journal of Mechanical Science and Technology*, 27(10), 3161–3169.
- Kong, K. & Jeon, D. 2006. *Design and control of an exoskeleton for the elderly and patients*. *Mechatronics, IEEE/ASME Transactions on*, 11(4), 428–432.
- Kong, K. & Tomizuka, M. 2009. *Control of exoskeletons inspired by fictitious gain in human model*. *Mechatronics, IEEE/ASME Transactions on*, 14(6), 689–698.
- Kopell, N., Ermentrout, G. & Williams, T. 1991. *On chains of oscillators forced at one end*. *SIAM Journal on Applied Mathematics*, 51(5), 1397–1417.

- Kordasz, M., Kuczkowski, K. & Sauer, P. 2011. *Study on possible control algorithms for lower limb rehabilitation system*. In: *Rehabilitation Robotics (ICORR), 2011 IEEE International Conference on*. IEEE, 1–6.
- Large, E.W. 2000. *On synchronizing movements to music*. *Human Movement Science*, 19(4), 527–566.
- Lewis, C.L. & Ferris, D.P. 2011. *Invariant hip moment pattern while walking with a robotic hip exoskeleton*. *Journal of biomechanics*, 44(5), 789–793.
- Lewis, F.L., Dawson, D.M. & Abdallah, C.T. 2003. *Robot manipulator control: theory and practice*. CRC Press.
- Lintzen, C. 2011. *Oscillator-based walking assistance*. Ph.D. thesis, TU Delft, Delft University of Technology.
- Liu, G.L., Habib, M.K., Watanabe, K. & Izumi, K. 2008. *Central pattern generators based on Matsuoka oscillators for the locomotion of biped robots*. *Artificial Life and Robotics*, 12(1-2), 264–269.
- Makinson, B. 1971. *Research and development prototype for machine augmentation of human strength and endurance. hardiman i project*. Tech. rep., DTIC Document.
- Marey, E.J. 1873. *De la locomotion terrestre chez les bipedes et les quadrupedes*. Impr. E. Martinet.
- Matsuoka, K. 1985. *Sustained oscillations generated by mutually inhibiting neurons with adaptation*. *Biological cybernetics*, 52(6), 367–376.
- Matsuoka, K. 1987. *Mechanisms of frequency and pattern control in the neural rhythm generators*. *Biological cybernetics*, 56(5-6), 345–353.

- McCrea, D.A. 1996. *Supraspinal and segmental interactions*. *Canadian journal of physiology and pharmacology*, 74(4), 513–517.
- Mefoued, S., Mohammed, S. & Amirat, Y. 2011. *Knee joint movement assistance through robust control of an actuated orthosis*. In: *Intelligent Robots and Systems (IROS), 2011 IEEE/RSJ International Conference on*. IEEE, 1749–1754.
- Meirovitch, L. 1975. *Elements of vibration analysis*. McGraw-Hill.
- Merabet, A. & Gu, J. 2010. *Advanced Nonlinear Control of Robot Manipulators*. INTECH Open Access Publisher.
- Mondal, S., Nandy, A., Verma, C., Shukla, S., Saxena, N., Chakraborty, P. & Nandi, G.C. 2011. *Modeling a Central Pattern Generator to Generate the Biped Locomotion of a Bipedal Robot Using Rayleigh Oscillators*. In: *Contemporary Computing*. Springer, 289–300.
- Moore, J. 1986. *Pitman: A powered exoskeleton suit for the infantryman*. Los Alamos Nat. Lab., Los Alamos, NM, Tech. Rep. LA-10761-MS.
- Mu, X. & Wu, Q. 2003a. *A complete dynamic model of five-link bipedal walking*. In: *American Control Conference, 2003. Proceedings of the 2003*, vol. 6. IEEE, 4926–4931.
- Mu, X. & Wu, Q. 2003b. *Synthesis of a complete sagittal gait cycle for a five-link biped robot*. *Robotica*, 21(05), 581–587.
- Muybridge, E. 1882. *The Horse in Motion as Shown by Instantaneous Photography*.
- Nguyen, C. 2009. *Van der Pol Oscillators Synchronization: Methods and Applications*.
- Nor, N.M. & Ma, S. 2014. *A simplified CPGS network with phase oscillator model for locomotion control of a snake-like robot*. *Journal of Intelligent & Robotic Systems*, 75(1), 71–86.

- Paul, J. 2005. *The history of musculoskeletal modelling in human gait. Theoretical Issues in Ergonomics Science*, 6(3-4), 217–224.
- Perko, L. 2013. *Differential equations and dynamical systems*, vol. 7. Springer Science & Business Media.
- Pohl, M., Werner, C., Holzgraefe, M., Kroczeck, G., Wingendorf, I., Hoölig, G., Koch, R. & Hesse, S. 2007. *Repetitive locomotor training and physiotherapy improve walking and basic activities of daily living after stroke: a single-blind, randomized multicentre trial (DEutsche GAngtrainerStudie, DEGAS). Clinical rehabilitation*, 21(1), 17–27.
- Pons, J., Moreno, J., Brunetti, F. & Rocon, E. 2007. *Lower-limb wearable exoskeleton*. INTECH Open Access Publisher.
- Pons, J.L. *et al.* 2008. *Wearable robots: biomechatronic exoskeletons*.
- Quintero, H., Farris, R.J., Goldfarb, M. *et al.* 2011. *Control and implementation of a powered lower limb orthosis to aid walking in paraplegic individuals*. In: *Rehabilitation Robotics (ICORR), 2011 IEEE International Conference on*. IEEE, 1–6.
- Red, E. 2000. *A dynamic optimal trajectory generator for Cartesian Path following. Robotica*, 18(05), 451–458.
- Rifai, H., Hassani, W., Mohammed, S. & Amirat, Y. 2011. *Bounded control of an actuated lower limb orthosis*. In: *Decision and Control and European Control Conference (CDC-ECC), 2011 50th IEEE Conference on*. IEEE, 873–878.
- Righetti, L., Buchli, J. & Ijspeert, A.J. 2005. *From dynamic hebbian learning for oscillators to adaptive central pattern generators*. In: *Proceedings of 3rd International Symposium on Adaptive Motion in Animals and Machines–AMAM 2005*, BIOROB-CONF-2005-011. Verlag ISLE, Ilmenau.

- Righetti, L., Buchli, J. & Ijspeert, A.J. 2006. *Dynamic hebbian learning in adaptive frequency oscillators*. *Physica D: Nonlinear Phenomena*, 216(2), 269–281.
- Righetti, L., Buchli, J. & Ijspeert, A.J. 2009. *Adaptive frequency oscillators and applications*. *The Open Cybernetics and Systemics Journal*, 3(BIOROB-ARTICLE-2010-001), 64–69.
- Righetti, L. & Ijspeert, A.J. 2006. *Programmable central pattern generators: an application to biped locomotion control*. In: *Proceedings 2006 IEEE International Conference on Robotics and Automation, 2006. ICRA 2006..* IEEE, 1585–1590.
- Rinderknecht, M.D., Delaloye, F.A., Crespi, A., Ronsse, R. & Ijspeert, A.J. 2011. *Assistance using adaptive oscillators: Robustness to errors in the identification of the limb parameters*. In: *Rehabilitation Robotics (ICORR), 2011 IEEE International Conference on*. IEEE, 1–6.
- Ronsse, R., Koopman, B., Vitiello, N., Lenzi, T., De Rossi, S.M.M., van den Kieboom, J., van Asseldonk, E., Carrozza, M.C., van der Kooij, H. & Ijspeert, A.J. 2011. *Oscillator-based walking assistance: A model-free approach*. In: *Rehabilitation Robotics (ICORR), 2011 IEEE International Conference on*. IEEE, 1–6.
- Ronsse, R., Vitiello, N., Lenzi, T., Van Den Kieboom, J., Carrozza, M.C. & Ijspeert, A.J. 2010. *Adaptive oscillators with human-in-the-loop: Proof of concept for assistance and rehabilitation*. In: *Biomedical Robotics and Biomechatronics (BioRob), 2010 3rd IEEE RAS and EMBS International Conference on*. IEEE, 668–674.
- Rosheim, M.E. 1990. *Man-amplifying exoskeleton*. In: *1989 Advances in Intelligent Robotics Systems Conference*. International Society for Optics and Photonics, 402–411.

- Roy, P. & Demiris, Y. 2005. *Analysis of biped gait patterns generated by van der Pol and Rayleigh oscillators under feedback*. In: *3rd International Symposium on Adaptive Motion in Animals and Machines (AMAM2005)*, pp. Ilmenau, Germany, in *Proceedings Of AMAM2005*.
- Sankai, Y. 2006. *Leading edge of cybernics: Robot suit hal*. In: *SICE-ICASE, 2006. International Joint Conference*. IEEE, P-1.
- Sawicki, G.S. & Ferris, D.P. 2009. *Powered ankle exoskeletons reveal the metabolic cost of plantar flexor mechanical work during walking with longer steps at constant step frequency*. *Journal of Experimental Biology*, 212(1), 21–31.
- Schöner, G., Jiang, W.Y. & Kelso, J.S. 1990. *A synergetic theory of quadrupedal gaits and gait transitions*. *Journal of theoretical Biology*, 142(3), 359–391.
- Seireg, A. & Grundmann, J. 1981. *Design of a multitask exoskeletal walking device for paraplegics*. *Biomechanics of Medical Devices*, 569–644.
- Seo, K., Hyung, S., Choi, B.K., Lee, Y. & Shim, Y. 2015. *A new adaptive frequency oscillator for gait assistance*. In: *Robotics and Automation (ICRA), 2015 IEEE International Conference on*. IEEE, 5565–5571.
- Shih, C.L. 1997. *Gait synthesis for a biped robot*. *Robotica*, 15(06), 599–607.
- Slight, T.J., Romeira, B., Wang, L., Figueiredo, J.M., Wasige, E. & Ironside, C.N. 2008. *A Liénard oscillator resonant tunnelling diode-laser diode hybrid integrated circuit: model and experiment*. *Quantum Electronics, IEEE Journal of*, 44(12), 1158–1163.
- Spivak, D.I. & Kent, R.E. 2012. *Ologs: a categorical framework for knowledge representation*. *PLoS One*, 7(1), e24274.

- Strausser, K.A. & Kazerooni, H. 2011. *The development and testing of a human machine interface for a mobile medical exoskeleton*. In: *Intelligent Robots and Systems (IROS), 2011 IEEE/RSJ International Conference on*. IEEE, 4911–4916.
- Strickland, E. 2012. *Good-bye, wheelchair*. *Spectrum, IEEE*, 49(1), 30–32.
- Strogatz, S.H. 2014. *Nonlinear dynamics and chaos: with applications to physics, biology, chemistry, and engineering*. Westview press.
- Swevers, J., Ganseman, C., Tükel, D.B., De Schutter, J. & Van Brussel, H. 1997. *Optimal robot excitation and identification*. *Robotics and Automation, IEEE Transactions on*, 13(5), 730–740.
- Takemura, H., Onodera, T., Ming, D. & Mizoguchi, H. 2012. *Design and control of a wearable stewart platform-type ankle-foot assistive device*. *International Journal of Advanced Robotic Systems, Int J Adv Robotic Sy*, 9.
- Traven, H., Brodin, L., Lansner, A., Ekeberg, O., Wallén, P. & Grillner, S. 1993. *Computer simulations of NMDA and non-NMDA receptor-mediated synaptic drive: sensory and supraspinal modulation of neurons and small networks*. *Journal of neurophysiology*, 70(2), 695–709.
- Tsukahara, A., Kawanishi, R., Hasegawa, Y. & Sankai, Y. 2010. *Sit-to-stand and stand-to-sit transfer support for complete paraplegic patients with robot suit HAL*. *Advanced robotics*, 24(11), 1615–1638.
- Tzafestas, S., Raibert, M. & Tzafestas, C. 1996. *Robust sliding-mode control applied to a 5-link biped robot*. *Journal of Intelligent and Robotic Systems*, 15(1), 67–133.
- Uyar, E., Baser, Ö., Baci, R. & Özçivici, E. 2009. *Investigation of bipedal human gait dynamics and knee motion control*. *Izmir, Turkey: Dokuz Eylül University-Faculty of Engineering Department of Mechanical Engineering*. Retrieved August.

- Vallery, H., van Asseldonk, E.H., Buss, M. & van der Kooij, H. 2009. *Reference trajectory generation for rehabilitation robots: complementary limb motion estimation*. *Neural Systems and Rehabilitation Engineering, IEEE Transactions on*, 17(1), 23–30.
- van der Kooij, H., Koopman, B. & van der Helm, F.C. 2008. *Human motion control. Reader for Delft University course wb2407 and Twente University course, 115047*, 211–220.
- Van der Pol, B. & Van der Mark, J. 1927. *Frequency demultiplication*. *Nature*, 120, 363–364.
- Veskos, P. & Demiris, Y. 2006. *Experimental comparison of the van der Pol and Rayleigh nonlinear oscillators for a robotic swinging task*. In: *Proceedings of the AISB 2006 Conference, Adaptation in Artificial and Biological Systems, Bristol*. 197–202.
- Vukobratovic, M., Borovac, B., Surla, D. & Stokic, D. 1990. *Biped locomotion, Scientific fundamentals of robotics 7*.
- Vukobratovic, M. & Juricic, D. 1969. *Contribution to the synthesis of biped gait*. *Biomedical Engineering, IEEE Transactions on*, (1), 1–6.
- Wadden, T., Hellgren, J., Lansner, A. & Grillner, S. 1997. *Intersegmental coordination in the lamprey: simulations using a network model without segmental boundaries*. *Biological Cybernetics*, 76(1), 1–9.
- Wallén, P., Ekeberg, O., Lansner, A., Brodin, L., Traven, H. & Grillner, S. 1992. *A computer-based model for realistic simulations of neural networks. II. The segmental network generating locomotor rhythmicity in the lamprey*. *Journal of Neurophysiology*, 68(6), 1939–1950.

- Walsh, C.J., Pasch, K. & Herr, H. 2006a. *An autonomous, underactuated exoskeleton for load-carrying augmentation*. In: *Intelligent Robots and Systems, 2006 IEEE/RSJ International Conference on*. IEEE, 1410–1415.
- Walsh, C.J., Paluska, D., Pasch, K., Grand, W., Valiente, A. & Herr, H. 2006b. *Development of a lightweight, underactuated exoskeleton for load-carrying augmentation*. In: *Robotics and Automation, 2006. ICRA 2006. Proceedings 2006 IEEE International Conference on*. IEEE, 3485–3491.
- Wang, G. 2003. *Observer-based feedback control methods for an underactuated robot system*. Ph.D. thesis, Simon Fraser University.
- Wang, L., Wang, S., van Asseldonk, E.H. & van der Kooij, H. 2013. *Actively controlled lateral gait assistance in a lower limb exoskeleton*. In: *Intelligent Robots and Systems (IROS), 2013 IEEE/RSJ International Conference on*. IEEE, 965–970.
- Weber, W. & Weber, E. 1836. *Mechanic der Menschlichen Gehwerkzeuge*.
- Westlake, K.P. & Patten, C. . *Pilot study of Lokomat versus manual-assisted treadmill training for locomotor recovery post-stroke*. *Journal of neuroengineering and rehabilitation*, 6, 18.
- Williams, T.L. 1992. *Phase coupling by synaptic spread in chains of coupled neuronal oscillators*. *Science*, 258(5082), 662–665.
- Williamson, M.M. 1999a. *Designing rhythmic motions using neural oscillators*. In: *Intelligent Robots and Systems, 1999. IROS'99. Proceedings. 1999 IEEE/RSJ International Conference on*, vol. 1. IEEE, 494–500.
- Williamson, M.M. 1999b. *Robot arm control exploiting natural dynamics*. Ph.D. thesis, Citeseer.

- Wojtyra, M. 2000. *Dynamical analysis of human walking*. EUROPEAN ADAMS USERS CONFERENCE.
- Wolbrecht, E.T., Chan, V., Reinkensmeyer, D.J. & Bobrow, J.E. 2008. *Optimizing compliant, model-based robotic assistance to promote neurorehabilitation*. *Neural Systems and Rehabilitation Engineering, IEEE Transactions on*, 16(3), 286–297.
- Wu, X. & Ma, S. 2010. *CPG-based control of serpentine locomotion of a snake-like robot*. *Mechatronics*, 20(2), 326–334.
- Yagn, N. 1890. *Apparatus for facilitating walking*. US Patent 420,179.
- Yali, H. & Xingsong, W. 2008. *Kinematics analysis of lower extremity exoskeleton*. In: *Control and Decision Conference, 2008. CCDC 2008. Chinese*. IEEE, 2837–2842.
- Yan, T., Cempini, M., Oddo, C.M. & Vitiello, N. 2015. *Review of assistive strategies in powered lower-limb orthoses and exoskeletons*. *Robotics and Autonomous Systems*, 64, 120–136.
- Yu, Y., Liang, W. & Ge, Y. 2011. *Jacobian analysis for parallel mechanism using on human walking power assisting*. In: *Mechatronics and Automation (ICMA), 2011 International Conference on*. IEEE, 282–288.
- Zaroodny, S.J. 1963. *BUMPUSHER-A POWERED AID TO LOCOMOTION*.. Tech. rep., DTIC Document.
- Zarrugh, M. & Radcliffe, C. 1979. *Computer generation of human gait kinematics*. *Journal of biomechanics*, 12(2), 99–111.
- Zhang, J.F., Yang, C.J., Chen, Y., Zhang, Y. & Dong, Y.M. 2008. *Modeling and control of a curved pneumatic muscle actuator for wearable elbow exoskeleton*. *Mechatronics*, 18(8), 448–457.

- Zhao, Y.j. & Xu, C. 2008. *Design and simulation of human lower extremity exoskeleton. Journal of System Simulation*, 20(17), 4756–4759.
- Zheng, Y.F. & Shen, J. 1990. *Gait synthesis for the SD-2 biped robot to climb sloping surface. Robotics and Automation, IEEE Transactions on*, 6(1), 86–96.
- Zielińska, T. 1996. *Coupled oscillators utilised as gait rhythm generators of a two-legged walking machine. Biological Cybernetics*, 74(3), 263–273.
- Zielińska, T. 2009. *Biological inspiration used for robots motion synthesis. Journal of Physiology-Paris*, 103(3), 133–140.
- Zielinska, T., Chew, C.M., Kryczka, P. & Jargilo, T. 2009. *Robot gait synthesis using the scheme of human motions skills development. Mechanism and Machine Theory*, 44(3), 541–558.
- Zoss, A., Kazerooni, H. & Chu, A. 2005. *On the mechanical design of the Berkeley Lower Extremity Exoskeleton (BLEEX). In: 2005 IEEE/RSJ International Conference on Intelligent Robots and Systems, 2005. (IROS 2005).. 3465–3472.*

APPENDIX A. Nonlinear Oscillators

A.1 Introduction

Oscillators refer to mechanisms that are capable of generating repeated periodic action or rather, any measurable quantity capable of repetition. Examples of such mechanisms are; some neurons, cells (pacemaker cell), waves (vibrations in bridges), electric circuits (brightness of a bulb), etc. Oscillators could be termed "linear" or "nonlinear" depending on the number of frequencies its motion possesses. Linear oscillators oscillate with one frequency while nonlinear oscillators oscillate with more than one frequency. Describing nonlinear oscillators requires building blocks that depend on time. These building blocks are used to depict its behaviour and could be represented by a differential equation.

Among other characteristics of a nonlinear oscillator, one characteristic that is of particular interest is the existence of closed trajectories. The amplitude of closed trajectory depends on the initial energy supplied to the system. These closed trajectories could be referred to as *limit cycles*, and are often associated with periodic movement. However, the amplitude of a limit cycle depends on both the energy supplied to the system and the system parameters (building blocks). According to ([Meirovitch \(1975\)](#)), limit cycles can be considered as movements of "balance" in which the system performs periodic

movement. By "balance", it implies that energy is gained in parts of the cycle and energy is lost in the other parts of the cycle. Hence, the energy at the end of the cycle must be zero. Some of the oscillators which have been extensively used in works related to human movement are; the Van der Pol oscillators, Matsuoka oscillators and Hopf oscillators. In this appendix, the mathematical background behind these nonlinear oscillators and their coupling principles are presented and hence, provides the foundation for which their applications in robotic exoskeleton are built.

A.2 Van der Pol Oscillator

Van der Pol oscillator was proposed by a Dutch electrical engineer called Balthasar van der Pol (1889-1959) in 1920. With the aid of vacuum tubes, van der Pol investigated electric circuits and discovered that these circuits present stable oscillations which could be termed limit cycles. He became the first to present experimental studies on chaos ([Van der Pol and Van der Mark \(1927\)](#)). His model has since been actively used in the field of engineering, physical and biological sciences ([FitzHugh, 1961](#); [Slight, Romeira, Wang, Figueiredo, Wasige and Ironside, 2008](#); [Zielińska, 2009](#); [Nguyen, 2009](#)). The Van der Pol oscillator is governed by a second-order differential equation:

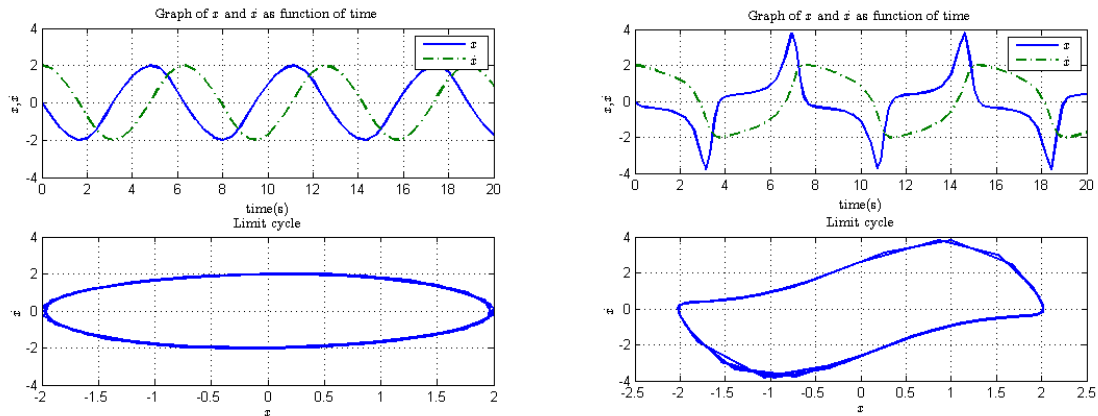
$$\ddot{x} + \mu(x^2 - 1)\dot{x} + x = 0 \tag{A.1}$$

where x is the dynamical variable and μ is the damping parameter.

In an electric circuit, oscillator parameters vary with an increase in voltage. With regard to the Van der Pol oscillators, an increase in voltage symbolise an increase of the frequency. Choosing values for \dot{x} and x and integrating the differential equation, it is possible to prove that the Van der Pol oscillator satisfies the Liénard's theorem¹ (see

¹ Liénard's theorem states that; for a certain class of differential equations called Liénard's system, one can prove the existence of a stable limit cycle. An example of such system is the Van der Pol oscillator.

Perko (2013)).



Left: $x = 2$ & $\mu = 0.1$. Right: $x = 2$ & $\mu = 2$.

Figure A.1: Graph of x and \dot{x} as function of time and the trajectory in the phase plane (limit cycle).

From Fig. A.1, it can be deduced that; for $\mu \ll 1$ the oscillator has a stable limit cycle with radius $r = 2$, and for $\mu \gg 1$ the oscillator becomes a relaxation oscillator, having a limit cycle that deviates from its ideal radius. However, relaxation oscillators are characterised by its stable limit cycles, or self-sustaining oscillation which makes them robust to perturbations. It was based on this observation that van der Pol and van der Mark modelled the electrical activity of the heart. It should be noted that the variation in oscillator parameters provides a platform for which the model of any system can be formulated. This is more eminent when the coupling of several oscillators is required to formulate the model of physical systems.

Considering forcing terms for the Van der Pol oscillator, van der Pol discovered that there seems to be a locking behaviour of the mean period of the dynamical variable x . This was further investigated by several researchers; which eventually motivated the investigation of phase-locking in neural tissue in (Guttman, Feldman and Jakobsson (1980)). The model used by van der Pol can be described as

$$\ddot{x} + \mu(x^2 - 1)\dot{x} + x = F \quad (\text{A.2})$$

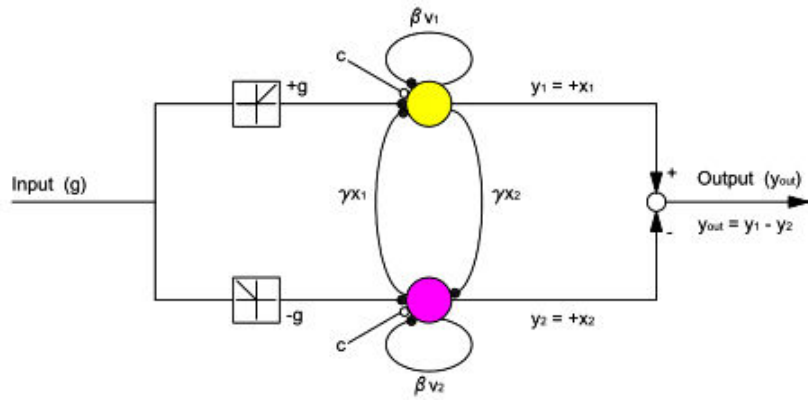
where $F = A\cos(\frac{2\pi t}{T})$ is the forcing term, T is the period of the forcing term, x and μ are same as above.

This forcing term could be used as an impulsive perturbation so as to observe the recovery time of the oscillator. The importance of this is to verify the recovery ability of the oscillator when dedicated to a specific joint pattern during human locomotion. This was investigated in (Zielińska (1996)). For more insight on forcing terms see (Jackson, 1992; Strogatz, 2014).

A.3 Matsuoka Oscillator

The Matsuoka oscillator was first developed by Kiyotoshi Matsuoka in (Matsuoka (1985)). In a bid to mathematically discuss the sustained oscillations generated by mutual inhibition of neurons, Matsuoka represented this effect by a continuous-variable model with adaptation. This model was since referred to as Matsuoka oscillator, and can be represented by some set of differential equations (see Eq. (4.13)). For the description of these parameters see subsection 4.5.2. This allows continuous inhibition of the neurons in conjunction with the nonlinear function (see Fig. A.2 for a structural view of the Matsuoka oscillator). The induction of a stable relaxation oscillation without external input could then be realised based on this phenomenon.

However, its control scheme lies in the oscillator's ability to vibrate some parts of the physical system with an introduction of certain sensor signals as input. Fig. A.3 shows the oscillation generated in the presence of an external input. The external input is defined by a periodic sine wave of the form $A\sin(\omega t)$. This exemplifies the oscillator's capability to adapt to the natural dynamics of the physical system and therefore pro-



Blanked dots represent excitatory, while filled dots symbolise inhibitory synapses.

Figure A.2: Structural view of the Matsuoka oscillator.

vides a means of energy-efficient actuation. This feature enables the application of the Matsuoka oscillator to robotic systems that perform diverse rhythmic movements.

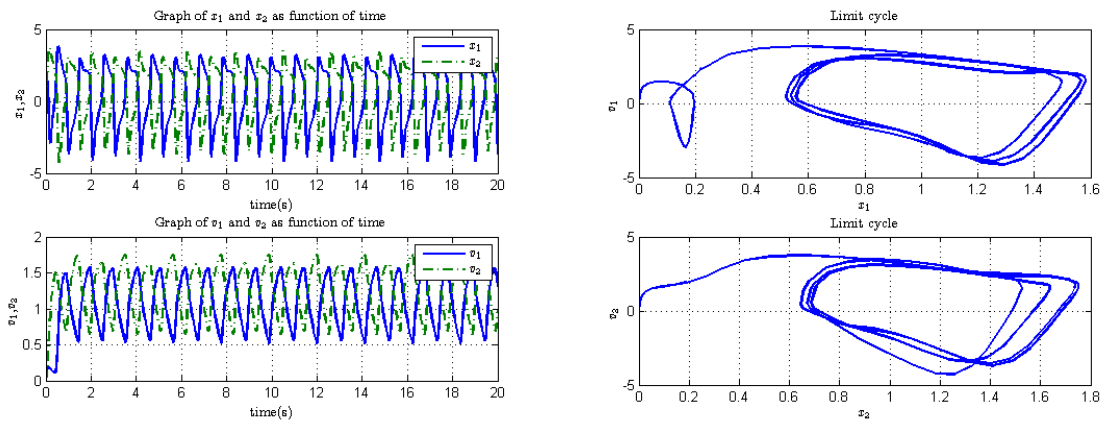


Figure A.3: Left: Graph of x and v as a function of time. Right: The trajectory in the phase plane (limit cycle).

A.4 Hopf Oscillator

The classical Hopf oscillator is given by:

$$\begin{aligned}\dot{x} &= (\mu - x^2 - y^2)x - \omega y \\ \dot{y} &= (\mu - x^2 - y^2)y + \omega x\end{aligned}\tag{A.3}$$

where μ is the strength and ω is the natural frequency of the oscillator.

This model establishes the fact that there is an equilibrium point at $(0,0)$, which is stable when $\mu = 0$. With reference to Hartman-Grobman theorem², linearising the model at the equilibrium point gives:

$$\begin{bmatrix} \mu & -\omega \\ \omega & \mu \end{bmatrix}\tag{A.4}$$

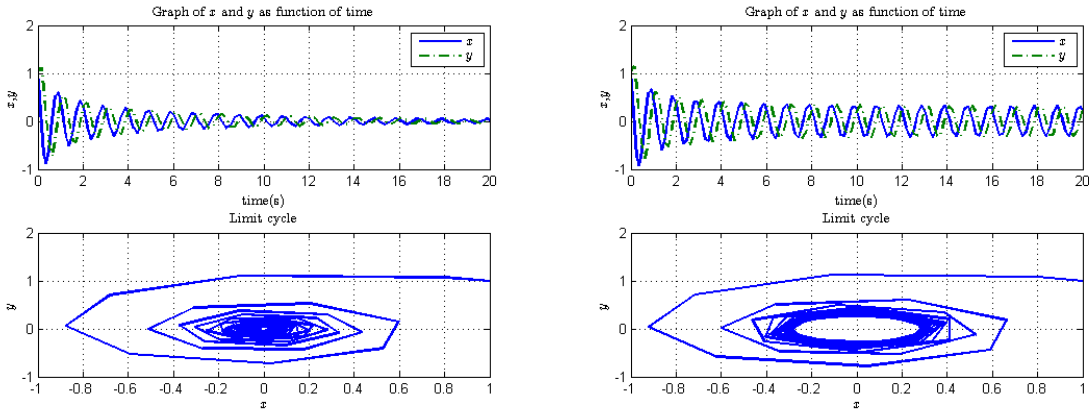
with eigenvalue $\lambda = \mu \pm i\omega$. The equilibrium point $(0,0)$ is locally asymptotically stable for $\mu < 0$ and unstable for $\mu > 0$. However, the system has a stable limit cycle when the amplitude is $\sqrt{\mu}$ if $\mu > 0$. This proves that there is a Hopf bifurcation at $\mu = 0$. Fig. A.4 presents two typical examples to buttress this point. It can be observed that when $\mu > 0$, there exist a limit cycle with radius $r = \sqrt{\mu}$, while all solutions are driven to the stable equilibrium point $(0,0)$ when $\mu < 0$. This certifies that $(0,0)$ is globally asymptotically stable.

In polar form, the Hopf oscillator can be written as

$$\begin{aligned}\dot{r} &= r(\mu - r^2) \\ \dot{\phi} &= \omega\end{aligned}\tag{A.5}$$

where r amplitude and ϕ is the phase. This “augmented-phase equation” is a special feature of this oscillator in particular. It clearly shows that the amplitude and the phase of this oscillator are completely independent.

²Hartman-Grobman theorem states that the behaviour of a dynamical system in a domain near a hyperbolic equilibrium point is qualitatively the same as the behaviour of its linearisation near this equilibrium point, provided that no eigenvalue of the linearisation has its real part equal to zero.



Left: $\mu = -0.1$. Right: $\mu = 0.1$. $\omega = 2\pi$ for both cases.

Figure A.4: Graph of x and v as a function of time and the trajectory in the phase plane (limit cycle).

In order for any oscillator to track the rhythmic movement of any physical system, there must be a way by which it could sense the fundamental parameters (e.g frequency) of the physical system. This requires the addition of a forcing term to the oscillator equation. To adapt the oscillator frequency to the frequency of the physical system does not appear as straightforward as it might seem. This is because the frequency of physical systems could vary based on its speed (velocity). Hence, continual re-adaptation of the oscillator frequency to the physical system is required. The development of the adaptive Hopf oscillator by (Righetti, Buchli and Ijspeert (2006)) is therefore needed for this purpose. Righetti added a third variable that allows the natural frequency of the oscillator to be varied.

The increasing interest in the use of nonlinear oscillators is based on their synchronisation capabilities with other oscillators or with external driving signals. Although, its synchronisation capabilities are limited, it could be achieved by carefully choosing the model parameters, which are principally the coupling strength and the frequency difference between the oscillator and other oscillators, intended to be synchronised or

the external driving signals. This is somewhat very difficult to achieve. However, to reduce the difficulties encountered when trying to choose model parameters to ensure synchronisation with the external driving signal, a learning/adaptation mechanism which adapts the oscillator frequency to the frequency of any periodic signal was proposed in (Righetti, Buchli and Ijspeert (2009)). This was achieved by tuning the parameter with the strongest influence on the frequency of the oscillator into a new state variable of the system. The mechanism was found to be generic enough to be applied to different types of oscillators. This frequency adaptation process goes beyond mere entrainment; which is an important feature of an oscillator. This is due to the fact that the learned frequency stays encoded in the oscillator even if the input signal disappears. The initial condition of the oscillator frequency is often trivial. Nevertheless, synchronisation of two or more oscillators could be achieved using classical control methods as demonstrated in (Nguyen (2009)).

Adaptive oscillators are oscillators which adapt their phase and frequency in response to an external input. These oscillators are particularly interesting when applied to rhythmic patterns. The Hopf oscillator forms the basic unit considered for this adaptation scheme. It possesses the ability to adapt the frequency of any periodic input signal, without requiring any external optimization algorithm. The system of equations required to transform a basic oscillator into an adaptive frequency oscillator (AFO) are given by

$$\begin{aligned}
 \dot{x} &= \gamma(\mu - x^2 - y^2)x - \omega y + \epsilon F(t) \\
 \dot{y} &= \gamma(\mu - x^2 - y^2)y + \omega x \\
 \dot{\omega} &= -\epsilon F(t) \left(\frac{y}{\sqrt{x^2 + y^2}} \right)
 \end{aligned} \tag{A.6}$$

where μ controls the amplitude of the oscillations, γ controls the speed of recovery after perturbation, ϵ is the coupling strength which must be greater than 0; $\epsilon > 0$, $F(t)$ is the periodic input to which the oscillator will adapt its frequency, ω controls the frequency of the oscillations, and this is the frequency adapted to periodic input $F(t)$.

To further investigate the validity of this AFO, simulations which provide educational insight into its parameter variation are presented accordingly.

A.4.1 Single Frequency Signal

Consider a periodic function $F(t) = \sin(ft)$; where f is the frequency of the function. Given a teaching signal defined as; $F(t) = \sin(30t)$, the adaptive oscillator is used to learn the teaching signal, i.e. adapting its frequency to the frequency of the teaching signal. Using MATLAB/SIMULINK, different initial conditions of the frequency of the adaptive oscillator $\omega(0) = 10, 15, 25, 35, 40$ is considered, with $\epsilon = 0.9, \mu = 0.2, \gamma = 0.2, x = 1, y = 0$. The plot is shown in Fig. A.5.

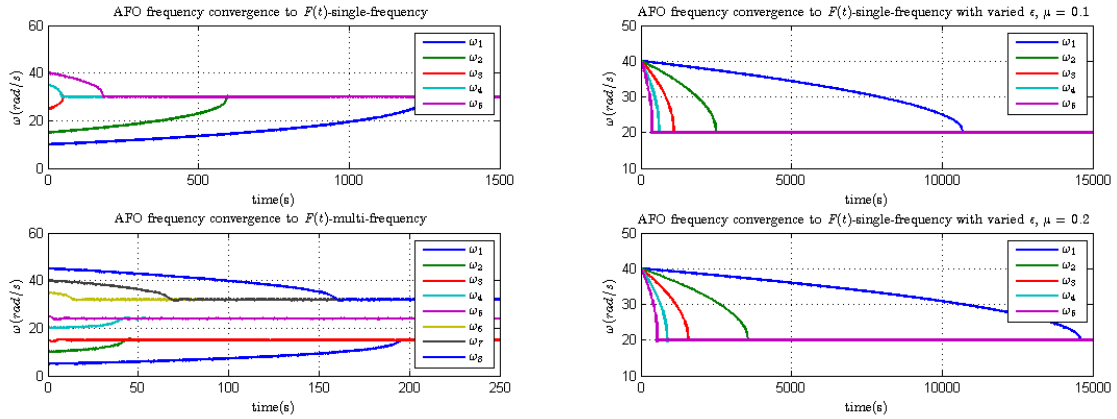


Figure A.5: Left: AFO frequency convergence to $F(t)$ with varied ω . Right: AFO frequency convergence to $F(t)$ with varied ϵ .

From the above, Fig. A.5 (Top-Left) shows that the oscillator could adapt its own frequency to the frequency of the input signal irrespective of the initial frequency $\omega(0)$ but the durations at which it occurs differs. This is based on the closeness of the initial frequency to the frequency of the teaching signal. It should be noted at this the juncture; that the need for carefully choosing the difference between the oscillator frequency and the frequency of the periodic signal is paramount. A large frequency difference may not allow the system to synchronise.

Furthermore, using a simple periodic function (teaching signal) $F(t) = \sin(20t)$, the adaptation of the oscillator's natural frequency at $\omega(0)$ for different values of the coupling strength and the amplitude control parameter; $\epsilon = 0.2, 0.4, 0.6, 0.8, 1$, $\mu = 0.1, 0.2$ and the speed of recovery control $\gamma = 0.2$ is simulated and as such the effect of the coupling strength is verified. μ , which controls the amplitude of the oscillations is also verified using the different values stated above (see Fig. A.5 (Right)).

It can be deduced from Fig. A.5 (Right) that the convergence speed of the frequency of the adaptive oscillator to the teaching signal is determined by the coupling strength.

A.4.2 Multi-Frequency Signal

Multi-frequency signals refer to a combination of single periodic signals. Given a multi-frequency signal expressed as; $F(t) = \sin(15t) + \cos(24t) + \sin(32t)$, the pattern of convergence of the frequency of the adaptive oscillator for $\omega(0) = 5, 10, 15, 20, 25, 35, 40, 45$ to the multi-frequency signal is verified. Values for the other constants are given as; $\epsilon = 0.9, \mu = 0.2, \gamma = 0.2, x = 1, y = 0$. From Fig. A.5 (Bottom-Left), it can be seen that the frequency of the adaptive oscillator converges to the closest frequency component of the multi-frequency signal. Therefore, it establishes the fact that an AFO possesses the ability to learn one frequency component of a multi-frequency signal. This tends to prove the convergence principle for multiple signals and further lay down the possibility of using coupled oscillators for learning multi-frequency signals.

A.5 Coupled Oscillators System

A system of coupled oscillators in a way, possess a medium by which individual oscillators interact with each other. This medium provides a means of coordination between them. The need for a coupling scheme is therefore required; which represent the type

and topology of coupling (see Fig. 2.4) envisaged for a particular system behaviour. Representing this medium mathematically allows the use of certain coupling terms, which indicates the mode of interaction of the oscillators.

It is important to note that coupled nonlinear oscillators with forcing terms and those without forcing terms may follow the same coupling principle, but the method required to determine the desired result may differ. Basically, the latter is used to generate specific patterns while the former may be used to learn specific generated patterns. In human locomotion control, coupled nonlinear oscillators without forcing terms may be used as CPGs to generate behavioural patterns similar to human gaits; providing the trajectories of the human lower limb as in pre-specified trajectory control. In contrast, the coupled nonlinear oscillators with forcing terms requires certain means to acquire the required behavioural pattern that needs to be followed, as in motion intention detection. CPGs are characterised as mutually coupled nonlinear oscillators; where each oscillator has its own amplitude and frequency parameters, linked by certain coupling terms to other oscillators (Acebrón, Bonilla, Vicente, Ritort and Spigler (2005)). For this purpose, a simplified example of the phase relationship used as the coupling term is modelled for the AFO as in (Righetti, Buchli and Ijspeert, 2009; Righetti and Ijspeert, 2006; Righetti, Buchli and Ijspeert, 2005).

A.5.1 Learning Multi-Frequency Signal

Here, coupled oscillators which allow the use of its adaptive characteristics of the oscillators to learn the different frequencies of a periodic teaching signal is presented. The idea behind this is such that each oscillator encodes one frequency component of the learning signal. Fig. A.6 illustrates multi-frequencies learning method using a negative feedback loop to couple a set of AFO, thereby allowing each oscillator learn one frequency component of the teaching signal. The already learned frequencies are removed from the

teaching signals and the remaining oscillators can be made to adapt to the remaining frequency components.

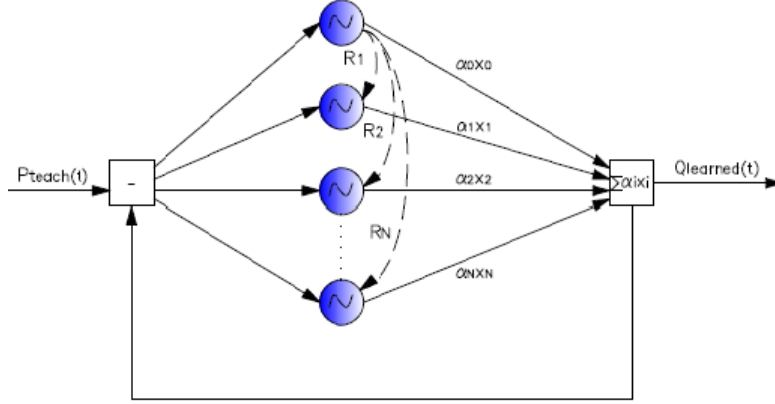


Figure A.6: Structure of a pool of AFO used in the reproduction of a given multi-frequency signal.

For simplicity, two oscillators are considered in this example. Hence, given $P_{teach}(t) = 0.8\sin(15t) + \cos(30t)$, with $\epsilon = 2, \eta = 0.5, \tau = 2, \mu = 1, \gamma = 8$ as constants, $\phi_i(0) = \alpha_i(0) = 0, x_i(0) = 1, y_i(0) = 0$ are the initial conditions for the variables.

$$\begin{aligned}
\dot{x}_i &= \gamma(\mu - x_i^2 - y_i^2)x_i - \omega_i y_i + \epsilon F(t) + \tau \sin(\theta_i - \phi_i) \\
\dot{y}_i &= \gamma(\mu - x_i^2 - y_i^2)y_i - \omega_i x_i \\
\dot{\omega}_i &= -\epsilon F(t) \left(\frac{y_i}{\sqrt{x_i^2 + y_i^2}} \right) \\
\dot{\alpha}_i &= \eta x_i F(t) \\
\dot{\phi}_i &= \sin \left(\frac{\omega_i}{\omega_0} \theta_0 - \theta_i - \phi_i \right) \\
\theta_i &= \text{sgn}(x_i) \cos^{-1} \left(-\frac{y_i}{\sqrt{x_i^2 + y_i^2}} \right) \\
F(t) &= P_{teach}(t) - Q_{learned}(t) \\
Q_{learned}(t) &= \sum_{i=0}^N \alpha_i x_i
\end{aligned} \tag{A.7}$$

where τ and ϵ are coupling constants and η is a learning constant. $Q_{learned}(t)$, represents the weighted sum of the outputs of each oscillator, while $F(t)$ is the negative feedback,

representing the difference between the learned signal and the teaching signal $P_{teach}(t)$ about to be learned. α_i is the amplitude associated to the frequency ω_i of oscillator i . α increases only if ω_i have converged to a frequency component $F(t)$, and will stop increasing when ω_i disappears from $F(t)$ due to the negative feedback loop. ω_i is the phase difference between oscillator i and 0. This converges to the phase difference between the instantaneous phase of oscillator i , θ_0 scaled at frequency ω_i and the instantaneous phase of oscillator i , θ_i . Each adaptive oscillator is coupled with oscillator 0, with strength τ to keep correct phase relationships between oscillators, using Kuramoto algorithm.

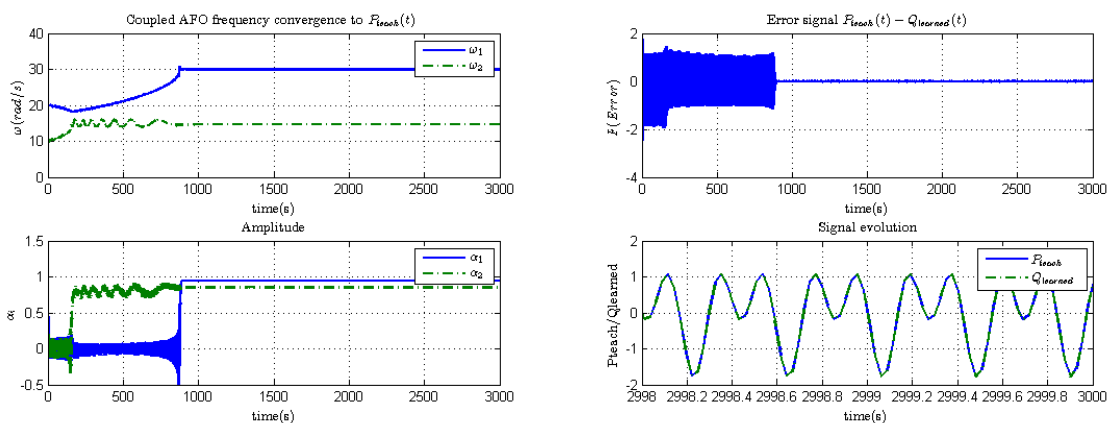


Figure A.7: Top-Left: Coupled AFO frequency convergence to $P_{teach}(t)$. Bottom-Left: Amplitude α . Top-Right: Error Signal $F(t)$. Bottom-Right: Signal evolution of P_{teach} and $Q_{learned}$.

It can be deduced from Fig. A.7 (Bottom-Right) that the network was able to learn the input signal accurately. This implies that the frequency of the oscillator has been effectively matched to the teaching signal. This was further verified by Fig. A.7 (Top-Left). This shows the ability for each of the coupled oscillators to adapt to one frequency component of the teaching signal. Fig. A.7 (Top-Right) illustrates the evolution of the error as regard the negative feedback which tends to zero with time. In addition, Fig. A.7 (Bottom-Left) validate the evolution of the amplitude α_i to the correct values of the teaching signal with regard to the frequency ω_i of the teaching signal adapted to.

In light of the above, it is expedient to consider a practical problem, and as such the next section presents the implementation of the control of an inverted pendulum using adaptive oscillators.

A.6 Inverted Pendulum Control

Performing periodic or quasi-periodic tasks in robotics and animal motor control remains a perpetual research problem. This is due to the difficulties encountered in trajectory generation and modulation. The success of the imitation of the generated motion lies in the ability of the controller-robot system to constantly and dynamically track and re-adapt the control parameters to maintain the motion dynamics. Hence, tracking the frequency of the periodic or quasi-periodic motion pattern helps provide an exciting way of achieving this purpose. Controlling the motion of robots has been likened to an inverted pendulum control problem. This motivated the implementation of the control of an inverted pendulum using adaptive frequency oscillator. This approach is based on frequency adaptation and it allows the system to learn the trajectory of the inverted pendulum dynamics. The modulation is achieved via the tuning of the frequency, amplitude and offset of the adaptive oscillator while keeping all the features of the original trajectory.

This control concept focuses on stabilising a simple one DoF inverted pendulum by establishing a way of tracking the trajectory of the motion dynamics. The validation of this control concept requires two basic building blocks:

- Inverted Pendulum Dynamics.
- Adaptive Frequency Oscillator.

A.6.1 Inverted Pendulum Dynamics

The inverted pendulum is represented by a vertically placed stiff bar of length (L) which is supported at one end by a frictionless pin (s) (see Fig. A.8). The dynamic equation of the inverted pendulum without considering the oscillating vertical motion at which it vibrates with is given by:

$$\ddot{\theta}(t) = \frac{g}{L} \sin(\theta) + u(t) \quad (\text{A.8})$$

where θ is the angular position of the stiff bar to the vertical, L is the length of the stiff bar, g is the gravitational force and $u(t)$ is the input torque.

The oscillating (periodic) vertical motion about the frictionless pin is defined by:

$$s(t) = A_{ref} \sin(\omega_{ref} t) + \pi \quad (\text{A.9})$$

where A_{ref} is the amplitude of the vertical motion and ω_{ref} is the frequency at which the vertical motion occurs. The task required by the inverted pendulum is to continually evolve about a specific oscillating vertical motion defined by the parameters above.

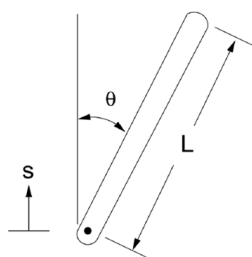


Figure A.8: Inverted pendulum.

A.6.2 Adaptive Frequency Oscillator

The differential equation which represents the adaptive frequency oscillator block is same as in Eq. A.6. However, learning the parameters of the vertical motion requires the difference between the actual position θ and the learned signal (estimated signal)

$\hat{\theta}$ (Righetti and Ijspeert (2006)), which is fed in as the input i.e. $F(t) = \theta - \hat{\theta}$. This necessitates the following equation to compute the estimated signal:

$$\begin{aligned}
\hat{\theta} &= \alpha_0 + \alpha_1 x \\
\dot{\hat{\theta}} &= \alpha_1 \omega y \\
\ddot{\hat{\theta}} &= -\alpha_1 \omega^2 x \\
\dot{\alpha}_0 &= \eta F(t) \\
\dot{\alpha}_1 &= \eta x F(t).
\end{aligned} \tag{A.10}$$

where $\hat{\theta}, \dot{\hat{\theta}}, \ddot{\hat{\theta}}$ is the estimated angular position, velocity and acceleration of the stiff bar respectively, while the amplitude α_1 and offset α_0 can be learned their integrators in Eq. A.10. η is a constant representing the integrator gain. These parameters are used to estimate the input torque $u(t)$ in Eq. A.8.

With regard to the inverted pendulum dynamics as in Eq. A.8; $u(t)$ is a combination of the actual control input $u_c(t)$ and the estimated control input $u_e(t)$, i.e. $u(t) = u_c(t) + u_e(t)$. The control input is defined by a PD controller:

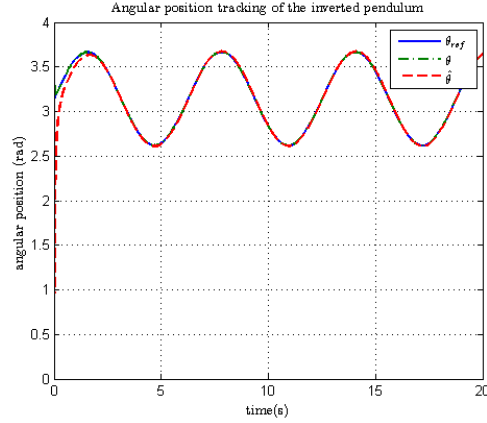
$$u_c(t) = K_p e + K_d \dot{e} \tag{A.11}$$

where e is the error signal; the difference between the oscillating vertical motion and the actual angular position of the stiff bar. K_p, K_d are the proportional and derivative gains of the controller.

Estimating the control input requires taking the inverse of the inverted pendulum dynamics, and can be written as:

$$\hat{u}(t) = \ddot{\hat{\theta}} - \frac{g}{L} \sin(\hat{\theta}) \tag{A.12}$$

$\hat{u}(t)$ is directly proportional to $u_e(t)$ and mathematically related by: $\hat{u}(t) = \kappa u_e(t)$. This allows $u_e(t)$ to be varied. Note that in this case, no variation of $u_c(t)$ is required.



θ_{ref} refers to the oscillating vertical motion $s(t)$. θ & $\hat{\theta}$ are defined in Eq. A.8 and Eq. A.10 respectively. Adaptive oscillator parameter: $\epsilon = 20, \eta = 5, \mu = 1$ & $\gamma = 8$. Inverted pendulum parameters: $L = 0.4m, g = 9.8m/s$. Control input gains: $K_p = 145, K_d = 43$.

Figure A.9: Angular position tracking of the inverted pendulum.

Fig. A.9 presents the angular position tracking of the inverted pendulum. It shows that the AFO-controller could effectively track the inverted pendulum motion dynamics by re-adapting its parameters to the oscillating vertical motion. The interesting aspect of this is that the disappearance of the oscillating motion signal is trivial. This is because the signal has been learned by the AFO and will continually provide the appropriate torque to keep the inverted pendulum within the limits of the oscillating vertical motion, ensuring the system stability.

A.7 Conclusion

The goal of this appendix is to establish a harmonious composition of nonlinear oscillators and also their control capabilities. This was achieved by presenting the mathematical principles behind the theory of nonlinear oscillators and their coupling (synchronisation) scheme. A clear distinction between classical nonlinear oscillators and adaptive oscillators, with the inclusion or exclusion of forcing terms has been demon-

strated. Relevant examples constituting practical problems were given to support this claim. Nonlinear oscillators; based on its rhythmic nature provide a very appealing concept in the area of assistance and rehabilitation robotics. This is because movement in humans is practically controlled by CPG, which may be referred to as spinal or neural oscillators. In the main body of this work, practical applications of the oscillators examined are detailed further where necessary, with specifics.

APPENDIX B. Stability Theory

B.1 Vectors and Matrix Norms

B.1.1 Vector Norms

Norms offers certain measures to calculate the distance between vectors and matrices. This provides a measure of “closeness” that is used to understand convergence in control system analysis.

A vector norm $\|\cdot\|$ is a functional ($\|\cdot\| : \mathfrak{R}^n \rightarrow \mathfrak{R}$) satisfying the following properties:

- $\|x\| \geq 0$, $\|x\| = 0 \leftrightarrow x = 0, x \in \mathfrak{R}^n$
- $\|x + y\| \leq \|x\| + \|y\|$, $x, y \in \mathfrak{R}^n$
- $\|\alpha x\| = |\alpha| \|x\|$, $\alpha \in \mathfrak{R}, x, y \in \mathfrak{R}^n$

B.1.2 P-norms

P-norms can be defined by the expression:

$$\|x\|_p = (|x_1|^p + |x_2|^p + \cdots + |x_n|^p)^{\frac{1}{p}}, \quad p \geq 1 \quad (\text{B.1})$$

- $\|x\|_1 = |x_1| + |x_2| + \cdots + |x_n|$ One norm

- $\|x\|_2 = (|x_1|^2 + |x_2|^2 + \dots + |x_n|^2)^{\frac{1}{2}}$ Euclidean norm
- $\|x\|_\infty = \max_{1 \leq i \leq n} |x_i|$ Infinity norm

The most important properties of p-norms are:

- The Holder inequality:

$$|x^T y| \leq \|x\|_p \|y\|_q, \quad \frac{1}{p} + \frac{1}{q} = 1$$

- The Cauchy-Schwartz inequality ($p = q = 2$)

$$|x^T y| \leq \|x\|_2 \|y\|_2$$

B.1.3 Matrix Norms

Matrix norms tend to calculate the sensitivity of a matrix to perturbations.

A matrix norm $\|A\|$, $A \in \mathfrak{R}^{m \times n}$ is functional satisfying the following properties:

- $\|A\| \geq 0$, $\|A\| = 0 \leftrightarrow A = 0$
- $\|A + B\| \leq \|A\| + \|B\|$
- $\|\alpha A\| = |\alpha| \|A\|$ $\alpha \in \mathfrak{R}$

Vectors induced matrix norms are defined in terms of p-norms of vectors as:

- $\|A\| = \max_{x \neq 0} \frac{\|Ax\|_p}{\|x\|_p} = \max_{\|x\|_p=1} \|Ax\|_p$

Note that *max* can be replaced by *sup* which stands for supremum (also known as least upper-bound).

One norm is the maximum absolute column sum and can be expressed as:

$$\|A\|_1 = \max_j \sum_{i=1}^m |a_{ij}| \quad (\text{B.2})$$

Infinity norm is the maximum absolute row sum and expressed as:

$$\|A\|_\infty = \max_j \sum_{j=1}^m |a_{ij}| \quad (\text{B.3})$$

Euclidean norm (2-norm) requires eigenvalue analysis and is given as:

$$\|A\|_2 = [\lambda \max(A^T A)]^{\frac{1}{2}} \quad (\text{B.4})$$

B.1.4 Existence and Uniqueness of Solutions

There are two important (standard) conditions which guarantee the existence and uniqueness of a solution, as given below:

- Piecewise Continuous

A function $f(t, x)$ is piecewise continuous in t on an interval $D \subset \mathfrak{R}$ if for every bounded subinterval $D_0 \subset \mathfrak{R}$, f is continuous in $t \forall t \in D_0$, except, possibly, at a finite number of points where f may have finite-jump discontinuities.

- Lipschitz Continuous

A function $f(t, x)$, is locally Lipschitz in x at a point x_0 if there exists a neighbourhood $N(x_0, r) = \{x \in \mathfrak{R}^n \mid \|x - x_0\| < r\}$: where $f(t, x)$ satisfies the Lipschitz condition:

$$\|f(t, x) - f(t, y)\| \leq L\|x - y\|, L > 0$$

B.2 Lyapunov Stability Theory

Since exoskeleton control is time dependent, it is expedient to review the tools of Lyapunov stability theory for non autonomous systems.

Consider the non-autonomous system:

$$\dot{x} = f(x, t) \quad x(t_0) = x_0 \quad x \in \mathfrak{R}^n \quad (\text{B.5})$$

Let's assume that $f(t, x)$ meets the standard conditions for existence and uniqueness of solutions:

B.2.0.1 Stability

The equilibrium point $x^* = 0$ of Eq. B.5 is:

- Stable at $t = t_0$ if for any $\epsilon > 0$, there exists a $\delta(t_0, \epsilon) > 0$ such that

$$\|x(t_0)\| < \delta \Rightarrow \|x(t)\| < \epsilon, \quad \forall t \geq t_0$$

- Uniformly stable at $t = t_0$ if for any $\epsilon > 0$, there exists a $\delta(\epsilon) > 0$ such that

$$\|x(t_0)\| < \delta \Rightarrow \|x(t)\| < \epsilon, \quad \forall t \geq t_0$$

B.2.1 Asymptotic Stability

The equilibrium point $x^* = 0$ of Eq. B.5 is:

- Asymptotically stable at $t = t_0$ if $x^* = 0$ is stable and there exists $\delta(t_0)$ such that

$$\|x(t_0)\| < \delta \Rightarrow \lim_{t \rightarrow \infty} x(t) = 0$$

.

- Uniformly Asymptotically stable at $t = t_0$ if $x^* = 0$ is uniformly stable and there exists δ such that

$$\|x(t_0)\| < \delta \Rightarrow \lim_{t \rightarrow \infty} x(t) = 0$$

.

B.2.2 Globally Stable

An equilibrium point x^* is globally stable if it is stable for all initial conditions $x_0 \in \mathfrak{R}^n$.

B.2.2.1 Unstable

An equilibrium point x^* is unstable if it is not stable.

B.2.3 Exponential Stability

The equilibrium point $x^* = 0$ is an

- exponentially stable equilibrium point of Eq. B.5 if there exist constants $m, \alpha > 0$ and $\epsilon > 0$ such that

$$\|x(t)\| \leq m e^{-\alpha(t-t_0)} \|x(t_0)\| \quad \forall \|x(t_0)\| \leq \epsilon \ \& \ t \geq t_0.$$

The largest constant α is called the rate of convergence.

B.2.3.1 Globally Exponentially Stable

A system is globally exponentially stable if the bound in

$$\|x(t)\| \leq me^{-\alpha(t-t_0)}\|x(t_0)\| \quad \forall \|x(t_0)\| \leq \epsilon \ \& \ t \geq t_0$$

is satisfied $\forall x_0 \in \mathfrak{R}^n$.

B.2.3.2 The Direct Lyapunov

This method entails the study of the rate of change of the energy of a system in order to determine stability if and only if there exists a *measure of energy* in the system. Defining the exact *measure of energy* is a cumbersome task, but for the purpose of analysis we shall consider an example by stating that:

Let B_ϵ be a ball of size ϵ around the origin, $B_\epsilon = \{x \in \mathfrak{R}^n : \|x\| < \epsilon\}$

B.2.4 Locally Positive Definite Functions

Locally positive definite function is locally like an energy function. A continuous function $V : \mathfrak{R}^n \times \mathfrak{R}_+ \rightarrow \mathfrak{R}$ is a locally positive definite function if for some $\epsilon > 0$ and some continuous, strictly increasing function $\alpha : \mathfrak{R}_+ \rightarrow \mathfrak{R}$,

$$V(0, t) = 0 \ \& \ V(x, t) \geq \alpha(\|x\|) \quad \forall x \in B_\epsilon, \ \forall t \geq 0.$$

B.2.5 Positive Definite Functions

Positive definite functions are functions which are globally like energy functions. A continuous function $V : \mathfrak{R}^n \times \mathfrak{R}_+ \rightarrow \mathfrak{R}$ is a positive definite function if for some $\epsilon > 0$ and some continuous, strictly increasing function $\alpha : \mathfrak{R}_+ \rightarrow \mathfrak{R}$, and $\alpha(p) \rightarrow \infty$ as $p \rightarrow \infty$.

B.2.6 Decrescent Functions

Decrescence is used to bound energy functions. This theorem states that when $V(x, t)$ is a locally positive definite function $\dot{V}(x, t) \leq 0$ then we can conclude stability of the equilibrium points. The time derivative of V is taken along the trajectories of the system.

$$\dot{V}|_{\dot{x} = f(x, t)} = \frac{dV}{dt} + \frac{dV}{dx}f \quad (\text{B.6})$$

A continuous function $V : \mathfrak{R}^n \times \mathfrak{R}_+ \rightarrow \mathfrak{R}$ is decrescent if for some $\epsilon > 0$ and some continuous, strictly increasing function

$$V(x, t) \leq \beta(\|x\|) \quad \forall x \in B_\epsilon, \quad \forall t \geq 0.$$

B.2.6.1 Basic Theorem of Lyapunov

Let $V(x, t)$ be a non-negative function with derivative $\dot{V} \leq 0$ along the trajectories of the system.

- If $V(x, t)$ is locally positive definite and $\dot{V}(x, t) = 0$ locally in x and for all t , then the origin of the system is locally stable.
- If $V(x, t)$ is locally positive definite and decrescent and $\dot{V} \leq 0$ locally in x and $\forall t$ then the origin of the system is uniformly locally stable.
- If $V(x, t)$ is locally positive definite and decrescent and $-\dot{V} \leq 0$ locally positive definite, then the origin of the system is uniformly asymptotically stable.
- If $V(x, t)$ is positive definite and decrescent and $-\dot{V} \leq 0$ positive definite, then the origin of the system is globally uniformly asymptotically stable

B.2.7 The Indirect Lyapunov

This method verifies the local stability of a system by utilising the linearised equation of that same system. Let's consider a system: $\dot{x} = f(x, t)$ with $f(0, t) = 0 \forall t \geq 0$. The Jacobian matrix of $f(x, t)$ with respect to x , evaluated at the origin is given as:

$$A(t) = \left. \frac{df(x, t)}{dx} \right|_{x=0} \quad (\text{B.7})$$

This implies that for each fixed t , the remainder $f_1(x, t) = f(x, t) - A(t)x$ approaches zero as x approaches zero. Though, the remainder may not approach zero uniformly. For this to be true we require a stronger condition that:

$$\lim_{\|x\| \rightarrow 0} \sup_{t \geq 0} \frac{\|f_1(x, t)\|}{\|x\|} = 0 \quad (\text{B.8})$$

If the Eq. B.8 holds, then the system

$$\dot{z} = A(t)z \quad (\text{B.9})$$

is referred to as the uniform linearisation of Eq. B.5 about the origin. If this linearisation exists then its stability determines the local stability of the original nonlinear system.

B.2.8 Lasalle's Invariance Principle

This theorem enables us to conclude asymptotic stability of an equilibrium point even when $-\dot{V}(x, t)$ is not locally positive definite. This applies only to autonomous or periodic systems; hence we shall not dwell on it.

B.2.8.1 Lasalle's Invariance Principle

Let $f : \mathfrak{R} \rightarrow \mathfrak{R}$ be a uniformly continuous function on $[0, \infty]$. Suppose that $\lim_{t \rightarrow \infty} \int_0^t f(\tau) d\tau$ exists and is finite. Then $f(t) \rightarrow 0$ as $t \rightarrow \infty$.

APPENDIX C. Transformed Inertia Matrix - Relative Angles

With reference to Eq. (5.4) & Eq. (5.24) the Inertia matrix vector $D(q)$ are given below:

C.1 Inertia matrix

$$\begin{aligned}
 D_{11} = & I_1 + I_2 + I_3 + I_4 + I_5 + l_1^2 m_2 + l_1^2 m_3 + l_1^2 m_4 + l_1^2 m_5 + l_2^2 m_3 + l_2^2 m_4 \\
 & + l_2^2 m_5 + l_4^2 m_4 + l_4^2 m_5 + l_5^2 m_5 + l_{c1}^2 m_1 + l_{c2}^2 m_2 + l_{c3}^2 m_3 + l_{c4}^2 m_4 + l_{c5}^2 m_5 - 2l_4 l_{c4} m_4 \\
 & - 2l_5 l_{c5} m_5 - 2l_2 l_5 m_5 \cos(q_2 + q_3 - q_4) + 2l_2 l_{c5} m_5 \cos(q_2 + q_3 - q_4) - 2l_2 l_4 m_4 \cos(q_2 + q_3) \\
 & - 2l_2 l_4 m_5 \cos(q_2 + q_3) + 2l_1 l_{c3} m_3 \cos(q_1 + q_2) + 2l_2 l_{c4} m_4 \cos(q_2 + q_3) + 2l_1 l_2 m_3 \cos(q_1) \\
 & + 2l_1 l_2 m_4 \cos(q_1) + 2l_1 l_2 m_5 \cos(q_1) + 2l_4 l_5 m_5 \cos(q_4) + 2l_1 l_{c2} m_2 \cos(q_1) + 2l_2 l_{c3} m_3 \cos(q_2) \\
 & - 2l_4 l_{c5} m_5 \cos(q_4) - 2l_1 l_5 m_5 \cos(q_1 + q_2 + q_3 - q_4) + 2l_1 l_{c5} m_5 \cos(q_1 + q_2 + q_3 - q_4) \\
 & - 2l_1 l_4 m_4 \cos(q_1 + q_2 + q_3) - 2l_1 l_4 m_5 \cos(q_1 + q_2 + q_3) + 2l_1 l_{c4} m_4 \cos(q_1 + q_2 + q_3)
 \end{aligned} \tag{C.1}$$

$$\begin{aligned}
D_{12} = & -I_2 - I_3 - I_4 - I_5 - l_2^2 m_3 - l_2^2 m_4 - l_2^2 m_5 - l_4^2 m_4 - l_4^2 m_5 - l_5^2 m_5 - l_{c2}^2 m_2 \\
& - l_{c3}^2 m_3 - l_{c4}^2 m_4 - l_{c5}^2 m_5 + 2l_4 l_{c4} m_4 + 2l_5 l_{c5} m_5 + 2l_2 l_5 m_5 \cos(q_2 + q_3 - q_4) \\
& - 2l_2 l_{c5} m_5 \cos(q_2 + q_3 - q_4) + 2l_2 l_4 m_4 \cos(q_2 + q_3) + 2l_2 l_4 m_5 \cos(q_2 + q_3) - l_1 l_{c3} m_3 \cos(q_1 + q_2) \\
& - 2l_2 l_{c4} m_4 \cos(q_2 + q_3) - l_1 l_2 m_3 \cos(q_1) - l_1 l_2 m_4 \cos(q_1) - l_1 l_2 m_5 \cos(q_1) - 2l_4 l_5 m_5 \cos(q_4) \\
& - l_1 l_{c2} m_2 \cos(q_1) - 2l_2 l_{c3} m_3 \cos(q_2) + 2l_4 l_{c5} m_5 \cos(q_4) + l_1 l_5 m_5 \cos(q_1 + q_2 + q_3 - q_4) \\
& - l_1 l_{c5} m_5 \cos(q_1 + q_2 + q_3 - q_4) + l_1 l_4 m_4 \cos(q_1 + q_2 + q_3) + l_1 l_4 m_5 \cos(q_1 + q_2 + q_3) \\
& - l_1 l_{c4} m_4 \cos(q_1 + q_2 + q_3)
\end{aligned} \tag{C.2}$$

$$\begin{aligned}
D_{13} = & -I_3 - I_4 - I_5 - l_4^2 m_4 - l_4^2 m_5 - l_5^2 m_5 - l_{c3}^2 m_3 - l_{c4}^2 m_4 - l_{c5}^2 m_5 + 2l_4 l_{c4} m_4 \\
& + 2l_5 l_{c5} m_5 + l_2 l_5 m_5 \cos(q_2 + q_3 - q_4) - l_2 l_{c5} m_5 \cos(q_2 + q_3 - q_4) + l_2 l_4 m_4 \cos(q_2 + q_3) \\
& + l_2 l_4 m_5 \cos(q_2 + q_3) - l_1 l_{c3} m_3 \cos(q_1 + q_2) - l_2 l_{c4} m_4 \cos(q_2 + q_3) - 2l_4 l_5 m_5 \cos(q_4) \\
& - l_2 l_{c3} m_3 \cos(q_2) + 2l_4 l_{c5} m_5 \cos(q_4) + l_1 l_5 m_5 \cos(q_1 + q_2 + q_3 - q_4) - l_1 l_{c5} m_5 \cos(q_1 + q_2 + q_3 - q_4) \\
& + l_1 l_4 m_4 \cos(q_1 + q_2 + q_3) + l_1 l_4 m_5 \cos(q_1 + q_2 + q_3) - l_1 l_{c4} m_4 \cos(q_1 + q_2 + q_3)
\end{aligned} \tag{C.3}$$

$$\begin{aligned}
D_{14} = & -I_4 - I_5 - l_4^2 m_4 - l_4^2 m_5 - l_5^2 m_5 - l_{c4}^2 m_4 - l_{c5}^2 m_5 + 2l_4 l_{c4} m_4 + 2l_5 l_{c5} m_5 \\
& + l_2 l_5 m_5 \cos(q_2 + q_3 - q_4) - l_2 l_{c5} m_5 \cos(q_2 + q_3 - q_4) + l_2 l_4 m_4 \cos(q_2 + q_3) + l_2 l_4 m_5 \cos(q_2 + q_3) \\
& - l_2 l_{c4} m_4 \cos(q_2 + q_3) - 2l_4 l_5 m_5 \cos(q_4) + 2l_4 l_{c5} m_5 \cos(q_4) + l_1 l_5 m_5 \cos(q_1 + q_2 + q_3 - q_4) \\
& - l_1 l_{c5} m_5 \cos(q_1 + q_2 + q_3 - q_4) + l_1 l_4 m_4 \cos(q_1 + q_2 + q_3) + l_1 l_4 m_5 \cos(q_1 + q_2 + q_3) \\
& - l_1 l_{c4} m_4 \cos(q_1 + q_2 + q_3)
\end{aligned} \tag{C.4}$$

$$\begin{aligned}
D_{15} = & I_5 + l_5^2 m_5 + l_{c5}^2 m_5 - 2l_5 l_{c5} m_5 - l_2 l_5 m_5 \cos(q_2 + q_3 - q_4) + l_2 l_{c5} m_5 \cos(q_2 + q_3 - q_4) \\
& + l_4 l_5 m_5 \cos(q_4) - l_4 l_{c5} m_5 \cos(q_4) - l_1 l_5 m_5 \cos(q_1 + q_2 + q_3 - q_4) + l_1 l_{c5} m_5 \cos(q_1 + q_2 + q_3 - q_4)
\end{aligned} \tag{C.5}$$

$$D_{21} = D_{12} \tag{C.6}$$

$$\begin{aligned}
D_{22} = & I_2 + I_3 + I_4 + I_5 + l_2^2 m_3 + l_2^2 m_4 + l_2^2 m_5 + l_4^2 m_4 + l_4^2 m_5 + l_5^2 m_5 + l_{c2}^2 m_2 + l_{c3}^2 m_3 + l_{c4}^2 m_4 \\
& + l_{c5}^2 m_5 - 2l_4 l_{c4} m_4 - 2l_5 l_{c5} m_5 - 2l_2 l_5 m_5 \cos(q_2 + q_3 - q_4) + 2l_2 l_{c5} m_5 \cos(q_2 + q_3 - q_4) \\
& - 2l_2 l_4 m_4 \cos(q_2 + q_3) - 2l_2 l_4 m_5 \cos(q_2 + q_3) + 2l_2 l_{c4} m_4 \cos(q_2 + q_3) + 2l_4 l_5 m_5 \cos(q_4) \\
& + 2l_2 l_{c3} m_3 \cos(q_2) - 2l_4 l_{c5} m_5 \cos(q_4)
\end{aligned} \tag{C.7}$$

$$\begin{aligned}
D_{23} = & I_3 + I_4 + I_5 + l_4^2 m_4 + l_4^2 m_5 + l_5^2 m_5 + l_{c3}^2 m_3 + l_{c4}^2 m_4 + l_{c5}^2 m_5 - 2l_4 l_{c4} m_4 \\
& - 2l_5 l_{c5} m_5 - l_2 l_5 m_5 \cos(q_2 + q_3 - q_4) + l_2 l_{c5} m_5 \cos(q_2 + q_3 - q_4) - l_2 l_4 m_4 \cos(q_2 + q_3) \\
& - l_2 l_4 m_5 \cos(q_2 + q_3) + l_2 l_{c4} m_4 \cos(q_2 + q_3) + 2l_4 l_5 m_5 \cos(q_4) + l_2 l_{c3} m_3 \cos(q_2) - 2l_4 l_{c5} m_5 \cos(q_4)
\end{aligned} \tag{C.8}$$

$$\begin{aligned}
D_{24} = & I_4 + I_5 + l_4^2 m_4 + l_4^2 m_5 + l_5^2 m_5 + l_{c4}^2 m_4 + l_{c5}^2 m_5 - 2l_4 l_{c4} m_4 - 2l_5 l_{c5} m_5 \\
& - l_2 l_5 m_5 \cos(q_2 + q_3 - q_4) + l_2 l_{c5} m_5 \cos(q_2 + q_3 - q_4) - l_2 l_4 m_4 \cos(q_2 + q_3) - l_2 l_4 m_5 \cos(q_2 + q_3) \\
& + l_2 l_{c4} m_4 \cos(q_2 + q_3) + 2l_4 l_5 m_5 \cos(q_4) - 2l_4 l_{c5} m_5 \cos(q_4)
\end{aligned} \tag{C.9}$$

$$\begin{aligned}
D_{25} = & -I_5 + 2l_5 l_{c5} m_5 - l_5^2 m_5 - l_{c5}^2 m_5 + l_2 l_5 m_5 \cos(q_2 + q_3 - q_4) - l_2 l_{c5} m_5 \cos(q_2 + q_3 - q_4) \\
& - l_4 l_5 m_5 \cos(q_4) + l_4 l_{c5} m_5 \cos(q_4)
\end{aligned} \tag{C.10}$$

$$D_{31} = D_{13} \tag{C.11}$$

$$D_{32} = D_{23} \tag{C.12}$$

$$\begin{aligned}
D_{33} = & I_3 + I_4 + I_5 + l_4^2 m_4 + l_4^2 m_5 + l_5^2 m_5 + l_{c3}^2 m_3 + l_{c4}^2 m_4 + l_{c5}^2 m_5 - 2l_4 l_{c4} m_4 \\
& - 2l_5 l_{c5} m_5 + 2l_4 l_5 m_5 \cos(q_4) - 2l_4 l_{c5} m_5 \cos(q_4)
\end{aligned} \tag{C.13}$$

$$\begin{aligned}
D_{34} = & I_4 + I_5 + l_4^2 m_4 + l_4^2 m_5 + l_5^2 m_5 + l_{c4}^2 m_4 + l_{c5}^2 m_5 - 2l_4 l_{c4} m_4 - 2l_5 l_{c5} m_5 \\
& + 2l_4 l_5 m_5 \cos(q_4) - 2l_4 l_{c5} m_5 \cos(q_4)
\end{aligned} \tag{C.14}$$

$$D_{35} = -I_5 - l_5^2 m_5 + 2m_5 l_5 l_{c5} - l_4 m_5 \cos(q_4) l_5 - m_5 l_{c5}^2 + l_4 m_5 \cos(q_4) l_{c5} \tag{C.15}$$

$$D_{41} = D_{14} \tag{C.16}$$

$$D_{42} = D_{42} \tag{C.17}$$

$$D_{43} = D_{44} = D_{34} \tag{C.18}$$

$$D_{45} = D_{35} \tag{C.19}$$

$$D_{51} = D_{15} \tag{C.20}$$

$$D_{52} = D_{25} \tag{C.21}$$

$$D_{53} = D_{54} = D_{35} \tag{C.22}$$

$$D_{55} = I_5 + m_5 l_5^2 - 2m_5 l_5 l_{c5} + m_5 l_{c5}^2 \tag{C.23}$$